Capacitive Energy Harvesting and Capacitive Icing Detection on High-Voltage Overhead Power Lines

PhD Thesis

submitted to the Faculty of Electrical and Information Engineering

by
Dipl.-Ing. Michael Johannes Moser

in candidacy for the academic degree
"Doktor der technischen Wissenschaften" (Doctor technicae)

Institute of Electrical Measurement and
Measurement Signal Processing

Graz University of Technology

Supervisor: Univ.-Prof. Dipl.-Ing. Dr.techn. Georg Brasseur
Co-Supervisor: Prof. Dr.-Ing. Michiel J. Vellekoop

Graz, November 2013

EIDESSTATTLICHE ERKLÄRUNG

Ich erkläre an Eides statt, dass ich die vorliegende Arbeit selbstständig verfasst, andere als die angegebenen Quellen/Hilfsmittel nicht benutzt und die den benutzten Quellen wörtlich und inhaltlich entnommenen Stellen als solche kenntlich gemacht habe.

Graz, am …… ……..
(Unterschrift)

Englische Fassung:

STATUTORY DECLARATION

I declare that I have authored this thesis independently, that I have not used other than the declared sources / resources and that I have explicitly marked all material which has been quoted either literally or by content from the used sources.

…… ……..
date (signature)

This work is dedicated to my parents, who always supported my studies.
Also, this thesis is dedicated to Eva, for her love and care and for her continuous motivation.
The reader should keep in mind that a powerful source of innovation is given by combining knowledge from different fields of research.

Abstract

This PhD thesis describes the evolution of an autonomous monitoring system for continuous on-line icing condition monitoring of the surface of high-voltage overhead power transmission lines. Continuous monitoring is required since icing events are hard to predict, occur rarely and very locally but can cause severe damages. On-line information on the icing status is useful to trigger countermeasures. The desired autonomous monitoring system consists of a capacitive energy harvesting system, a capacitive icing detection system and the related data transmission circuitry. In both laboratory and field tests, the functionality of a test device was successfully tested. It could be shown that capacitive icing detection can be employed in the vicinity of a high-voltage conductor and that the harvested energy allows the use of commercial radio networks as main measurement data transmission channel. In addition to that, the capacitive measurement principle was implemented in an industrial measurement device for condition monitoring of overhead power transmission lines.

Zusammenfassung

Diese Arbeit beschreibt die Entwicklung eines autonomen Überwachungssystems für die kontinuierliche Aneisungserkennung an der Leiterseiloberfläche von Hochspannungsfreileitungen. Die kontinuierliche Zustandsüberwachung ist notwendig, weil Aneisungsereignisse schwierig vorauszusagen sind, selten und räumlich stark begrenzt auftreten und gleichzeitig schwere Schäden verursachen können. Die aktuellen Informationen über Aneisungsereignisse am Leiterseil dienen der zeitgerechten Einleitung von Gegenmaßnahmen. Das gesuchte autonome Überwachungssystem besteht aus einem kapazitiven Energy Harvesting-System, einem Messsystem zur Erkennung von Eisschichten basierend auf kapazitiver Sensorik und einer Datenübertragung zu einer Basisstation per Funk. Sowohl in Labor- als auch in Feldversuchen konnte die Funktionalität erfolgreich gezeigt werden. Die durch das kapazitive Energy Harvesting bereitgestellte Energie ist ausreichend, um die Daten über kommerzielle Funknetzwerke (z.B. GSM) und somit ohne zusätzliche Repeater zu übertragen. Weiters wird der Betrieb kapazitiver Messtechnik im Bereich starker elektrischer Wechselfelder demonstriert. Das Sensorprinzip wurde darüberhinaus in einem industriellen Produkt zur Überwachung des Zustandes von Freileitungen implementiert und an einem Prüfstand getestet.

I wish to express my sincere gratitude to my supervisor, Univ.Prof. Dipl.-Ing. Dr.techn. Georg Brasseur, Head of the Institute of Electrical Measurement and Measurement Signal Processing, Graz University of Technology, for giving me the opportunity to carry out this work and for his continuous support during the work on the present thesis.

My sincere thanks are due to my co-supervisor, Prof. Dr.-Ing. Michiel J. Vellekoop, Head of the Institute for Microsensors, -Actuators and -Systems, University of Bremen, Germany, for his detailed comments on this work from an external point of view.

I warmly thank Univ.Prof. Dipl.-Ing. Dr.techn. Hubert Zangl, Head of the Sensors&Actuators Department at the Institute of Smart Systems Technologies, Alpen-Adria-Universität Klagenfurt, for his openness to unconventional solutions, numerous discussions and his valuable advice during this work.

I wish to thank all the current and former members of the Sensors and Instrumentation Group at the Institute of Electrical Measurement and Measurement Signal Processing, Graz University of Technology, for their support of the present work.

I am grateful to Dipl.Ing. Dr.techn. Werner Lick and his colleagues at the Institute of High Voltage Engineering and System Management, Graz University of Technology, for their support with high-voltage experiments during the development of the test device.

I would also like to express my thanks to Dipl.-Ing. Herbert Lugschitz and his colleagues at Austrian Power Grid for the funding of the project and for giving me the opportunity to carry out field tests of the test device on a real-world overhead power transmission line. Also, I warmly thank Mr. Horst Hopitzan for his efforts on the industrialization of the developed measurement principle.

I would like to thank Assoz.Univ.-Prof. Mag. Dr.rer.nat. Ulrich Foelsche from the Institute of Physics, University of Graz, for his introduction to the field of atmospheric icing and meteorology.

I warmly thank Dr. Lasse Makkonen from VTT, Finland for his helpful comments on my work.

Also, I would like to thank Hamid Banitalebi Dehkordi, Pierre Camirand and Prof. Masoud Farzaneh at CIGELE Atmospheric Icing Research Wind

Tunnel (University of Québec at Chicoutimi) for their fruitful collaboration.

I also thank Ao. Univ.Prof. Dipl.-Ing. Dr.techn. Johann Nicolics from the Department of Applied Electronic Materials (AEM) at Vienna University of Technology for his introduction to LTCC technology.

During the course of this work, I received assistance from several further colleagues at the Institute of Electrical Measurement and Measurement Signal Processing, Graz University of Technology, to whom I wish to express my thanks. Especially, I wish to express my thanks to Mr. Werner Schwartz for providing me with his sound experience in mechanical construction.

My loving thanks are due to Eva, my parents and my family for their support all throughout my work on this thesis.

Graz, October 2013

Michael J. Moser

Contents

List of Figures

List of Tables

Chapter 1

Introduction

At the beginning, a short overview on the topic is given, followed by the author's motivation for carrying out this PhD work. Section 1.3 defines the problem and presents the aims of this work. Section 1.4 describes the novel concept pursued in this work - an integrated autonomous measurement device. Section 1.5 briefly explains the fields of research. At the end of this chapter, Section 1.6 lists articles which the author and his co-authors published during this work.

1.1 Overview

Distribution of electric energy by means of high-voltage overhead lines is a standard technique due to low installation costs, reasonable maintenance costs and long operational times (typically several decades). Due to the exposure to the environment, several factors causing possible damages have to be taken into account. For instance, the distance between the line and the objects in the vicinity (the so-called line sag) may change, for example, due to growing trees or temperature expansion, snow or ice deposition. In order to maintain safe operating conditions, power lines need to be inspected in regular intervals. This so-called "condition monitoring" is usually done by means of on-ground and helicopter-aided inspection. As this is time-consuming and comparatively costly, the intervals between inspections usually are in the range of months or years. Of course, this is a suitable interval for parameters that only change notably within that time such as tree growth. Meteorological conditions (pre-

cipitation, ice, snow, wind, high or low temperatures) however, can change in orders of magnitude within hours or even minutes. Especially, the combination of low temperatures (within a specific range), high air humidity or precipitation and wind can lead to ice accumulation at the conductor surface. This is the phenomenon called "atmospheric icing", which is hard to predict, occurs locally and rarely but potentially poses heavy problems to the power lines as the transmission towers have to bear the additional weight. The additional weight can lead to the collapse of transmission towers or the destruction of the entire transmission line, causing danger for passersby, economic losses due to interruption of power supply and enormous costs for re-building.

1.2 Motivation

In order to give an impression of the range of possible damages due to ice accretion on the conductor rope, this Section provides a short list of example events, all of them within the recent 15 years.

One of the worst occurrences was an ice storm in eastern Canada and the US in January 1998. Super-cooled rain droplets freezing at cold surfaces (so-called freezing rain) led to a quick buildup of thick ice layers. In the province of Québec, 3 million people were affected for up to 5 weeks, when more than 150 transmission towers collapsed due to the weight load of the ice [11]. As a consequence, several people died, mainly because of lacking electrical energy for heating [12].

From December 2004 to February 2005, a large-scale icing event affected 700 million people in the Chinese provinces of Hunan, Hubei and Chongqing. In total, more than 1000 ice accidents were recorded in China since 1954 and occurred more frequently in the recent past due to the fast economic growth of the country [13].

Between November 24 and 27, 2005, a heavy snow storm hit the region of Muensterland in Germany. While the air temperature ranged around 0°C, wet, and therefore heavy snow coincided with high wind speeds, thus accreting thick wet snow layers to the conductor ropes. Besides effects at surfaces like roads (causing more than 1200 car accidents) and trees (breaking and damaging power lines), a total of 83 transmission towers collapsed due to the weight of

the accreted snow. Based on photographs, diameters of wet snow accretions in the range of 15 cm were estimated, corresponding to a maximum wet snow load of approx. 50 N/m according to [14]. 250000 residents were affected for up to 4 days.

On March 5, 2006, snow load on conductors caused ground short circuits on multiple lines in the surroundings of Ljubljana, Slovenia. Due to the circumstances, a 110 kV line faced both additional current and snow load which caused the line sag to increase until the line touched the ground. The power line was later automatically re-connected to the grid, started to melt down the ice layer due to the continuous ground connection and broke. The simulation of the snow load yielded a layer of approx. 30 mm with a density of 0.6 [15].

The ice storm in southern China in early 2008 was among the most severe events in he last few years. More than 7500 transmission lines above 10 kV were out of service in 570 counties of 13 provinces in southern China. This event was recognized to be the most serious ice accident since 1937 and in total over 2000 transmission towers being part of power lines with a system voltage equal to or above 220 kV collapsed. Thereof, nearly 900 transmission towers were totally destroyed [16].

On January 27-28, 2009, four 110 kV transmission towers of an important line were lost in a rime icing storm in northern Slovenia. More than 50 cm of snow caused interruption of supply. The redesign and reconstruction works needed 30 days to be completed [17].

On May 4, 2011, the temperature went down to 0°C together with snow, heavy fog and frost in south-western Poland. About 100000 people suffered from power outages due to power lines caused by falling trees, for example, in Walbrzych and Wroclaw.

Summing up the above: these events occur rarely but cause big damages.

1.3 Problem Statement and Aim of this Work

Unobserved icing on power lines causes the following problems:

- Increasing line sag, which reduces the safety distance towards the environment.

- Formation of thick ice layers, which are very difficult to cope with (lines have to be taken off the grid and de-iced manually).
- Changes in the dynamics of a transmission line [18], for example, so-called aeolian vibrations, wake-induced oscillations and galloping of conductors; all of them induced due to the changes in aerodynamic properties, causing mechanical stress.
- In severe cases, heavy damages and/or destruction of entire power lines occur, for example, due to material fatigue.
- Reduction of supply reliability.
- Limited applicability of so-called dynamical thermal rating (DTR) due to falling ice chunks. For transmission lines, dynamical thermal rating describes the maximization of the current while not threatening the health of the equipment by exceeding certain temperature limits. In the presence of ice, an increased conductor temperature may lead to faster melting processes.

Hence, it is the interest of electric supply companies who operate power transmission lines in endangered areas to avoid the accumulation of ice or detect as soon as possible in order to take adequate precautions like, for example, thermal de-icing (details on de-icing can be found in Section 2.3.2). This interest is extended to any company or consumer who by their nature strongly depend on the stability of the power grid.

Therefore, the aim of this work is the design and realization of an icing detection system for operation at high voltage over-head power transmission lines fulfilling the following requirements:

- Detection of ice at small thicknesses at the surface of a power line or as close to the line surface as possible to allow for early counter measures.
- High measurement accuracy and repeatability with respect to the detection of ice.
- Autonomy from external power supplies, i.e. implementation of a suited energy harvesting technique.

- Data transmission to a central database collecting information from multiple measurement devices, for example, over a wireless communication path.
- Mechanical and electrical robustness against the harsh environment (High Voltage (HV), Alternating Current (AC) electric and magnetic field, winter weather conditions).
- Maintenance intervals in the range of several years.
- Realization of test devices for laboratory and field tests.

1.4 Novel Concept and Outline

Figure 1.1 depicts the basic block diagram of the proposed system.

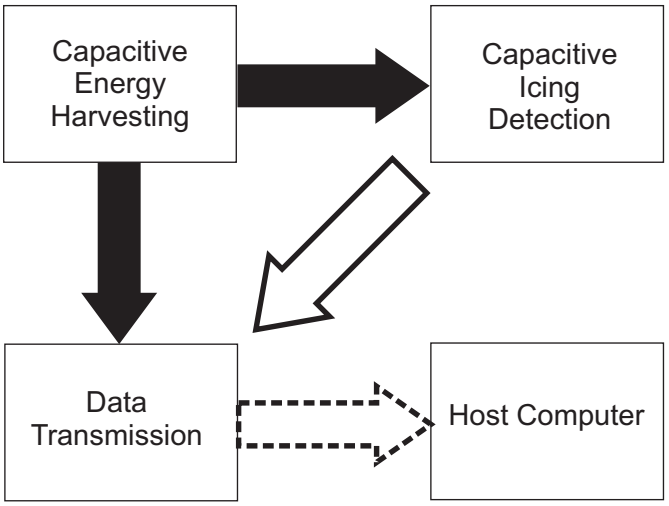

Figure 1.1: Block diagram of the proposed measurement system, comprising capacitive energy harvesting, capacitive icing detection and data transmission circuitry, which transmits the icing data to a base station or remote host computer. Black arrows indicate energy supply paths while white arrows indicate data paths.

The system comprises the following components:

- An energy harvesting system, i.e. the implementation of a suitable energy harvesting technique is required to ensure autonomy from external power supply or batteries, thus providing maintenance intervals in the range of many years. Chapter 4 explains the available technologies which may be useful or are already in use on high-voltage power lines. After a comparison, it turned out that a capacitive energy harvester [19] obtaining the energy from the electrical field would be the optimum solution most of all due to its independence from the current load state and from weather or pollution.

- An icing detection system is required for the detection of ice at small thicknesses at the surface of a power line or as close to the line surface as possible while providing high measurement accuracy and repeatability. The measurement concept thus focuses on a measurement based on an electrode assembly which is in close vicinity (i.e. within few millimeters or less) of the conductor surface. Chapter 3 outlines a survey on icing detection principles and realizations and then compares the available technologies against each other. After carefully examining the available technologies, it turned out that a measurement based on capacitances (which in fact is a subtype of impedance measurement) looks most promising. Model, simulation, architecture, properties, materials and challenges with this type of sensor are explained in Chapter 5.

- Wireless data transmission and practical solutions to ensure electrical robustness against the environment (HV AC field, winter weather conditions) are described in Chapter 6. Moreover, Chapter 6 also describes the test device platforms which were used to obtain and transmit the measurement data from the sensor front-end to a base station for evaluation purposes.

Chapters 7 and 8 cover test procedures and results from single components to the entire field test device, respectively. In Chapter 10, a conclusion and an outlook on future work is given.

Beforehand, Chapter 2 gives a short introduction on the nature of atmospheric icing, its origins and various appearances. Furthermore, it presents strategies to prevent icing and to remove ice which has already accreted.

1.5 Related Research Fields

The aim of this work touches various fields of research:

- **Atmospheric Icing**. Atmospheric icing is a phenomenon that usually occurs when air temperature, precipitation, air humidity and wind speed meet certain levels. Man-made structures on top of mountains are often exposed to rime icing, while in other areas, wet snow or freezing rain likewise endangers infrastructures at lower altitudes [20]. Critical structures, which are subject to atmospheric icing are, for instance, antennas, wind turbines and transmission lines. In the latter case, the transmission towers can collapse due to the additional weight. Several organizations such as the International Electrotechnical Commission (IEC) and the International Council on Large Electrical Systems (CIGRÉ) are taking effort in establishing international standards and methodologies in the environment of the icing of power lines [21], [22].

- **Ice Detection**. The detection of the presence of ice on surfaces and the quantification of its quality and thickness is a sensing task which can be approached by means of various physical principles. These range from the alteration of a resonating mass-spring-damper system to impedance and reflection measurements in the domain of light, microwaves or radio frequencies or even below. The early and precise detection of ice is of importance on aircraft wings, road surfaces and wind turbines as well as on conductor lines. For the latter, special methods such as weight or line sag measurement have been implemented. Ice detection in most cases triggers some kind of measures to remove the ice or at least leads to watchful waiting or modified power line operation modes.

- **Energy Harvesting**. This term generally relates to the generation of electrical energy from sources like a temperature difference (thermoelectric energy harvesting), vibration or alternating pressure (with

a piezoelectric generator), solar energy (solar cells, for example, used for watches) or a electromagnetical field (e.g. used for passive RFID tags, compare with [23]). Typically, energy harvesting is employed with wireless devices (mobile devices, sensor nodes, portable devices) whenever the average power demand is comparatively low and primary batteries or wired power connections have to be avoided. In the environment of power lines, strong magnetic and electrical fields are present, but also solar energy or wind could be useful sources from which energy could be harvested.

- **High-Voltage Engineering**. This field within electrical engineering deals with voltages above 1 kV. Typically, research and testing in this field covers high-voltage energy transmission and the relevant devices and plants such as generators, transformers, cables, overhead power lines and all the necessary components such as insulators and materials. In this work, voltage levels range up to 220 kV system voltage at 50 Hz. In a three-phase system, system voltage equals $\sqrt{3}$ times the phase voltage of approx. 127 kV.

1.6 Publications

[1] presents the system concept for the observation of power lines 24 hours a day, 7 days a week, providing a higher accuracy than remote monitoring: an autonomous condition monitoring device for high-voltage overhead lines which relies on energy harvesting, several sensors (such as line sag, conductor temperature and degree of icing) and a data processing and transmission unit. It is shown that the energy harvested from the electric field which surrounds the conductor is sufficient to power the measurement circuitry. Two ways of data transmission seem feasible: a 433 MHz ISM band RF link or the GSM or UMTS mobile phone grids, the latter demanding far more power but being independent from dedicated relay stations. [1] also contains preliminary investigations on a capacitive icing sensor.

[2] presents a capacitive principle to detect the formation and accumulation of ice at a conductor line surface (connected to an autonomous monitoring system). Both a linear and a circular type electrode geometry are presented.

The inter-electrode capacitances are evaluated by means of a commercially available capacitance-to-digital converter and laboratory measurement results show good agreement with finite element simulations. The degree of icing is estimated by measuring multiple capacitances formed by electrode pairs at different distances with respect to each other. The variation in time of the measurement capacitances is exploited to estimate the ice origin.

[3] publishes first field-test results on a high-voltage overhead line. At this stage, the autonomous sensor system is powered by a capacitive energy harvester (i.e. energy harvesting from the electric field) and mounted on a 220 kV transmission line in the Austrian alps in winter 2009-10. Reference data collection was performed by means of a weather camera system. Several icing and snow deposition events could be successfully detected.

[4] focuses on the problems which arise due to the implementation of both a power harvesting system based on a capacitive principle and a capacitive measurement device in one electronic system for icing detection on high-voltage overhead lines. The overall capacitance of the measurement circuitry between the conductor and the energy harvester shell must remain within a well-defined range to keep the energy harvesting circuitry operational and to operate the capacitance-to-digital converter within its specifications. A decoupling solution for both the data path and the power supply unit has been implemented and verified experimentally.

Furthermore, parts of this PhD work were presented at the ARGE Sensorik PhD Summits in Vienna and Linz, in 2009 and 2011, respectively [5]. The approach of capacitive icing detection was also demonstrated for a planar setup for the usage on wind turbines at the scientific conference Winterwind 2011, Umea, Sweden [6] as well as a sensor-fusion approach at scientific conference Winterwind 2012, Skelleftea, Sweden [7].

1.7 Own Contributions

The major contributions of the author also within the mentioned publications are listed below:

- Investigations on suitable data paths including GSM data transmission

- Design and implementation of laboratory icing setups
- Design and implementation of a temperature measurement system
- Review and choice of components for test device implementation
- Design and implementation of the sensor front-end including the electrode assembly
- Design and manufacturing of measurement electrode setups for lab and field tests
- Design and implementation of the data path decoupling concept
- Design, supervision and evaluation of laboratory and field tests of the prototype
- Investigations on materials and technologies for industrialization
- Test device implementations and tests with various material systems for industrialization

Chapter 2

Atmospheric Icing, Anti-Icing and De-Icing

This chapter explains the phenomenon of atmospheric icing and describes the methods to avoid icing or to cope with ice once accreted. A profound survey on atmospheric icing is required as different forms of atmospheric icing have variable physical properties (for example, a density between 0.05 and 0.9 kg/dm^3). Other variable physical properties comprise the adhesive power, the refractive index and the dielectric permittivity. This wide range is highly relevant for both the choice of the measurement principle and the effects on the power line. Section 2.1 gives an overview of these effects. Section 2.2 provides a closer view on the parameters that characterize the forms of icing and on the different modes of icing such as freezing rain or rime ice. Section 2.3.1 lists the various methods to avoid icing ("anti-icing") such as hydrophobic coatings or heat-dissipating layers. Section 2.3.2 describes the approaches to ice shedding once it accreted to the overhead power line. In combination with a measurement system capable of detecting thin layers, anti-icing and de-icing can be employed to keep lines ice-free and thus fully operational.

2.1 Icing Effects on Power Transmission Lines

Power transmission lines are most often composed of two layers, characterized by the cross-section surface of aluminium and steel (e.g. Al/St 340/110), where

aluminium carries the electric current while the steel core bears the mechanical load. In between there is a special grease with a drop point above 80°C which should prevent the steel core from corrosion.

Power lines seem to have a comparatively small surface. However, even neglecting the surface structure consisting of multiple strands, the surface of a standard 220 kV conductor with a diameter of 28 mm results in approx. 0.1 square meters per meter conductor length. Assuming 250 meters between two transmission towers and 6 conductors (two three-phase systems), the conductor surface subject to icing exceeds 150 square meters (!).

In this configuration, a 10 mm layer of clear ice accumulates to an additional weight load of approx. 1800 kg per transmission tower. At that point, the surface exposed to icing conditions has already nearly doubled. This simple calculation shows how atmospheric icing can heavily endanger transmission line systems. Furthermore, wind becomes a greater issue due to the increased working surface.

In order to stay within safe operation conditions, new power transmission lines need to be dimensioned appropriately according to historic icing events at the desired location. In the simplest method, a Gaussian distribution is assumed where 45 % of the maximum ice load known so far is considered to be the mean value and the standard deviation is 50 % of this value.

Numbers of standard and elevated ice load are calculated differently in nearly every country or national standard specification. Most often they are defined in Newton per meter of conductor line, for example, by a constant plus a value depending on the conductor line diameter (e.g. in Austria: $4 + 0.2\ d$ where d is the conductor line diameter) [24].

2.2 Atmospheric Icing

This section gives an introduction to atmospheric icing and describes the conditions which can lead to atmospheric icing. Atmospheric icing is a phenomenon which usually occurs when the relevant weather parameters combine to defined constellations [21], [25]:

- Wind Speed

- Wind Direction
- Air Temperature
- Relative Air Humidity
- Water Droplets in Air (Liquid water content of air, LWC)

In meteorology, atmospheric icing events are divided into two classes of events: precipitation icing and in-cloud icing. In case of precipitation icing, additional parameters are the precipitation rate, the surface temperature and the liquid water content of snow flakes, for example. For in-cloud icing, the liquid water content (LWC) in the cloud and the droplet size distribution are of interest. This happens, for instance, in Japan, Canada, UK, Iceland, Finland, Hungary, Norway, Russia, China and several more countries all over the world. Man-made structures on top of mountains are often exposed to rime icing, while in other areas, wet snow or freezing rain likewise affect infrastructures at lower altitudes [20]. Critical structures which are subject to atmospheric icing are, for example, antennas, wind turbines (compare [26]) and power transmission lines. In the latter case, atmospheric icing can lead to accretions of more than 300 kg per meter wire length (as occurred in Norway in April 1961). Several organizations such as the International Electrotechnical Commission (IEC) and the International Council on Large Electrical Systems (CIGRÉ) are making an effort to establish international standards and methodologies in the environment of the icing of power lines.

Besides precipitation icing and in-cloud icing, also hoarfrost icing can occur on conductor lines. Hoarfrost forms when vapor directly changes into solid ice, especially at low temperatures and also at relatively low air humidity levels. Typically, its density is low and hoarfrost alone does not cause relevant ice loads. However, it has a significant impact on corona discharges due to both the enhanced surface and its needle shape [27].

2.2.1 Precipitation Icing

Any form of water, snow or ice which can be described as liquid or frozen particles falling from the sky and adhering to a surface on ground can be regarded as precipitation icing. Various types of precipitation can lead to

ice accretion in different shapes. What determines the icing scenario is the vertical temperature distribution in the air, the air temperature at ground level and the temperature of the ground surface or the geometry of the structure. Depending on the temperature, water crystallizes in shapes ranging from thin plates (between 0 and 4°C) over needles, columns, dendrites (typically referred to as snow) and thicker plates to hollow columns at temperatures below -22°C. These crystals may stick together and form snow flakes [28]. At the same time, the amount of water vapor which can be dissolved in air is increasing with temperature. Given the fact that water freezes at 0°C, it can be estimated that icing can be most intense just a few degrees below zero. Depending on the vertical temperature profile in the atmosphere, snow forming in higher altitudes may arrive at the ground level in the form of snow, snow that melts and freezes again (sleet), snow that melts and arrives as a liquid, supercooled drop freezing at the surface (freezing rain) or just rain at temperatures above 0°C. In a convective cloud, freezing and melting processes may work at a single snow flake for a prolonged time, leading to precipitation forms like rimed snowflakes or graupel (snow pellets) [28].

Precipitation icing events can be roughly categorized as follows:

- **Freezing rain.** Glaze ice forms on the substrate, the density of the accreted ice lies between 0.7 and 0.9 kg/dm^3. The air temperature typically ranges between -10 and 0°C. This type of precipitation icing results in transparent ice layers and may include icicles [22]. Due to the compact material, removal of this type of ice is difficult. In January 1998, an event of that type hit Eastern Canada and North-Eastern USA (compare Section 1.2).

- **Dry snow.** Thin, light, fragile layers of dry snow are formed in the clouds due to the nucleation of so-called "freezing nuclei" at temperatures below -12°C or by the freezing of droplets at temperatures between -3 and -35°C. The single crystals are bound together by mechanical forces [29]. Typically, wind speed during formation is low, i.e. below 2 m/s [22]. Layer densities range between 0.05 and 0.1 kg/dm^3.

- **Wet snow.** Thick and heavy layers of snow usually can build up at temperatures around the freezing point of water [30]. This situation is

often observed in countries such as Japan, Iceland, Norway and many other European countries [20]. The density of the accreted ice ranges between 0.1 and 0.85 kg/dm^3, the air temperature during formation lies between 0 and 3°C [31]. During the formation, the crystals lose sharpness and agglomerate to sub-millimetric ice granules. This material can have a liquid water content of up to 40 % and more and thus has a comparatively high density. Snow accretion on a small conductor grows towards the windward side first, may then rotate around the conductor and develop into a cylindrical sleeve [32].

- **Icicles.** Water melting and freezing (also due to de-icing measures) can lead to the formation of icicles, which are often a big part of the ice load in freezing precipitation [33].

2.2.2 In-Cloud Icing

In-cloud icing usually occurs within clouds which contain different amounts (Liquid Water Content, LWC) of supercooled water droplets of different sizes (Median Volume Diameter, MVD). Typically, **soft rime** (density 0.1-0.3 kg/dm^3) occurs at low MVD and LWC values, while **hard rime** (0.3-0.7 kg/dm^3) is accreted to the surface when exposed to a cloud with higher MVD and LWC. Both intensity and duration of an in-cloud icing event depend on the flux of liquid water in the cloud [20]. Usually, air temperatures are well below 0°C; this icing process can occur down to -20°C and the resulting layer is an opaque, porous ice deposit [22].

2.3 Anti-Icing and De-Icing

According to the CIGRÉ Technical Report 438 [22], Anti-Icing for overhead power lines techniques are defined as measures which prevent or reduce accumulation of ice or snow on conductors. This is achieved by weakening ice adhesion strength on one side or by preventing freezing of supercooled droplets on the other side. In particular, this goal is achieved by the use of icephobic coatings. According to [22], the main influences on ice adhesion are the electrostatic forces present at the ice-solid interface and the surface roughness of

the substrate. Section 2.3.1 briefly summarizes state-of-the-art approaches.

On the other hand, de-icing techniques cover all methods which remove or reduce ice accretion, thus being activated during or after ice accretion processes. An overview is given in Section 2.3.2.

2.3.1 Anti-Icing

Passive anti-icing makes use of natural forces such as wind, gravity or solar radiation in order to limit the effects of ice loads on overhead lines [22]. Another possibility is the application of de-icing methods (see Section 2.3.2) in early stages of an approaching icing event.

It is hoped that **hydrophobic coatings** (i.e. an adaptation of the physical-chemical properties of the conductor surface) can reduce ice loads. No material has been found so far to be perfectly icephobic [34]. Materials in use for that purpose are, for instance, Polytetrafluoroethylene (PTFE) [35] or (modified) silicones which both have demonstrated sufficient wet snow accretion reduction effect [36], [37]. Surface roughness plays an important role as ice de-bonding can be observed due to the fact that air can be trapped in closed pores in the ice layer and pressure builds up. Consequently, by choosing an optimum surface roughness, a super-hydrophobic surface can be obtained. On the other hand, porosity can have negative effects during in-cloud icing, when droplets are small enough to penetrate and freeze in the pores. Further parameters that influence ice adhesion include the precipitation type and impact speed and the ice crystal grain size and shape [38]. Also, the density and the liquid water content (LWC) of wet snow influence the adhesion to a conductor surface [39].

Moreover, **chemical substances** such as freezing point depressant liquids may be used to prevent icing. However, the necessity of frequent applications fails to make this approach feasible for a large scale application.

2.3.2 De-Icing

De-icing or ice shedding will rely on one of the following physical principles, independently from the actual triggering mechanism:

- **Ice mechanical breaking and snow shedding** - adhesive/cohesive failure of accretion as ice is brittle at high strain rates [40].

- **Ice melting** - due to temperatures of the outer ice surface above 0°C. Parameters are air temperature, wind speed and solar radiation.

- **Ice sublimation** - water vapor released to the air from the ice layer, a slow, usually natural process.

Thereof, mechanical breaking and melting are technically used for ice shedding. The following **mechanical** methods are in use:

- Ice Scraping: this can be achieved by manual scrapers, rollers or cutters or robots on the line (e.g. LineROVer, [41]).

- Shock Waves: mechanical application either manually or by knotted ropes or weights on a rope bound to a helicopter, with insulated poles or cylinder pistons [42].

- Electromagnetic Impact Shock Waves (EIDI): on pairs of strands [43], on bundle conductors [44] or on insulated strips.

- Induced vibrations by means of devices mounted on the conductor (compare e.g. [45]).

- Twisting of Conductors

Methods which **melt** ice in order to force its shedding can again be separated by their general approach to heat generation [29].

The first group uses active coatings which generate heat in a layer which is permanently attached to the conductor surface, thus preventing ice or snow accretion:

- Dielectric coatings made from ferroelectric materials allow to maintain the conductor surface temperature above the freezing point by taking energy from the alternating electric field. Usually, this requires a higher frequency than the standard grid frequency which needs to be injected separately. Hence, this system is not yet available commercially but only in test setups.

- LC-Spiral Rods generate heat from the alternating magnetic field generated by the conductor current, preventing snow and ice from accumulating on the conductor. This method has been applied in Japan for more than 20 years in a large scale [46].

The second group covers all types of de-icing methods which rely on the joule effect:

- Load Shifting Method: A power line which is subject to critical weather conditions can be posed with additional load due to interventions in the power grid such as shutting down other transmission lines, activation or shutdown of power plants. Typically, this method is only suitable for single-conductor lines as too high currents would be necessary for bundled conductor lines. As an advantage of this method, the line can still be used for power transmission and no dedicated equipment is required [12].

- On-load Network De-icer (ONDI): This method also works while keeping the iced power transmission line on the grid and even pre-heating of a power line prior to icing is feasible. A phase-shifting transformer allows for the de-icing of lines of a length of up to 900 km [47], [48].

- Reduced-Voltage, Short-Circuit Method: A line is three-phase short-circuited at one line end while being fed from the other. Thus, the line heats up but is not available in the grid while de-icing.

- DC Current: After disconnecting the line from the grid, a closed DC current loop must be established for de-icing and additional equipment is necessary [16]. The speed of DC de-icing depends on the ice layer density and thickness, current density, environmental air temperature and wind speed. The melting process includes the formation of an air gap between ice and conductor due to the weight of the remaining ice. [16]

- Contactor Load Transfer: conductors within conductor bundles can be switched in a way so that the current through the single conductors is drastically increased during de-icing [49], [50].

Besides these approaches, various other heat sources may be used:

- Transportable Radio Wave Sources
- Transportable Steam Sources
- High Frequency (HF) De-Icing: dielectric Losses in the ice layer cause the thermal effect [51].
- Pulse Electrothermal De-icer: the conductor is covered with a dielectric layer and an additional conductive layer [52], [53].

Summarizing the above, various methods for de-icing of high-voltage overhead lines have been available for decades and are successfully tested in the field. The deployment of a sensor capable of detecting thin layers of ice (e.g. early stages of icing) at the conductor surface represents an optimal trigger mechanism for early and easy counter measures.

Chapter 3

Survey on Ice Detection

In this chapter, a survey and a comparison of available methods and devices for icing detection and/or ice layer thickness estimation are presented. The approaches for detecting atmospheric icing conditions can be divided into three groups: prediction from meteorological data (Section 3.1), indirect measurement (Section 3.2) and direct measurement principles (Section 3.3). Icing detection is necessary for an early-stage triggering of counter measures such as de-icing.

3.1 Meteorological Prediction and Icing Condition Measurement

Modern meteorological forecasting models of the atmosphere allow for the estimation of the amount of ice which has already accreted to a conductor and for a forecast of ice build-up. These methods have been evaluated in large-scale research projects [54] and also for exposed mountain terrains [55]. Systems collecting weather data are widely used. Approaches for conductor icing prediction relying on weather data typically use measurement systems mounted on transmission towers and collect weather data such as air temperature, air humidity, precipitation and wind speed. In meteorology, various devices for ice measurement are in use - usually, passive devices are designed which resemble the structure exposed to by icing. These passive devices can, for instance, be tubular steel-rod racks representing geometries similar to a power transmission tower and then they are observed by personnel or by a camera. Icing events

are recorded and collected in databases and models can be developed for the forecast of icing [56].

Furthermore, the term "meteorological icing" is defined as the duration of a meteorological event or perturbation which causes icing (unit: time). It can be characterized by the duration of the icing event, and/or the meteorological conditions, and possibly with additional information such as the total amount of ice accreted on a standard (reference) object during the icing event as well as with the average and maximum accretion rate [57].

[11], [58], [59], [60] and [61] describe weather data based systems for icing condition detection and forecasting on transmission towers. In some applications, weather data methods are combined to a sensor network and extended by surface moisture detectors or other icing detectors [17]. For the detection of in-cloud icing, another approach is the combination of a temperature measurement and a humidity sensor designed for operation below zero [62].

3.2 Indirect Measurement Methods

Indirect measurement methods are considered to not directly detect ice on a sensitive area of a sensor but to measure other quantities which change most likely but not only due to an ice load. These methods comprise conductor weight measurement and line sag measurement. Typically, small changes due to thin ice layers are hard to detect using indirect methods.

3.2.1 Weight Measurement

One method of indirect icing detection is weight measurement. The weight of a conductor line between two transmission towers is measured in regular intervals by means of special electrically insulated load cells. The method is comparatively old and widely used in high voltage applications [63].

In [64], a standard ice-measurement device is recommended for all structures except overhead lines. A smooth cylinder with a diameter of 30 mm placed with the axis vertical and slowly rotating around the axis. The cylinder length should be a minimum length of 0.5 m, but, if heavy ice accretion is expected, the length should be 1 m. The cylinder is placed 10 m above terrain and recordings of ice weight may be performed automatically [57].

A commercially available device based on weight measurement is the Combitech IceMonitor [65]. Another realization is the ICEmeter manufactured by the Institute of Atmospheric Physics, Prague, CZ [66].

3.2.2 Sag Measurement

The line sag can be measured, for instance, by means of ultrasound distance measurement between conductor and ground. However, the angular position of the sensor aperture can not be determined exactly because of the conductor rope's rotation over its length axis, which is mainly due to temperature variations. Furthermore, the line sag also depends on the conductor temperature and solar radiation. By absorption of solar radiation only, the conductor temperature can be up to 10°C over air temperature, without any current load [67].

3.3 Direct Measurement Methods

Direct measurement methods are considered to detect ice on a sensitive area of the sensor. This is achieved by exploiting the differences in the physical properties of air, water and ice and most often rely on wave propagation (light, microwaves, ultrasound, low frequency (LF) electric fields) or changes in mass-spring-damper dynamic systems (resonant sensors). Besides, also gamma rays and thermal material properties can be exploited.

3.3.1 Optical Ice Detectors

Optical ice detection relies on diffraction, reflection or absorption of light. Systems for aircrafts detect the presence of rime ice and clear ice in air using a collecting surface facing an upcoming air stream. Light is crossing a prismatic window being thus refracted in different angles depending on the presence of ice [68]. Special icing condition detectors similar to dew point detectors have been developed; the latter use a thermoelectric element which keeps a polished surface at a desired adjustable temperature. The presence of water or ice is then detected by measuring the intensity of light reflected by that surface [69]. Ice detectors based on fiber optic sensors are described in [70]

(based on the determination of the sensor's incident angle of reflected light) and [71], where thickness and type of ice accreted to an aircraft wing are determined by measuring scattered and reflected light as a function of the ice growth, obtaining characteristic light intensity growth curves. Related approaches are described in [72] and [73]. Optical measurement methods may suffer from pollution which might be difficult to handle, as in the environment of power grids the maintenance intervals can be years or more.

A commercial example of an optical ice detector is the T series from HoloOptics, which relies on reflection characteristics changes when a mirror in an infrared beam path is covered with ice [57].

3.3.2 Microwave Ice Detectors

Microwave ice detection can be carried out by using different principles. It can be realized using a radiometer system detecting naturally occurring atmospheric microwave radiation in multiple bands (e.g. at approximately 20, 30, and 90 GHz [74]). From the measurement data, the total ice column in the atmosphere, the liquid water and water vapor content in the atmosphere are calculated. Other systems detect ice at exterior surfaces by transmitting a relatively low power microwave electromagnetic signal into a dielectric layer which operates as a surface waveguide. By monitoring the signals transmitted into and reflected from the waveguide while an ice layer builds up, the impedance or reflection characteristics of the composite waveguide comprising the ice layer and the permanent surface waveguide change and characterize the presence and location of the ice [75]. In [76], a principle of ice accretion detection is described on the wings of an aircraft. Coplanar transmission lines are used as a sensor for time domain reflectometry (TDR) at low microwave frequencies. As travel time, phase velocity, effective dielectric constant and further parameters are evaluated, presence and thickness of known dielectric materials can be detected.

3.3.3 Ultrasonic Ice Detectors

Ultrasonic ice detection relies on measurement of the signal level (attenuation) or the time-of-flight of ultrasonic pulses.

As described in [77], the attenuation of ultrasound transmitted through a thread-like or tape-like transducer mounted at a planar surface is measured and then compared with a signal of the same setup after heating up the sensor area. [78] describes a principle of detecting ice using ultrasonic guided shear waves, while in [79], a method based on the monitoring of variations on the transmission of flexural waves is presented. Furthermore, [80] proposes an ultrasound ice detection principle by means of attenuation measurement in a frequency range between 20 and 300 kHz. The sensor can identify various aggregate states of water at the surface of a structure. A similar concept is described in [81]. The ice detector proposed for the use in refrigeration machines in [82] derives the icing status from the degree of attenuation in a system of two electroacoustic transducers connected to membranes.

[83] describes a miniaturized icing sensor based on the propagation of surface acoustic waves. The propagation of Love waves is greatly dependent on the physical properties of the substance present at the surface of the thin-film (few microns) wave-guide through which the waves propagate. Both, wave velocity and damping are affected by substances present on the wave-guide.

[84] describes an apparatus for the measurement of ice thickness by ultrasound time-of-flight. Ultrasonic pulses are emitted from a transducer at the surface of a structure, the pulse is reflected at the periphery of the accreted ice and the reflection is detected. The time delay is related to ice thickness and accretion rate. In [85], a sensor for detecting the presence of frost uses two coils and an acoustic transmitting medium made of a magnetostrictive material of a ribbon shape.

A commercial product is the Labkotec LID series, which detects the attenuation of an ultrasonic signal on the ice detector structure due to the presence of ice.

3.3.4 Resonant Ice Detectors

Resonant detectors usually make use of a vibrating surface area (e.g. one or more vibrating fingers [86], [87], [88]). The vibrating surface area is subject to ice deposition, thus its resonant frequency is altered which is then detected and indicated as ice deposition. Alternatively, the deposition of an ice layer can prevent an oscillator from oscillation [89] or the alteration of the stiffness-

to-mass ratio itself is the measurand [90]. The sensor can also be realized by means of a vibrating tube excited by a coil which is sealed by a diaphragm that is exposed to the air under icing conditions [91]. Instead of the coil, a piezoelectric element can be used [92]. There are also realizations for aircrafts which by means of geometry and aerodynamics change the pressure field around the ice detector to cause a lower temperature region on the probe assembly compared to the aircraft. As a consequence, the probe is supposed to be the first point of the surface where ice deposits and the information from the system can be used as an early warning [93]. The vibrating diaphragm excited by a piezoelectric element can also be thermally connected to a Peltier element for heating and/or cooling above and below ambient temperature. The excessive change of the resonance frequency thus indicates the presence of icing conditions [94]. The micro-electro-mechanical (MEMS) ice detector described in [95] operates at a principle that the presence of ice alters the mechanical properties of a diaphragm which represents the interface of the MEMS to the environment. A further realization of this principle is described in [96], where a lead zirconate titanate (PZT) disk transducer allows for detection of the freezing transition of a water layer by detection of an abrupt resonance frequency change at the freezing temperature. Rosemount Inc. produces a series of vibrating ice probes based on magnetostriction which are widely used in meteorology. Ice accretion on the probe decreases the vibration frequency [97]. After an accretion of a few hundred micrometers of ice, the device de-ices itself and accretion can re-start [98]. Another commercially available instrument based on a resonant transducer is the ice rate meter (IRM) as used for icing investigations in Canada [99].

3.3.5 Capacitive Ice Detectors

Capacitive sensing usually relies on the change in amount, geometry, material or material properties of the dielectric component of a capacitor. The measurement technology is frequently used for humidity measurement [100] as the high relative permittivity of water leads to a good signal-to-noise ratio. A capacitive sensor is easily scalable and due to its measurement principle it is most sensitive for thinnest ice layers, i.e. it allows for a detection of an icing process at early stages, which is desired in most application cases. An

early design of an icing detector based on a capacitive principle is given in [101]. Impedance type ice detectors for the detection of the presence of ice on aircrafts is described in [102] and [103].

A more advanced approach is described in [104] and [105]: The detector is designed for characterization of heterogenous ice on aircrafts. It comprises a multi-electrode setup with different inter-electrode distances and detects both ice presence and ice thickness and suggests the usage of different excitation frequencies. Temperature information is also an input to the measurement signal processing.

In [106], an ice and water detector for roads and runways is presented. Two measurement frequencies are used to be able to distinguish between air, water and ice. Based on experimental results, an algorithm for the state estimation (dry versus wet versus icy) was developed that uses the derivatives of the capacitance signals. In [107], an impedance-type discriminator between air water and ice based on a fingerprint sensor is described.

[108] presents a proof of concept for a capacitance and resistance based ice meter which consists of two conductive cylindrical probes. An LCR bridge is used to evaluate the capacitance between the two cylinders which are subject to ice accretion. Feasibility could be shown both in laboratory and in icing laboratory tests, also showing that wind direction has a big impact on the measurement results.

The Instrumar IM101 measures the surface electrical impedance and the temperature of a ceramic probe [109].

As not only the presence but also the layer thickness is of interest, multiple measurement capacitors can be evaluated in order to eliminate ambiguities in the measurement result given knowledge from the measurement model. Section 5 presents details on the design of a multi-electrode icing detector purpose-made for the use on high-voltage overhead lines.

3.3.6 Other Principles

Especially for aircrafts, systems that generate mechanical pulses at different (typically including high) levels have been invented, whereof the high-level pulses should be sufficiently strong to remove ice. An accelerometer records the pulse response of the metal-ice system and ice presence is calculated by

means of a threshold level [110].

Also, the difference in heat flow within materials can be exploited to detect presence and/or formation of ice [111]. The measurement is carried out by means of a Peltier element and a temperature sensor. As long as ice is present, the temperature level will not change although heat is transferred into the probe. Similar principles are used in [112].

A related icing sensor based on heat capacity is described in [113]. The latency in temperature change due to a cold conductor covered with ice or snow is detected, for example, by a current measurement. A variation of the same principle is used in an early icing rate detector for aircrafts [114]. A thermoelectric switch is sensitive to the deposition of ice. Closing of the switch activates a heater which melts the ice and causes the switch to open again. Thus, the rate of power consumption is proportional to the icing rate.

Gamma rays can be employed for ice detection on aircraft wings [115]. A high energy radioactive gamma ray source (^{241}Am) penetrating the airfoil substrate generates secondary photons, which are backscattered to a photodetector. By choosing a proper sensor geometry, the photodetector is most sensitive to photons which are generated within the ice layer.

[116] presents an icing detection method operating in the Very High Frequency (VHF) range. Here, state and thickness of water accumulation at a surface are evaluated by means of multiple electrically resonant circuits and a radio frequency transmitter for exciting the circuits. The excitation frequency is variable and a receiver detects the resonant signal from each circuit. At a resonance frequency of 75 MHz, for example, no water or ice is present while a significantly lower resonant frequency corresponds to a layer building up. [117] describes a detection principle based on the phase delay of a radio frequency in the gap between line electrodes. In [118], an inductive measurement system for aircraft wings based on multiple sensor electrodes and a thermocouple is described. [119] presents a combined monitoring system mounted on transmission towers. The icing status is derived from a combination of weather parameters, insulator deflection angle, line weight, vision-based measurement data and the conductor gallop frequency. Conductor gallop is the low-frequency (typically around 1 Hz) wave motion of the overhead power line due to wind. The oscillation frequency is altered by the additional mass originating from ice

layers.

Furthermore, a video camera or stereo imaging could be a method to detect ice accretion. However, it is complicated to get a clear view over the typically large distance between camera and conductor rope and also to keep the camera ice-free [26].

3.4 Comparison

Table 3.1 compares the relevant measurement parameters of the measurement methods mentioned above. The selectivity regards the potential of a measurement system to distinguish between impacts from the desired measurand and other measurands. Except for pollution impacts, which are addressed separately, most methods will not respond to other impacts than snow, ice or water. One exception is the line sag, as this can also be caused by thermal expansion of the conductor.

Pollution impairs weather-data based methods (e.g., a dirty anemometer will change its characteristics). Optical methods suffer from dust or dirt on optical transducers or fiber outlets. Moreover, ultrasound or resonant detectors can be significantly disturbed by offsets due to dust or dirt.

Concerning the power demand, it can be noted that most methods are miniaturized enough so that the energy consumption is low. Methods which employ the emission of a reasonable amount of energy such as ultrasound, microwaves or heat have a disadvantage. Power for operation has to be harvested from the environment or taken from the power line. For this reason, less power consumption has its advantages for the system.

Complexity needs to be interpreted with respect to the constructional effort and the costs per unit. The systems are comparable except for methods based on ionizing radiation.

The ability to measure thickness is a critical requirement for a measurement system in the given application. This is not feasible with weather data estimation, conductor weight or line sag measurement nor with heat flow based measurements due to the averaging character of this measurement methods.

At last, measurement accuracy is critical especially at small ice thicknesses. Weather data estimation lacks measurement accuracy due to its predictive

	Measurement Parameters					
	selectivity	pollution	power	complexity	thickness	accuracy
Weather Data	+	o	o	+	-	-
Cond. Weight	+	+	o	o	-	o
Line Sag	-	+	+	+	-	+
Optics	+	-	o	+	+	+
Microwaves	+	+	-	o	+	+
Ultrasound	+	o	-	+	o	+
Capacitance	+	+	+	+	+	+
Resonant	+	o	+	+	+	+
Heat Flow	+	+	-	o	-	o
Gamma Rays	+	+	o	-	+	+

Table 3.1: Comparison of icing detection techniques for operation at high-voltage power lines. "+" denotes high selectivity, minor effects of pollution, low power demand, low complexity, good suitability for thickness measurement and high accuracy. "−" denotes the opposite, "*o*" denotes properties in-between.

character.

As it is required to detect thin layers (early accumulation of ice) while operating at a restricted power budget, impedance/capacitance type measurements, optical methods and resonant probes remain promising. The capacitance/impedance measurement approach seems most promising as resonant probes contain moving parts and optical methods may heavily suffer from pollution (e.g. bird droppings) without the possibility to calibrate for the offsets caused thereby.

Chapter 4

Survey on Energy Harvesting

As the typical operation time of a high-voltage overhead line amounts to several decades, also the monitoring systems should in principle be suitable to remain operational for a similar order of magnitude in time. For this reason, battery powered systems are - as of 2012 - not the preferred choice; and an energy harvesting principle should be implemented instead. Energy harvesting covers exploiting any form of energy provided by the immediate environment of the device. Usually, the energy source is more or less continuously available.

A survey on the available methods and devices for energy harvesting on a high-voltage overhead line is presented in this chapter. Energy harvesting techniques exploit a power source generally available (but subject to variability) in the environment of application. Transducers (solar cells, wind turbines, piezoelectric generators) are used to transform the energy into electrical energy (usually at a low efficiency and with low total output power in the range of mW to μW). The harvested energy is converted to a suitable voltage level and stored in a rechargeable battery or a capacitor. The following energy harvesting techniques have been investigated in the following sections:

- Solar radiation (Section 4.1)
- Wind (Section 4.2)
- Heat Flow (Section 4.3)
- Magnetic field (Section 4.4)
- Electrical field (Section 4.5)

4.1 Solar Energy

The photoelectric effect, discovered by Alexandre Becquerel in the 1830s, is the principle of operation of solar cells. Since the 1950s, solar cells have been produced for satellites, starting with an overall efficiency below 5 %. Nowadays, efficiency for silicon-based cells reach up to as much as 22 % for large-scale commercially available modules for on-grid application. The surface area required to supply measurement equipment on high voltage power lines is defined by the power demand of the measurement circuitry and the orientation of the equipment's surface and the variability of the mentioned orientation. For a standard poly-crystalline solar cell with an efficiency of 15 %, 1 cm^2 of cell area yields as much as 15 mW in full sunlight. Besides mono- and polycrystalline silicon solar cells, various other technologies such as amorphous silicon, gallium arsenide or other thin-film technologies are available; however, efficiency is remarkably lower.

Crystalline cells are brittle and typically have a thickness below 0.2 mm. For use on high-voltage power lines, the cells need to be protected from water and mechanical damages such as hail impacts by a robust yet transparent housing. This is achieved by encapsulation between glass layers or polymers. In order to optimize efficiency, a maximum power point tracker (MPPT) circuit is employed, which is a power converter with an auto-adjusted input impedance. The harvested energy can be stored in a capacitor or a rechargeable battery.

The energy source - the sun - is available independently from the state of the power line. Solar radiation is available daily and the available amount of energy can be calculated in advance for a given location. However, nights and phases of cloudy weather (the latter reducing the harvested power down to as little as 1 % of the nominal power) have to be bridged. As it is desired that the cells are mounted on an object that is itself mounted onto the conductor, one has to take care that the cells are aligned on an equipotential surface around the conductor, as they are conductive surfaces themselves. As the conductor may twist, it may be necessary to align the cells all around the conductor and employ a switching circuitry.

Once a relevant snow or ice layer accumulates on top of the cells, the amount of harvested energy reaches zero. Furthermore, pollution such as dust, pollen

and bird droppings may lower the performance of the solar harvesting system.

As the system does not contain any moving parts, aging is not a problem: typical commercial modules currently come with a guaranteed 80 % nominal output power after 25 years. In space, systems have shown to remain operational for 40 years and more, despite the harsh environment of cosmic gamma radiation and extremely low temperatures.

Solar cells are widely in use for wireless sensor networks also in the environment of high voltage transmission lines [120], [121].

4.2 Wind

Wind is available independently from the status of a power line as it is a regenerative source of energy originating from solar radiation. Similar to solar energy, a comparatively large temporary energy storage system is necessary for continuous operation as wind speed is heavily fluctuating.

As the distance between a HV power transmission line and ground level typically exceeds 10 m, sufficient average wind speeds can be expected. However, wind conditions are hard to predict on a very local and small-scale level [122]. Wind turbines may be down-scaled successfully for energy harvesting purposes; a wind flow harvester with an overall volume below 300 cm^3 and a turbine diameter of 6.3 cm has been described in literature to generate up to 10 mW at a wind speed of 16 km/h [123]. Several generators could be implemented in a device on a HV line in order to meet the power demand of a sensor node. However, maintenance costs are comparatively high due to the presence of moving mechanical parts.

Power generation strongly depends on weather conditions and icing might heavily decrease the output power as the moving parts (i.e. the rotor blades) may suffer from icing. During longer periods of cold weather, these generators might remain out of service for days or weeks. Additionally, attention needs to be paid to the design of bearings and their encapsulation.

4.3 Heat Flow

A heat flow can be exploited to harvest energy by forcing it through a Peltier element, which generates electricity by means of the thermoelectric or the so-called inverse Seebeck effect, discovered by Thomas Seebeck in 1821. Relevant heat sources are solar radiation or heat generated by the conductor itself (due to ohmic losses or by means of ferromagnetic or ferroelectric coatings (compare Section 2.3.2).

[124] presents a thermoelectric energy harvesting system to power wireless sensor nodes (WSNs). Up to 150 mW at a voltage level of 0.45 V can be harvested in an application on a domestic radiator heater at a temperature difference of 33°C. Compared to other energy harvesting sources, the power density is comparatively high (up to 130 W/kg at $\Delta T = 40C$). This is a property which qualifies this technique also for use in aviation [125].

On high-voltage transmission lines, three available temperature levels could be exploited: the (heated or unheated) conductor, the environmental air and a third temperature level generated as described in [126], for example: a miniature greenhouse is used to heat up a thermal mass from sunlight. Both hot and cold side of the thermoelectric modules have to be insulated properly in order to create and maintain the temperature gradient. An average collected energy of 8.2 mWh within an 8 hours period was feasible in an experiment even with rainy and cloudy weather.

4.4 Magnetic Field

Energy harvesting from the alternating magnetic field that surrounds a conductor is a comparatively old approach. As in transmission lines currents are at a high level (typically several hundred Ampere), few windings can extract an amount of power from the magnetic field that is sufficient to operate a measurement circuitry. By its construction, an energy harvesting system exploiting the magnetic field around a conductor can be compared to a transformer. In the environment of a high-voltage overhead line, a small transformer seems to be the easiest way to obtain power for the operation of a measurement device. In fact, a magnetic core is closed around the conductor and a secondary coil

is used to draw power. This approach is comparatively easy to implement. However, as the current in the conductor is hard to predict and heavily fluctuating, a certain minimum current is needed for operation, which can not be guaranteed. Therefore, an energy storage system is necessary here as well. Snow and ice neither interfere with the operation of the current transformer, nor are problems expected with respect to pollution or aging. A commercial magnetic harvester for a temperature monitoring device was developed in the early 1980s and proven to be operational in the laboratory [127] and in the field [128]. [129] describes a Rogowski coil around the conductor for magnetic harvesting.

4.5 Electrical Field

It could be shown that energy can be harvested from the alternating electric field between conductor line and earth by inserting a conductive shell between conductor and earth, thus forming a capacitive voltage divider [19]. Compared to energy harvesting from the magnetic field, its main advantage is the independence from the current load status, so this method will work at any time the power line is turned on. The displacement current to the environment through a conductive shell with a length of 40 cm and a diameter of 60 cm amounts to several hundred microamperes [19], [130]. The field strength far from the conductor is low and most of the potential decrease occurs in the immediate vicinity of the conductor. Thus, increasing the distance between the harvester and ground has a low impact: even a large increase of the distance between conductive shell and ground from 10 m to 500 m reduces the capacitance by less than 50 % according to FEM simulations.

The conductive shell can be realized through a conductive hollow cylinder around the conductor made from plastic sheet and aluminium foil, with a nonconductive spacer. This type of harvesting device only has the drawback that once a line is completely shut down for maintenance or due to a fault, no more energy can be harvested. Usually, this status is rare and can be bridged with a comparatively small energy storage which only might have to bear a few dozen charge/discharge within the device's lifetime. Ice or snow layers may lower the harvesting performance as an additional dielectric or conductive layer

may form between the conductor and the harvester shell, thus altering or even short-circuiting the inner capacitor. It is crucial that the ratio between the two capacitances (i.e. conductor-shell and shell-earth) is kept within certain limits to ensure continuous power output. Figure 4.1 depicts a realization of the described principle.

4.6 Comparison

Table 4.1 compares the relevant quantities with impact on the performance of harvesting circuitry.

Weather effects by nature influences harvesting techniques which rely on solar radiation or wind. Heat flow methods may suffer from small temperature differences between conductor, harvester and environment, for example, during cloudy weather.

Current load has effects on magnetic harvesters as they typically need a minimum current. Periods of low current loads need to be bridged. If conductor temperature is exploited for heat flow based harvesting, this is also an issue.

Pollution has effects on solar harvesting and wind energy, as there are moving parts which might get stuck. If solar radiation is exploited for heat flow based harvesting, efficiency may be lowered.

Maintenance efforts (cleaning excluded) are high only for wind energy as there are moving parts which may take damage or need to be lubricated.

Complexity in construction is lowest with solar harvesting and harvesting from the electrical field as only little and comparatively cheap material is required, weight is low and there are no moving parts.

It turns out that energy harvesting from the electrical field seems most promising. The negligible impact from environmental conditions and pollution distinguish the methods relying on environmental energy from those relying on energy supplied by the line itself. Other than magnetic harvesting, the capacitive harvester is not dependent on the current load status of the line, thus it does not require a minimum current flow. Concerning the implementation effort, the two methods are comparable. Section 6.1 shows details on the mechanical setup, the circuitry to make this displacement current appropriate

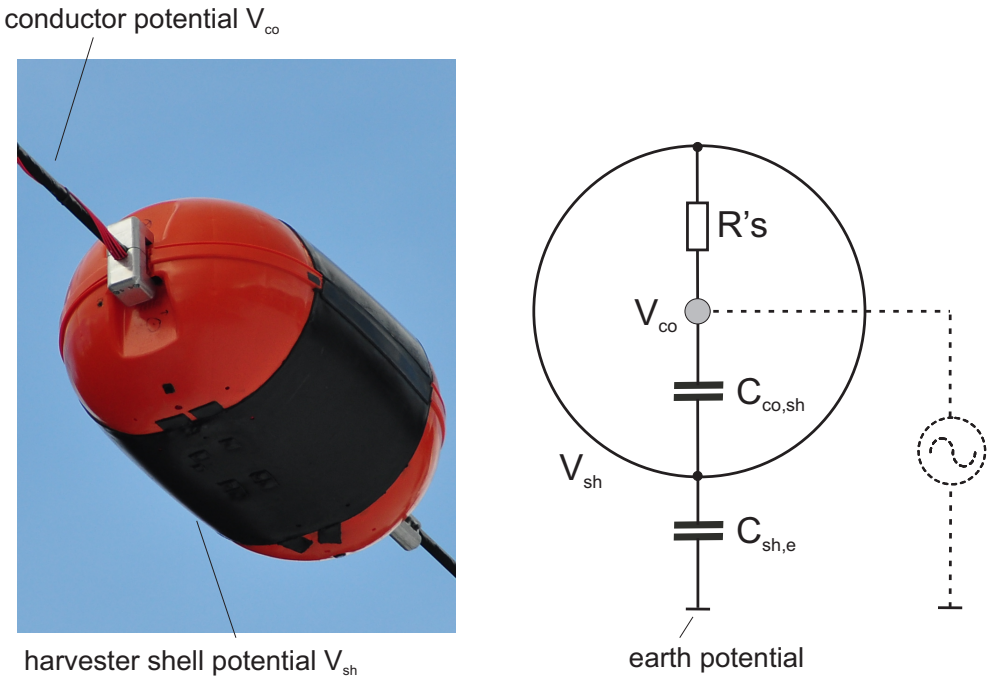

Figure 4.1: Example realization and block diagram of an energy harvesting device using the electric field: The capacitive voltage divider is established by means of two capacitances: The harvester capacitance $C_{co,sh}$ is the capacitance between the conductor at conductor rope potential V_{co} and the metal covered harvester shell at harvester shell potential V_{Sh}. The harvester ground capacitance $C_{sh,e}$ is the capacitance between the harvester shell and earth potential. Depending on the ratio between the two capacitors $C_{co,sh}$ and $C_{sh,e}$, a sufficient amount of energy will pass through the equivalent impedance $R's$ which by means of a suitable transformer converts the displacement current useable for powering measurement hardware. The dashed line indicates the high-voltage between conductor rope potential V_{co} and earth potential.

	Impact				
	weather	current load	pollution	maintenance	complexity
Solar Energy	-	+	-	+	+
Wind	-	+	-	-	o
Heat Flow	o	o	-	+	o
Magnetic Field	+	-	+	+	o
Electrical Field	+	+	+	+	+

Table 4.1: Comparison of energy harvesting techniques for operation at high-voltage power lines. "+" denotes a low weather impact, low dependence on the current load, minor effects of pollution, low maintenance effort and low complexity. "−" denotes the opposite, "*o*" denotes properties in-between.

for powering a measurement circuitry and the feasible power output.

Chapter 5

Sensor Architecture

This chapter covers three aspects: first, the design and evaluation of a capacitive sensor front-end for icing detection at the conductor rope surface of a high-voltage overhead line; second, its interaction with an energy harvesting system based on the alternating electrical field and, third, the related data evaluation. At first, Section 5.1 explains the selected capacitive approach to icing detection, with its geometry constraints determined by the geometry and the environment of a high-voltage overhead line. Section 5.2 explains in detail the electrical boundary conditions which have to be considered when a capacitive sensor is operated in the alternating electrical field in the immediate vicinity of the conductor rope of a high-voltage overhead line. After that, Section 5.3 covers the problems which arise due to the implementation of both a capacitive energy harvesting system and a capacitive measurement system in a single device. At the end of this chapter, Section 5.4 describes the data evaluation method used for the field test device, i.e. how to derive the icing status from the acquired measurement data.

5.1 Design of a Capacitive Sensor for Icing Detection

This section discusses the design principles for a capacitive sensor for icing detection on a conductor rope of a high-voltage overhead line. First, possible measurement electrode geometries are evaluated (Section 5.1.1). Then, the icing scenarios to be expected are described (Section 5.1.2). Section 5.1.3 ex-

plains the measurement model with respect to icing scenarios and the selected electrode layout. In Section 5.1.4, the results obtained from finite element simulation are presented and discussed.

5.1.1 Sensor Geometries

A capacitive sensor consists of two or more electrodes. The electrodes, representing, in fact, the conductive part of the sensor, can be abstracted to a geometry of two or more conductive parts insulated one from each other and all of them electrically insulated from the environment. The presence of a conductive element in order to establish a measurement common ground potential is useful, however, it is not a requirement. A common ground level is often introduced in the environment of a capacitive measurement setup in order to keep one "hemisphere" of the geometry constant with respect to capacitance changes (i.e. no or reduced sensitivity to changes of the dielectric matter). As far as the operation at a high voltage power line conductor rope is concerned, it seems useful to maintain the electrode geometry or distance constant. Only the amount or quality of the dielectric material that changes the permittivity link between the electrodes, on the other hand, should be variable. Due to the strong electrical field gradient in the immediate vicinity of the conductor's surface, the maximum distance between the conductor rope and the electrode is limited (see Section 5.1). Therefore, a flat, planar design is desirable. Different planar electrode topologies have been evaluated and tested in order to evaluate the function of the different electrode setups.

The standard operation environment is an aluminium conductor, steel reinforced (ACSR) conductor rope, a technology, which has been used for over 90 years for high voltage power transmission. This type of conductor rope consists of one or more layers of aluminium strands applied concentrically, with alternate right-hand and left-hand twisting directions, over a galvanized steel core consisting of one or more strands. The steel core provides mechanical strength, and the aluminium strands conduct most of the current [24], (cf. also Section 2.1).

Starting from the given geometry of a typical ACSR conductor rope's profile as depicted in Figure 5.1, the following design options are feasible:

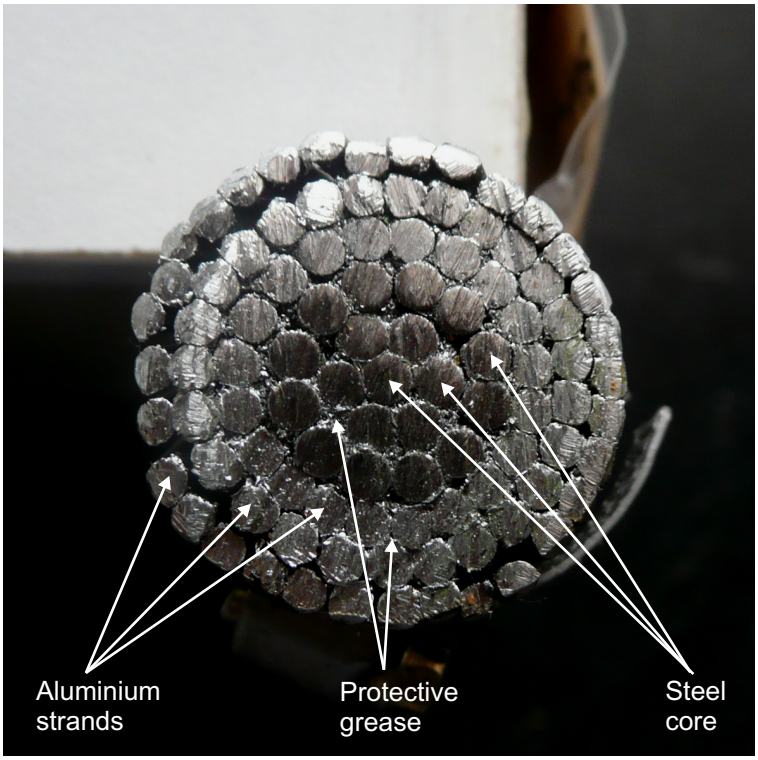

Figure 5.1: Standard profile of a conductor rope (cross section), consisting of a steel core and multiple (here: three) layers of aluminium strands.

- **Circular** (ring-shaped) electrodes around the conductor rope (cf. Figure 5.2). Insulated wires are mounted around the conductor rope's surface. The measurement capacitances are defined by electrode pairs. Each measurement capacitance has a different yet unique characteristic depending on the electrode distance. This setup provides the advantage of a tangentially uniform sensitivity around the conductor rope. At the same time, the sensor characteristic does not take into account non-uniform ice accretion, for example, due to the presence of wind. A drawback of this approach might be a potentially complicated mounting process on the line: a procedure needs to be developed that allows for mounting of rings on the line while at the same time ensuring a known distance between electrode and conductor rope's surface plus keeping the electrical insulation of the electrodes intact. This may lead to sensor electrodes, which have to consist of multiple parts or be very flexible, yet mechanically stable (such as conductive polymers). Furthermore, the measurement capacitance between two rings is not easily scalable to the desired

measurement circuitry input range without changing the overall sensor behavior.

- **Straight** (linear) electrodes along the conductor rope (cf. Figure 5.3). Insulated wires are mounted in the surface gaps between the aluminium conductor strands, following the twisting of the conductor rope. This setup allows for easy scaling as the electrode length changes both offset and measurement capacitance. As in the previous approach, the measurement capacitances are defined by electrode pairs. Also here, each measurement capacitance has a different yet unique characteristic depending on the electrode distance. The advantages of this setup are, on the one hand, the possibility to pre-produce the sensor elements with a holder, which can be easily mounted as long as the electrode length does not exceed half of the twisting length of the conductor rope. However, this configuration results in a limitation of the sensitive area. The major advantage of this setup is the position of the measurement electrodes: if placed into the surface gaps, the exposure to the electrical field and thereby the potential difference between measurement electrodes and conductor rope can be kept small due to its position "within" the surface.
- **Complex geometries** (for example, electrodes of different lengths, free-form geometries). In principle, any electrode shape that fits both the requirements of application on a high-voltage conductor rope and the required sensor characteristics, could be realized. However, sophisticated geometries typically lack scalability, which is regarded to be essential for the design of a first laboratory or field test device.

Due to the ease of scalability, the simple application onto the conductor surface and the advantage of not having to deal with too high voltages between conductor and measurement electrodes, the linear electrodes approach was chosen to be investigated in more detail. Besides, preliminary experiments have been carried out with ring-shaped electrode setups as well.

5.1.2 Sensing Scenarios

In consequence to Section 2.2, different standard sensing scenarios are expected. The following scenarios are most likely to occur:

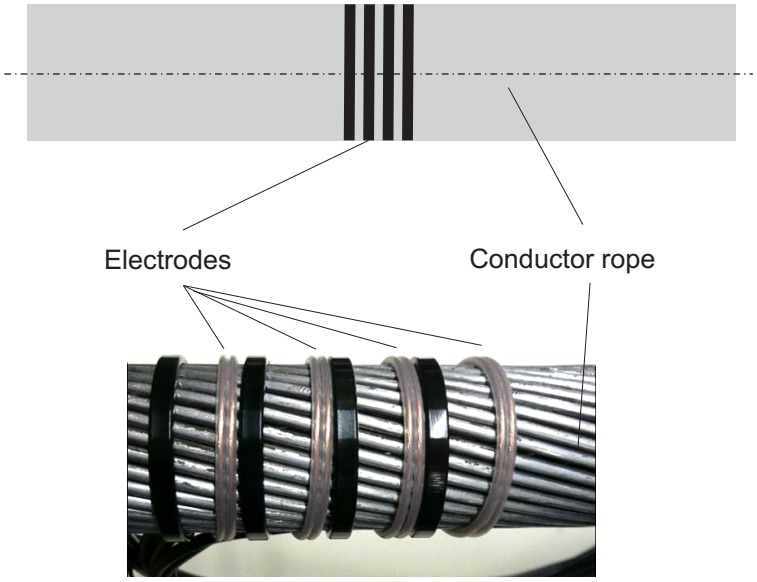

Figure 5.2: Geometric model and example photograph of a circular electrode setup on a conductor rope. Insulated wires are mounted along the circumference of the conductor surface. This setup provides the advantage of a tangentially uniform sensitivity around the conductor rope.

- **Dry conductor**. In this case, the medium surrounding the conductor and the sensor is air.

- **Rime icing** (air humidity induced ice deposition). Air humidity freezes and accumulates at the conductor surface. In this case, an ice layer is assumed to be present at the conductor surface and the sensor, with increasing or decreasing thickness.

- **In-cloud icing** (presence of water droplets). Similar to rime icing; no water layer but amounts of small water droplets in the air are assumed to be present during the icing process.

- **Snow deposition**. This process describes snow (ice of complex geometries containing various amounts of water and air) accumulating at the surface of the conductor and on the sensor.

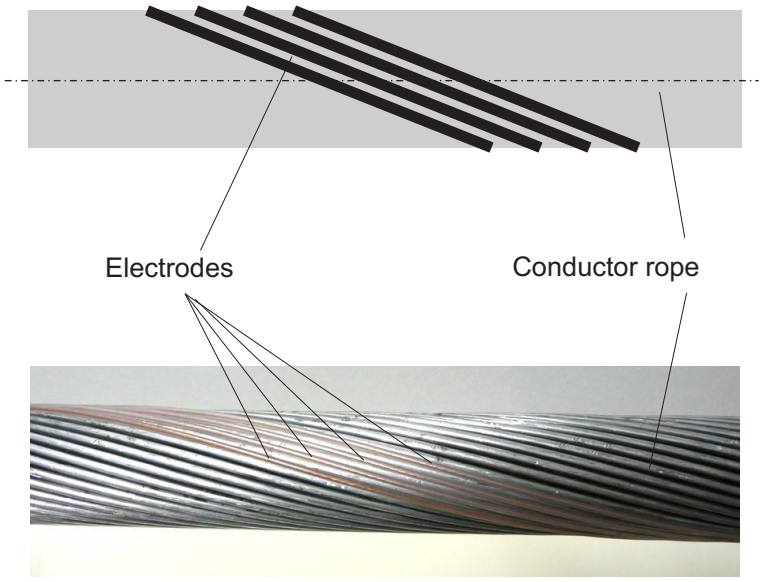

Figure 5.3: Geometric model and example photograph of a linear electrode setup on a conductor rope. Insulated wires are mounted in the surface gaps between the aluminium conductor strands, following the twisting of the conductor rope. This setup allows for easy scaling as the electrode length changes both offset and measurement capacitance.

- **Freezing rain**. Liquid water drops hit the conductor surface and form a clear ice layer of increasing thickness; this can be modeled by an ice layer with increasing thickness on the conductor and the sensor and on top a water layer of limited thickness.

- **Melting ice**. Typically, a conductor line would rather de-ice by solar radiation or increasing air temperatures. The situation concerning the layer structure of different permittivities is similar to a freezing rain event, although there is a longer duration of stable states.

- **Wet conductor**. The medium surrounding the conductor and the sensor is water, typically originating from precipitation or a melting thin ice layer. A water layer at the surface of a conductor is limited in its thickness by gravity, the viscosity of water, the surface geometry and

roughness and the hydrophilic/hydrophobic behavior of the surface.

Figure 5.4 depicts the sensing scenarios in the field as described above. It can be seen that in principle, three capacitances are present in this setup: a capacitance between each electrode and the conductor surface ($C_{g,1}$ and $C_{g,2}$) as well as the inter-electrode coupling capacitance C_c. The measured capacitance C_N is given by equation 5.1:

$$C_N = C_c + \frac{C_{g1} * C_{g2}}{C_{g1} + C_{g2}} \tag{5.1}$$

The capacitance model is explained in more detail in Section 5.1.3. Images of the corresponding states during laboratory tests are depicted in Figure 5.5.

In Figure 5.5, a laboratory linear electrode setup is depicted. Four equally spaced wire electrodes are positioned in the gaps between conductor strands.

Summarizing, a capacitive sensor for icing detection on a high-voltage power line conductor should be able to both detect and distinguish between any of the listed measurement scenarios. Further information may be extracted from the transitional states between the scenarios.

5.1.3 Capacitance Model

This section describes the electrical capacitance model of an electrode setup in the vicinity of the surface of a conductor line. The effects of the presence of water or ice in the vicinity of the conductor equipped with a two-electrode measurement capacitance are explained. As the expected measurement frequencies (i.e. the excitation frequencies) are below 10 MHz, wave propagation effects are neglected.

Figure 5.6 depicts a basic measurement setup, consisting of two measurement electrodes. A total of three conductive objects (Electrode E1, Electrode E2 and the Conductor) yield three inter-electrode capacitances. Figure 5.6 depicts the equivalent network of capacitances contributing to the evaluation result of a measurement capacitance C_N. For the application on a conductor, more than two electrodes are required in order to solve ambiguities.

- $C_{g,1}$ is the ground capacitance 1 between Electrode E1 (for instance, a transmitter) and the conductor rope. This capacitance can be approx-

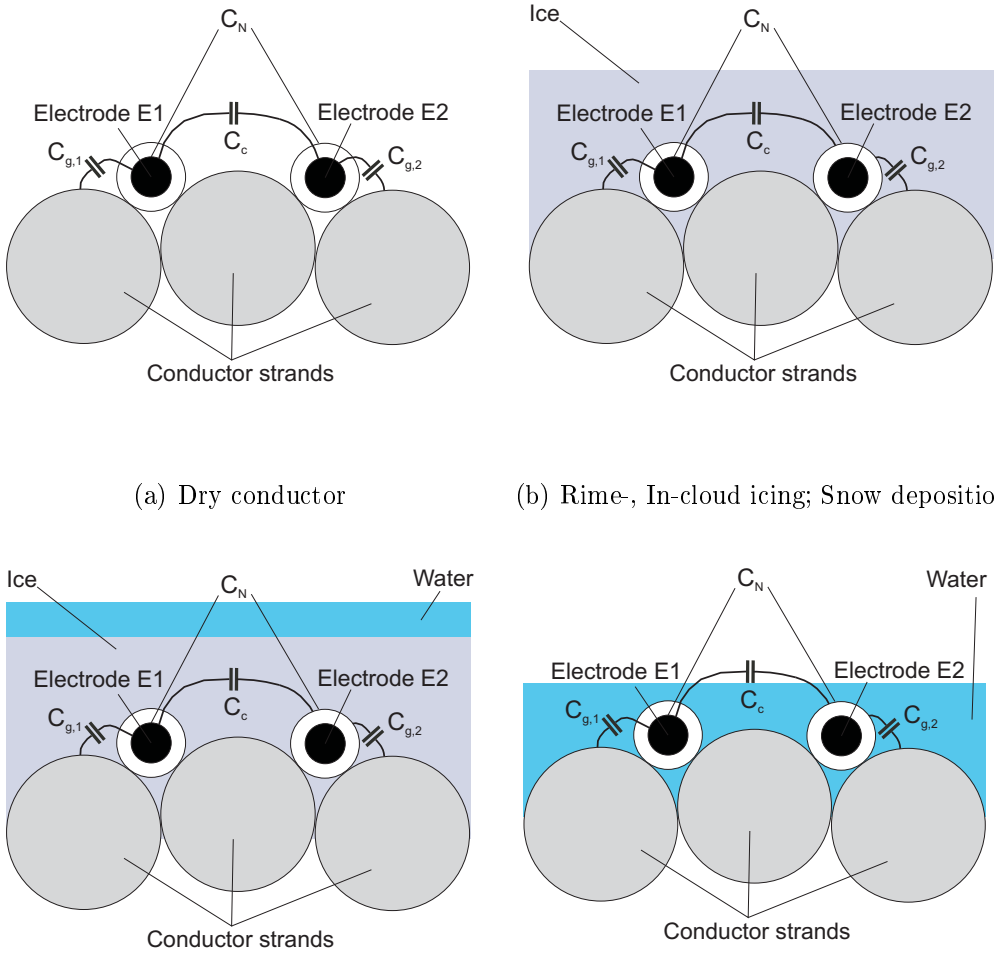

(a) Dry conductor

(b) Rime-, In-cloud icing; Snow deposition

(c) Freezing rain, Melting ice

(d) Wet conductor

Figure 5.4: Cross-section of a simplified capacitance model of example scenarios with linear electrode setups in a laboratory test cycle. First, the conductor rope's surface is dry (a). Ice accretes (b) and melts (c) during the experiment, leaving water on the conductor rope's surface (d). The capacitances between each electrode and the conductor rope's surface ($C_{g,1}$ and $C_{g,2}$) as well as the inter-electrode coupling capacitance C_c depend on the type and amount of material (ice, water or air) present on the conductor rope's surface and the electrodes. This capacitance model is explained in more detail in Section 5.1.3.

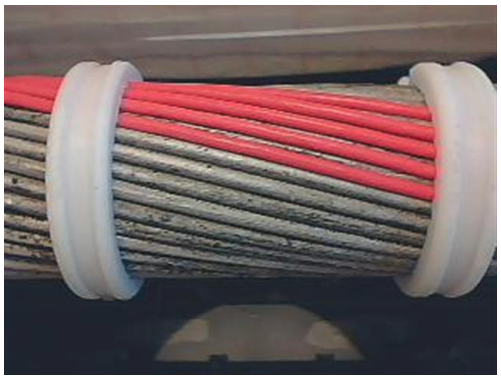

(a) Dry conductor

(b) Rime icing / In-cloud icing / Snow deposition

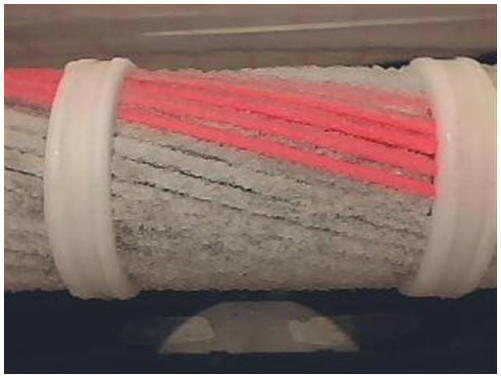

(c) Freezing rain / Melting ice

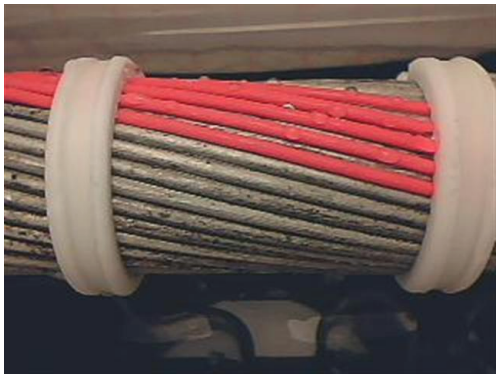

(d) Wet conductor

Figure 5.5: Images of example icing scenarios with linear electrode setups in a laboratory test cycle. First, the conductor surface is dry (a). Ice accretes (b) and melts (c) during the experiment, leaving water on the conductor surface (d).

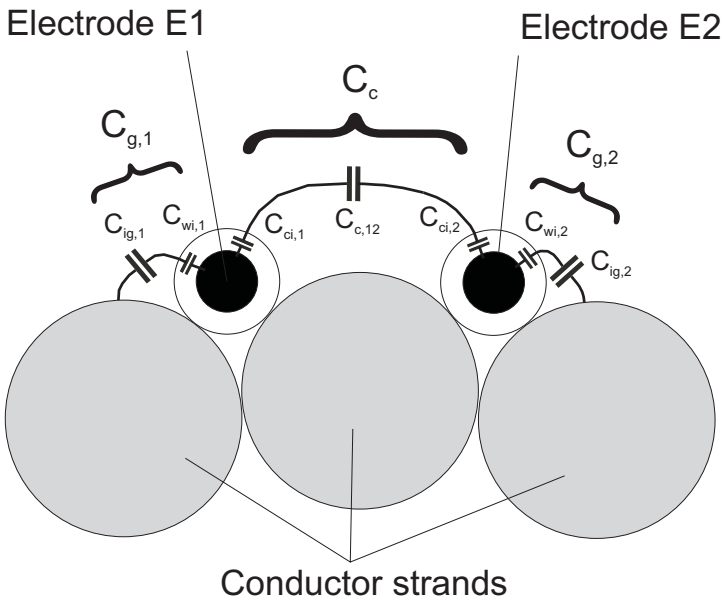

Figure 5.6: Capacitance model for a two-electrode linear setup (cross-section). The three inter-electrode capacitances $C_{g,1}$, $C_{g,2}$ and C_c consist of partial capacitances.

imated by a cylinder electrode (with the diameter of the wire) in the vicinity of a surface, which has a half-cylinder texture. The media in between the two conductive structures is the wire insulation of Electrode E1 (typically a polymer with a permittivity ($\varepsilon_r = 2...5$) and air. Thus, $C_{g,1}$ is the series connection of the capacitance between wire and insulation $C_{wi,1}$ and the capacitance $C_{ig,1}$ between insulation and conductor. However, the air gap is subject to be replaced by ice or water, thus significantly changing the capacitance $C_{ig,1}$.

- $C_{g,2}$ is the ground capacitance 2 between the receiver Electrode 2 (for instance, a receiver) and the conductor rope. The impacts on this capacitance are the same as for $C_{g,1}$.

- C_c is the coupling capacitance between Electrode E1 and Electrode E2; this is the measurement capacitance. This capacitance can be approximated as the capacitance between two cylindrical objects. A series connection of three capacitances contributes to the coupling capacitance: A

capacitance between Electrode E1 and the surface of its outer insulation $C_{ci,1}$, the same for Electrode E2 ($C_{ci,2}$) and the coupling capacitance $C_{c,12}$. Again, the capacitances $C_{ci,1}$ and $C_{ci,2}$ depend on the material of the wire insulation of Electrodes E1 and E2 (typically a polymer with a permittivity ($\varepsilon_r = 2...5$). $C_{c,12}$ is given by the air gap in between the two insulated electrodes. Replacement of the air gap by ice and/or water significantly alters the value of $C_{c,12}$.

Whenever a capacitance measurement setup consists of at least a transmitter, a receiver and a common ground potential, an object in-between can either increase ("coupling mode") or decrease ("shielding mode") the coupling capacitance (compare, for example, [131]), depending on the size and the permittivity of the object, its distance from the measurement capacitor and its capacitance with respect to ground. As described in Figure 5.7, this can lead to ambiguities when evaluating only a single measurement capacitance.

Figure 5.7 illustrates the measurement principle for four different measurement scenarios. The coupling capacitances between Electrodes E1, E2 and E3 are evaluated by means of a low-impedance measurement circuitry with Electrode E1 as a common transmitter.

Whenever air in the vicinity of the conductor is replaced by water, ice or snow, all the partial capacitances within one measurement electrode pair ($C_{g,1}$, C_c and $C_{g,2}$) are altered. The variation of all three capacitances potentially has effects on the measurement readout and might lead to ambiguous results. Consequently, the use of multiple electrodes (i.e. multiple measurement capacitances) is required for the evaluation of ice quality and thickness information. Ice could be distinguished from water even more easily due to an impact on the coupling capacitances which differs by orders of magnitude.

The behavior of a measurement capacitance is different but unique for any electrode distance. Overall, the sensor characteristics are determined by the electrode distance, the thickness of the wires, the thickness and the material of the isolation layer. Besides, it can be linearly scaled (in order to adapt the measurement capacitance to the readout circuitry) by increasing the respective electrode lengths [4].

As stated above, in order to be able to estimate the layer thickness from the measurement signal, multiple measurement capacitances need to be evaluated

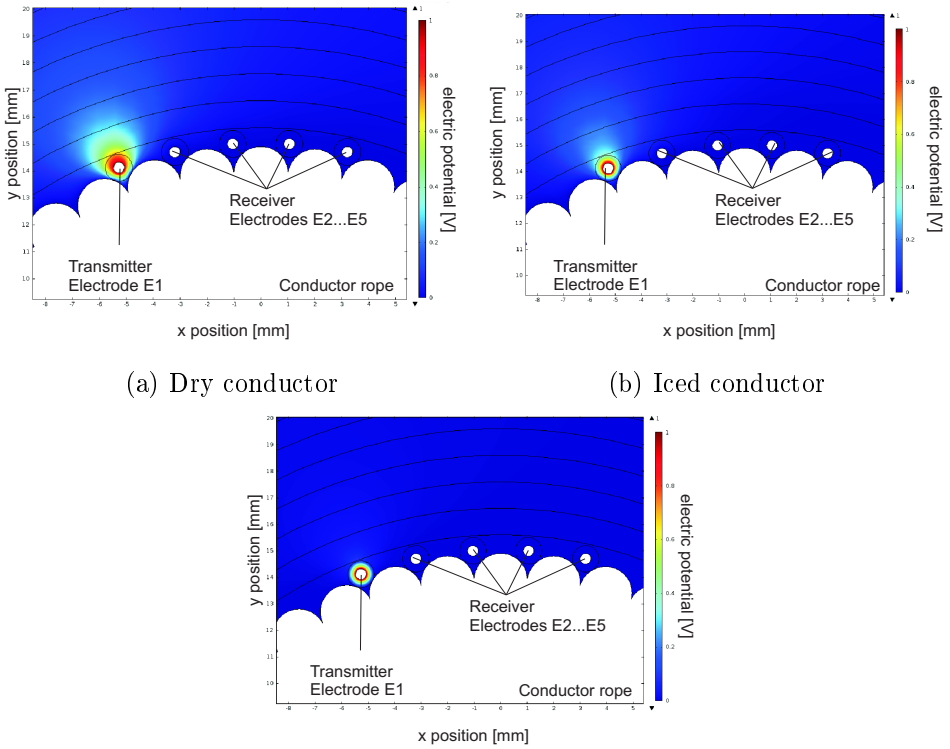

(a) Dry conductor

(b) Iced conductor

(c) Wet conductor

Figure 5.7: Surface states and the impact on the measured capacitance. (a) The low permittivity of air ($\varepsilon_r = 1$) causes a small displacement current which is concentrated around the transmitter; thus, coupling is weak and the capacitance measurement value is small.
(b) The displacement current increases for ice covered electrodes due to the higher permittivity of ice ($\varepsilon_r > 2$). Thus, also the coupling between the common transmitter Electrode E1 and the receivers Electrode E2 and Electrode E3 increases, i.e. the displacement current increases due to the higher permittivity; coupling is improved and the measured capacitance C_c increases. For increasing thicknesses of the ice layer, the displacement current is more and more directed away from the electrodes and the coupling capacitance C_c starts to decrease again. As the displacement current is directed further away, the coupling capacitance C_c decreases due to the increasing coupling between the dielectric layer and the conductor. If the distance between transmitter and receiver increases, the maximum capacitance value is reached at an increased ice layer thickness (here: compare the measurement capacitances between Electrodes E1-E2 and E1-E3, respectively).
(c) For very high permittivities (water, $\varepsilon_r = 80$), the displacement current strongly increases and is directed towards the conductor, even for very thin layers. Consequently, the field remains concentrated around Electrode E1 and the coupling to Electrodes E2 and E3 is poor.

and the achieved measurement signals must be merged by means of a suitable algorithm.

The maximum number of electrodes per electrode assembly is practically limited by the availability of circuits. That is, as per 2012, 16 receiver electrodes for commercially available devices. However, this limit can be worked around by means of multiplexers or other suitable devices. The theoretical minimum required number of measurement capacitors due to the presence of shielding mode and coupling mode would be two. However, for reasons of redundancy, ability for self diagnosis and data quality, it was decided to implement four measurement electrodes for the field setups, though several early experiments were also carried out with two or three measurement capacitances depending on the available sensor IC.

According to the operation modes of commercially available capacitance-to-digital converters, four measurement capacitors were designed by a single transmitter (excitation) electrode and multiple multiplexed receiver electrodes, which are continuously evaluated. As mentioned above, these measurement capacitors are designed to differ in their inter-electrode distance, thus having different nominal capacitances and different characteristics. A schematic of this setup, based on real-world dimensions, is depicted in Figure 5.8. The measurement capacitances between a common electrode (Electrode E1) and multiple measurement electrodes (Electrode E2...E5) are evaluated. The sensor electrodes consist of electrically isolated wires following the twisting of the conductor strands. This is an approach which primarily uses dimensions given by the surface to be observed.

5.1.4 Finite Element Simulation

After deriving the model (Section 5.1.3), a 2D finite element simulation of the measurement setup has been established.

Figure 5.9 depicts the measurement setup in the simulation software environment. The setup equals the field test setup (consisting of four measurement capacitances).

In the simulation framework, a layer of variable thickness of ice ($\varepsilon_r = 3$) is simulated at the conductor surface. The 2D finite element model results of this calculation are depicted in Figure 5.10.

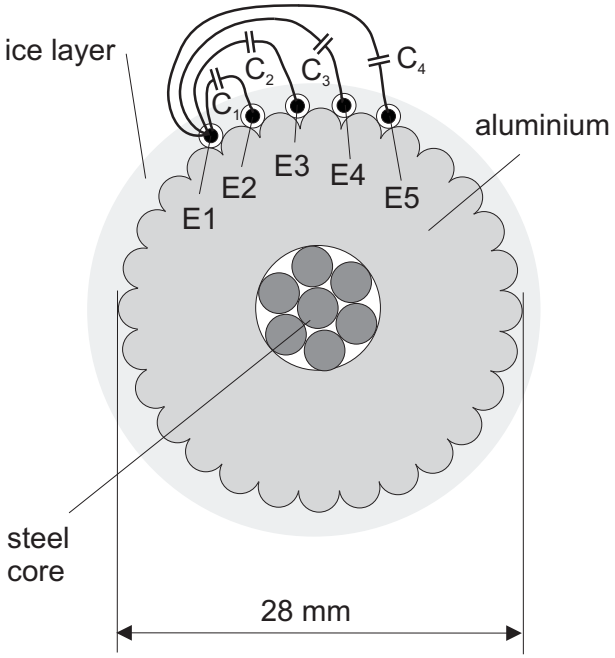

Figure 5.8: Electrode setup for a typical conductor rope with five linear electrodes E1...E5, forming the measurement capacitances C_N (i.e. C_1, C_2, C_3 and C_4).

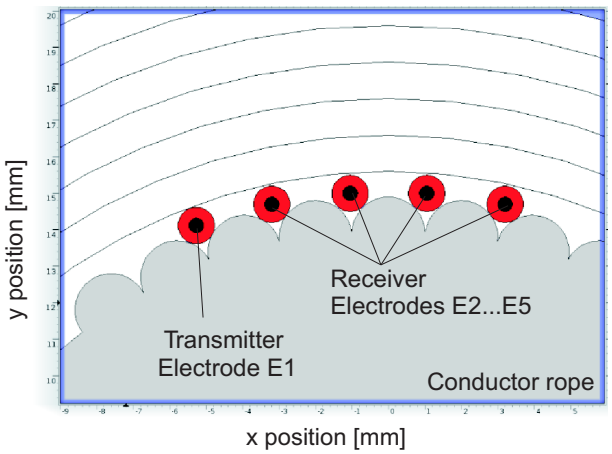

Figure 5.9: 2D model in the FEM simulation software. Electrodes E1...E5 form the measurement capacitances C_N (i.e. C_1, C_2, C_3 and C_4)

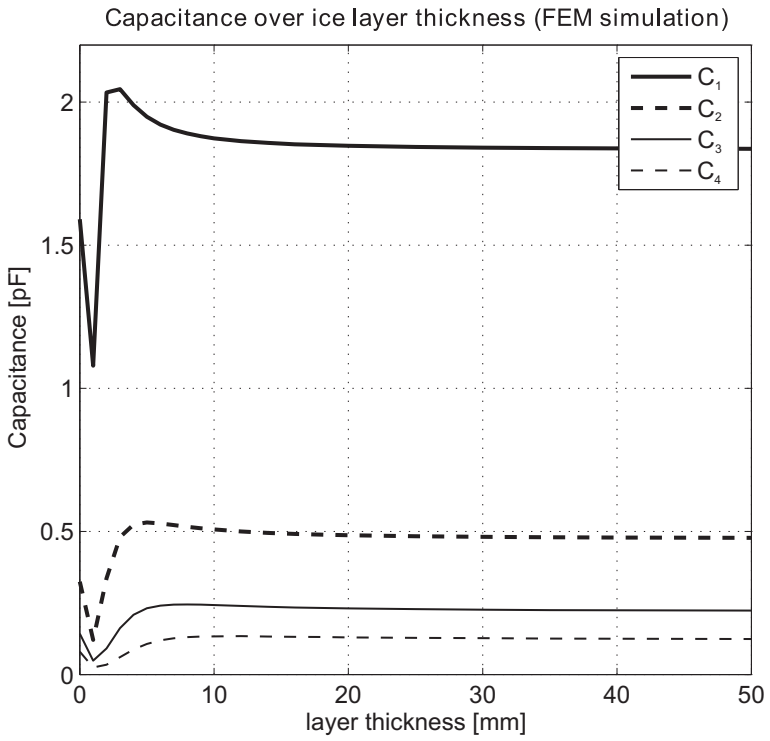

Figure 5.10: 2D FEM simulation results for ice layers with increasing thickness. It can be seen that for increasing inter-electrode distances (C_1 smallest, C_4 largest), the absolute dry value decreases and the maximum value is reached at a higher thickness for a larger inter-electrode distance. Furthermore, all measurement capacitances are lower than their "dry" value for small thicknesses (approx. 1 mm), resulting from the predominant shielding mode.

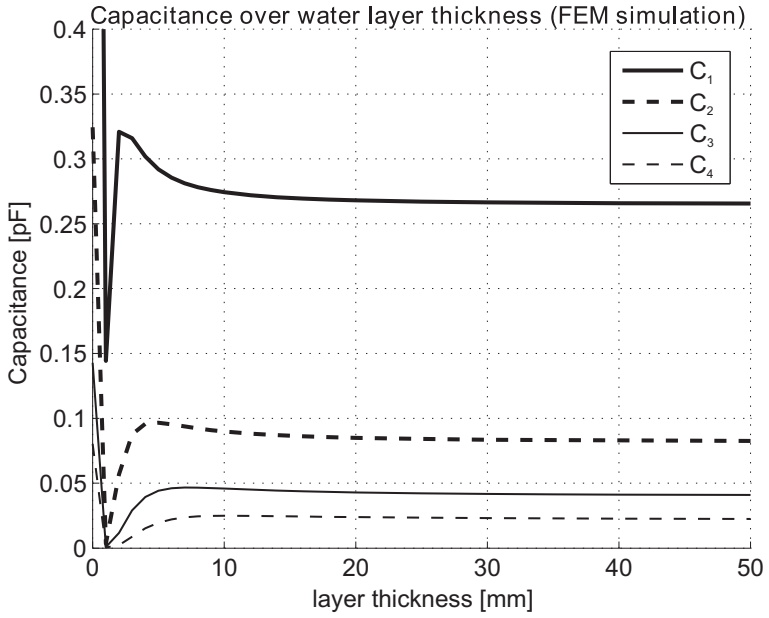

Figure 5.11: 2D FEM simulation results for water layers with increasing thickness. Compared to Figure 5.10, all capacitances are small. For increasing inter-electrode distances (C_1 smallest, C_4 largest), the behavior for higher layer thicknesses is similar. With the presence of water, the shielding effect dominates over the whole thickness range. It has to be noted that a water thickness of 50 mm is impossible, however, thick and very wet snow layers may show a similar behavior.

It can be seen that the behavior of the measurement capacitances is different for the various inter-electrode distances (cf. Section 5.1.3). The combination of multiple measurement capacitances will allow for the estimation of the layer thickness (to be discussed in Section 5.4).

Figure 5.11 shows the 2D finite element model results for a water layer of variable thickness ($\varepsilon_r = 80$). It is obvious that already at a comparatively small layer thickness, all measurement capacitances saturate at low capacitance values. However, as mentioned earlier in Section 5.1.2, a thick water layer is not expected to occur on a conductor line due to both the geometry of the setup and gravity. Nevertheless, a thick layer of very wet snow may behave similarly to a thick water layer.

5.2 High-Voltage Design for a Capacitive Icing Sensor

In a high-voltage environment, several constraints apply to the design of a capacitive sensor. While in principle, the required measurement capacitances can be formed by multiple conductive parts (sensor electrodes) of any shape, which have to be covered by a non-conductive layer, the following constraints have to be observed concerning materials and geometry [3]:

- No sharp edges or corners are allowed in order to avoid corona discharges due to field crowding.
- A trade-off needs to be found concerning the distance between conductor rope surface and measurement electrodes. While a larger distance leads to a lower offset capacitance and lower parasitic coupling, it also causes a higher potential difference in the magnitude of kilovolts between the CDC channels and measurement ground (i.e. the conductor rope).
- Similar to the sensor cables, the sensor electrode isolation needs to withstand the industrial temperature range (-40 to +85°C) and must be stable against the strong electrical field and partial discharges.
- A minimum electrode isolation thickness must be kept for long-term stability.
- A mechanically stable connection between sensor cable and sensor electrodes must be established.

These restrictions are discussed in Section 5.2.1 and 5.2.2.

5.2.1 Geometry

The first geometric boundary for a sensor on a high-voltage power line is (depending on the measurement principle) a low profile in order to avoid too high voltages between conductor and measurement electrodes. Secondly, any sharp edge, corner or peaks of any object can generate corona discharges into the air, which will lead to EMC disturbers and material degradation. Hence, from a high-voltage engineering point of view, two major requirements apply:

- Minimization of the electrode assembly's profile (i.e. height, length in radial direction).

- Maximization of the corner and edge radius of any part in the electrical field.

On the other hand, a larger distance between conductor surface and electrode assembly decreases the parasitic capacitances between both measurement electrodes and conductor potential, thus having a positive overall effect on the capacitive measurement.

5.2.2 Materials

Capacitive sensing in a high-voltage electrical field requires the sensor materials to be able to withstand the strong electrical field (i.e. carry the dielectric currents without degradation) and to also withstand partial discharges from its surface. Furthermore, the connecting cables have to meet the same requirements while not being sensitive to icing. The choice of materials is very limited: the materials have to suit the mechanical demands, be immune against UV radiation (i.e., no material degradation due to sunlight) and certified for the standard industrial temperature range (between -40 and +85 degrees Celsius). In high-voltage engineering, there are several materials that fulfill these requirements, such as ceramics, special silicone elastomers and Teflon (polytetrafluoroethylene, PTFE). The low permittivity of PTFE ($\varepsilon_r = 2$) ensures low dielectric load over the sensor lifetime. The only drawback of the material is its low friction coefficient; also, it is comparatively hard to join (no glue available, no simple thermal forming procedures). Moreover, silicone elastomers typically have similar material properties such as hydrophobic surfaces and sophisticated joining procedures.

The use of commercial PTFE or silicone insulated wires ensures mechanical stability concerning the insulation layer between measurement electrode and conductor potential. What needs to be ensured is a water-tight yet low-profile element where the sensor cables are connected to the sensor. Details on the realization of the icing sensor are given in Section 6.3.1.

5.3 Capacitive Harvesting versus Capacitive Measurement

This section covers the problems which arise due to the concurrent operation of a capacitive energy harvesting system and a capacitive measurement system. Section 5.3.1 describes in detail the interaction of the capacitor of the energy harvesting system with the capacitors, which are part of the measurement system. The approaches to solving this problem are discussed in Section 5.3.2. The selected solution approach and resulting boundaries for the implementation in a test device are described in Section 5.3.3.

5.3.1 Problem Description

Figure 5.12 depicts a block diagram of key components of a complete energy harvesting and icing detection system.

The primary coil of the 5 kV/20 V transformer is connected to both the conductor line (conductor rope potential V_{co}) and the energy harvester shell (harvester shell potential V_{sh}). The transformer output is rectified and regulated to the required supply voltage respect to the harvester shell (V_{co}). The energy harvesting circuitry is represented by the equivalent impedance $R's$. The energy supply is fed to all components of the circuitry.

The problem that arises during the design process is that one has to choose a proper potential for the supply lines of the capacitive icing sensor electrodes. This so-called shield potential could be set to the ground potential of the micro controller (on harvester shell potential V_{sh}). However, this results in a parasitic link (i.e. a lowered impedance) between conductor and harvester shell, potentially disturbing the operation of the energy harvesting system. On the other hand, magnetic fields are strong close to the conductor and the electric field gradient is highest in the immediate vicinity of the conductor, making it difficult to operate wireless data transmission systems (such as GSM and ISM) there, also due to the presence of metallic objects and restricted areas available for antennas.

Consequently, micro controller and data transmission circuitry should reside as close to the harvester shell due to the mentioned reasons, whereas the

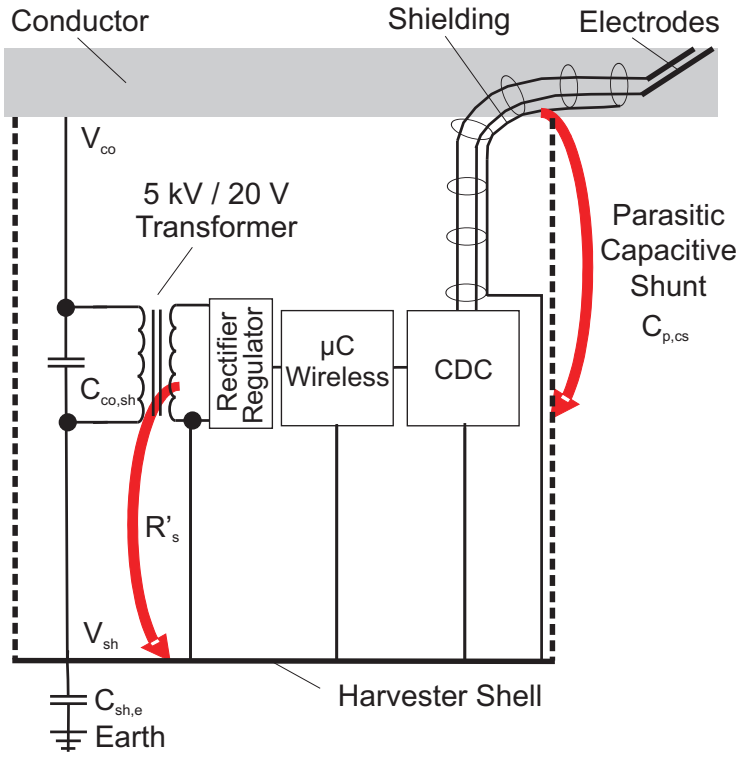

Figure 5.12: Schematic of the parasitic capacitive path problem. V_{co} is the conductor rope potential. V_{sh} is the harvester shell potential. $C_{sh,e}$ is the capacitance between harvester shell and ground, while $C_{co,sh}$ is the harvester capacitance. The capacitive shunt $C_{p,cs}$ is introduced by the sensor cables shielding with respect to ground, as they are routed to the conductor from the capacitance-to-digital converter (CDC).

measurement circuitry should reside as close to the conductor as possible. This allows to keep the voltage between measurement electrodes and measurement ground as small as possible.

Furthermore, the energy harvesting system is based on a capacitive voltage divider. As mentioned in Section 4.5, the ratio between the two divider capacitances is crucial for its operation. Therefore, additional (parasitic) paths between the conductor rope potential V_{co} and harvester shell potential V_{sh} decrease the amount of harvestable power due to the alteration of the mentioned divider ratio, and need to be taken into account.

These parasitic paths may be introduced by ice or snow layers on the outer side of the harvester shell, but also by the icing detection circuitry itself (compare Figure 5.12). For instance, assuming a harvester ground capacitance $C_{sh,e}$ of 10 pF between harvester shell and ground, a harvester clamping voltage of

5 kV and a system voltage of 220 kV RMS line-to-line (equaling 127 kV RMS voltage with respect to earth), the parallel connection of the harvester capacitance $C_{co,sh}$, the equivalent impedance of the energy harvesting circuitry R'_s and the parasitic capacitive shunt $C_{p,cs}$ between conductor and harvester shell must not exceed 250 pF in order to keep the voltage divider within its designed parameters. Consequently, an increased value of that capacitance would require an increase of the harvester ground capacitance $C_{sh,e}$ which can, in fact, only be achieved by enhancing the length (and thereby the weight) of the harvester shell, which is not desirable.

Assuming the circuitry residing in the vicinity of the harvester shell (i.e. on harvester shell potential V_{sh}), the shielding of the coaxial cables towards the sensor wires introduces already a relevant parasitic capacitance as they are connected to harvester shell potential V_{sh}. In order to keep the aerodynamical effects of the harvester shell on the icing behavior at the sensor location small, a minimum distance should be kept between harvester shell and icing sensor. A minimum of at three electrodes (one transmitter and two receiver electrodes) is required for a reliable icing detection in order to be able to resolve ambiguities. The capacity per unit length of a coaxial cable typically amounts to approx. 100 pF per meter. Assuming a distance of only one meter between harvester shell and icing sensor (yielding approx. 1.5 m of cabling per sensor electrode), at least 450 pF of additional parasitic capacitance are introduced. This value already exceeds the calculated maximum for reliable operation of the energy harvesting system. Consequently, the displacement current to the environment would no longer pass through the harvesting circuitry but through the parasitic path and the energy harvesting system would therefore no longer operate.

The operation of measurement circuitry in the immediate vicinity of a high voltage power line conductor poses several problems:

- High electrical field strengths which have influence on the sensors on one hand and on the measurement circuitry on the other hand. Due to the geometry which is similar to a line source over a conductive plane, the highest field gradient occurs closest to the conductor.

- In consequence to that, components mounted at different distances from

the conductor reside at different electrical potentials, unless they are mounted in a Faraday cage. However, such a device would introduce additional parasitic capacitances.

- High magnetic field strengths while high currents are present. High AC currents may induct voltages in any loop-shaped part of the circuitry of suited orientation towards the field.

- Disturbances / Transients during switching processes in both the electrical and the magnetic field regime [4].

Hence, for a realization of the system the following requirements have to be considered:

- The communication circuitry should reside as far as possible from the conductor to keep induced voltages in the antenna as low as possible.

- The measurement circuitry should reside as close to the conductor as possible in order to minimize 50 Hz disturbances between measurement ground and the measurement circuitry inputs.

- The sensor cables need to be shielded to make them sensitive only in the desired area. A shield potential needs to be defined. If the shield potential is set to harvester shell potential V_{sh}, the parasitic capacitances would by far exceed the limits that need to be respected for the operation of the energy harvester.

- The total parasitic impedance of the circuitry between conductor and harvester shell has to be small, because the capacitive voltage divider ratio is crucial for the operation of the energy harvester [4].

Following these considerations, it is not feasible to mount the entire circuitry on the inside of the harvester shell. In the next section, solutions approaches for this problem are described.

5.3.2 Solution Approaches

A minimum of two possible concepts seem feasible:

1. Placement of the entire circuitry **on conductor potential** on the inner side of the harvester shell or on the conductor. This approach provides the following advantages:

   - Short measurement cables, small additional offset capacitances
   - Virtually no parasitic capacitive shunt $C_{p,cs}$ in parallel to $R's$ and the harvester capacitance $C_{co,sh}$
   - Compact solution

   At the same time, the following drawbacks have to be dealt with:

   - GSM/ISM antenna placement in strong field area
   - GSM/ISM antenna placement within harvester shell - directional characteristics, shielding effects
   - Entire circuitry within strong magnetic field area
   - Additional weight due to the necessary magnetic shielding of the circuitry

   Figure 5.13 depicts the block diagram of this approach.

2. **Separation and decoupling** between measurement front end and the rest of the circuitry.

   The advantages of this approach are:

   - Communication circuitry and antenna resides on harvester shell
   - Minimal parasitic capacitive shunt $C_{p,cs}$ in addition to $R's$ and the harvester capacitance $C_{co,sh}$
   - Capacitance measurement circuitry close to the conductor, i.e. small additional offset capacitances

   Drawbacks of this approach:

   - Durable isolation between the two circuitry areas is necessary, possible problems with creeping currents

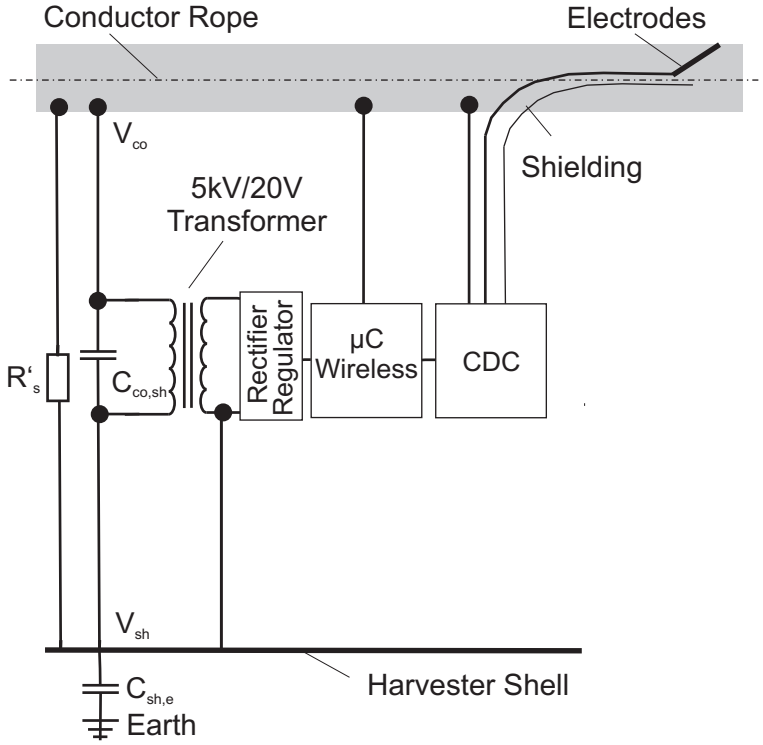

Figure 5.13: Block diagram of a decoupling solution with the measurement circuitry at the conductor rope potential V_{co}.

- Two signal ground levels are present at a potential difference of several thousand Volt
- Data and power transfer and/or measurement signal transfer between the two potential levels needs to be established

Given this, the following design rules for an implementation should be obeyed:

- The measurement circuitry and/or the measurement signals need to be decoupled from the harvesting and communication circuitry. Consequently, there are two ground levels (harvester ground and measurement ground) with a potential difference of several thousand Volts.
- Isolated data and/or measurement signal transmission is required between communication circuitry and measurement circuitry.
- Isolated power transmission can be required if the measurement circuitry is entirely decoupled.

- All capacitances introduced by these data and power paths represent again contributions to the parasitic capacitive shunt $C_{p,cs}$ and should therefore be kept as small as possible. [4]

In order to obtain the largest possible distance from the conductor (thus avoiding disturbances from the magnetic field), the inner side of the harvester seems the optimum mounting location for the measurement and data communication circuitry. This also allows for the integration of communication antennas in that area.

5.3.3 Decoupling Solution

As it seems that wireless data transmission in an environment of strong alternating magnetic fields is more difficult to handle in comparison with a strong electrical field and the related insulation issues, the approach to separation and decoupling was further investigated. Therefore, suitable methods of transferring either the measurement excitation and receiver signals or both power and data between the circuitry parts need to be implemented, as the main aim is the use of the conductor surface as measurement ground potential.

This aim can be achieved either by means of high-voltage high-frequency transformers or by means of high-voltage optical couplers (typically providing a coupling capacitance below 1 pF per unit) and a small-scale high-frequency insulated transformer (with a typical primary-to-secondary coupling capacitance below 5 pF).

Figure 5.14 depicts the solution approach for the decoupling problem. In comparison to Figure 5.12, a Data/Power Decoupling Unit is introduced into the setup. The main aim of this unit is the ground level translation - as most of the circuitry (including energy harvesting and wireless data transmission) is referred to the vanishes and a (de)coupling capacitance $C_{p,dc}$ is introduced by the decoupling circuitry. As mentioned above, this additional capacitance $C_{p,dc}$ is orders of magnitude below the expected values of the parasitic capacitive shunt $C_{p,cs}$.

Details on the implementation of the decoupling solution are given in Section 6.3.3.

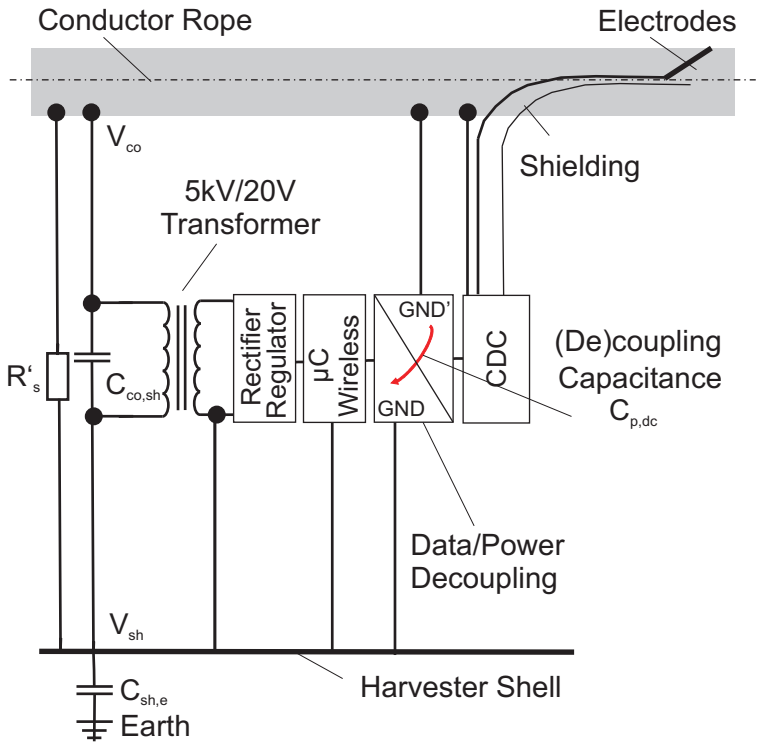

Figure 5.14: Block diagram of the capacitive path decoupling solution. The parasitic shunt $C_{p,cs}$ between the conductor rope potential V_{co} (GND') and the harvester shell potential V_{sh} (GND) disappears and is replaced by a small decoupling capacitance $C_{p,dc}$ which is orders of magnitude smaller than the parasitic shunt $C_{p,cs}$.

5.4 Data Evaluation and Algorithm Design

This section describes the path from the capacitance measurement raw data to the measurement data representing the icing status of the conductor surface presented to a responsible person such as the operator in charge. Section 5.4.1 investigates possible cross sensitivity effects on the measurement due to, for instance, temperature changes, and proposes approaches for automated correction. Section 5.4.2 explains how the actual icing status can be derived from the temperature compensated measurement data.

5.4.1 Cross Sensitivity Effects

In order to ensure proper data evaluation, cross sensitivity effects of the sensor have to be taken into account. Cross sensitivity in this context refers to

physical quantities or effects other than ice, water or air, having effects on the capacitive measurement data. The cross sensitivity effect, which will occur under all circumstances, is the temperature dependance of permittivities. On the other hand, other effects such as changing air humidity or pollution need to be taken into account. A short overview of these effects is also given in this section.

Temperature

As the measurement equipment is exposed to a cold environment, a maximum operational temperature range between -40°C and +85°C can be expected. Besides general effects on the circuitry, this temperature changes have also impact on the the icing measurement results. More in detail, this problem has multiple faces:

- Temperature dependence of the supply voltage causing a temperature dependence of the capacitance measurement due to the supply voltage drift.
- Temperature dependence of the capacitance measurement circuitry (ICs, passive components).
- Temperature dependence of ground capacitances $C_{g,1}$ and $C_{g,2}$ due to temperature dependence of the permittivity of the sensor wire insulation (capacitances between wire and insulation $C_{wi,1}$ and $C_{wi,2}$, compare Figure 5.6) as well as the sensor cable capacitances $C_{p,sc}$.
- Temperature dependence of the measurand on the sensor, i.e. temperature dependance of the coupling capacitance C_c.

While the first two error sources can be compensated by introducing correction factors, the change in offset capacitances in the measurement circuitry can be coped with by introducing reference capacitors with a value close to the sensor cable capacitance $C_{p,sc}$. Furthermore, possible temperature effects of protective filters in the sensor front-end (compare Section 6.3.4), the reference capacitors are also connected via input filter using the same filter structure as for the sensor electrodes.

The temperature dependance of the permittivity of water and ice has to be investigated more in detail: the dielectric properties of ice and snow vary over temperature, frequency and air content. According to [132], at frequencies below 100 kHz, the complex permittivity is highly dependent on the excitation (i.e. measurement) frequency. In the frequency range between 1 kHz and 10 kHz, a permittivity change of 20 % and more is caused by a temperature difference of only 7°C [132]. However, this effect disappears for excitation frequencies of 100 kHz and higher. Also for this reason, it is chosen to use excitation frequencies which exceed 100 kHz.

Air humidity, Pollution, Mechanical Effects

In general, very little dirt adheres to a conductor line surface. Usually, the initial surface oxidation of the aluminium and the diffusion of the steel core's protective grease may change the behavior of the sensor. Further effects to be taken into consideration are as follows:

- **Air Humidity.** Non-condensing air humidity is expected to have only minor effects. The maximum water content of air at 10°C is approx. 10 g per cubic meter and the permittivity of vapor is comparable to that of air. Condensing air humidity causes water droplets, drops or thin water layers on the electrode assembly, causing the measurement circuitry to detect water. A water layer from condensing air humidity can grow in thickness and drop off, it can freeze and form an ice layer or it can evaporate and vanish again.

- **Pollution.** Various sources of pollution with effects on the sensor are possible. For example, flue gases from domestic heating, traffic or industry may accumulate on the sensor surface. This may change offset capacitances and/or the surface properties of the sensor, however, it is supposed that such slow processes concern the whole sensor area uniformly. Bird droppings, leaving irregular pieces of dielectric material with varying water content, are less likely to occur as birds avoid high-voltage power lines as they cause displeasing corona discharges. The probability of such an event is small and there is the expectation that rain and wind would help cleaning the sensor.

- **Mechanical Effects.** Furthermore, there may be effects related to the mechanics of the conductor line. It is expected that there will be expansion, shrinking and torsional motion due to the thermal expansion of the conductor line. According to [133], the thermal expansion coefficient of aluminium is approx. $23.1 \cdot 10^{-6} \cdot K^{-1}$, whereas the value for steel is typically lower. Assuming a total sensor length of 150 mm, the variation over a maximum difference of 120°C is approx. 0.2 % or 0.3 mm. This is well within the typical range of elasticity of all used materials.

In the field tests conducted during this work, none of the mentioned effects could be observed having a significant influence on the measurement data.

5.4.2 Classification

Several parameters have to be considered in order to derive one or multiple indicators which deliver icing status information of the power line: besides the evaluation of multiple measurement electrode distances, also the evaluation of reference capacitors, conductor and circuitry temperature as well as the signal variances have to be taken into account.

Starting at the sensor model and the yielded FEM data, it can be seen that for a certain, relatively small inter-electrode distance (approx. 2 millimeters for a linear electrodes setup as described in Section 5.1.1), a measurement capacitance behavior can be achieved, which delivers a positive change in measured capacitance for ice accretion and a negative signal for water present on the electrodes due to the high shielding effect towards measurement potential.

Figure 5.15 depicts FEM simulated data show this behavior from a thickness of approx. 2 mm.

In all measurement setups (laboratory, field and industrialized setup), it is the main goal to obtain at least one electrode pair which can discriminate between ice and water as described above and to have a second electrode pair which indicates thicknesses above the distance of the discrimination electrode pair (with a maximum thickness typically in the range of the inter-electrode distance. This is the minimum configuration which equals three measurement electrodes and a measurement ground electrode. Not only the nominal capacitance depends on the electrode distance, but also both the minimum and the

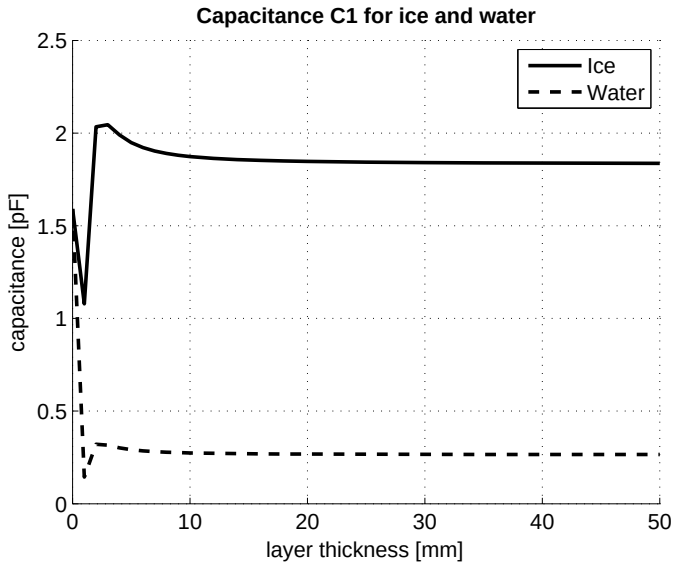

Figure 5.15: 2D FEM simulation data for ice (solid line) and water (dashed line) on an electrode setup with approx. 2 mm inter-electrode distance. From a distance of 2 mm, water and ice capacitance readouts do not share the same range of values.

maximum capacitance measurement value due to ice formation. Additional information can be extracted from the timely run of the capacitance signals, especially on growing or shrinking ice layers and water drying/evaporating processes.

Robustness can be achieved against artifacts, short but strong signal variations or small water droplets (not forming a layer) on or between measurement electrodes by inserting more electrodes, thus forming multiple measurement capacitances. For both field tests and industrial prototype, four measurement capacitances per sensor are used. The optimum electrode distance strongly depends on its geometry, the covering layer and its permittivity.

By means of evaluating the signal noise level during icing, the presence of droplets can be derived such that hoarfrost icing can be separated from in-cloud icing.

Icing from freezing rain and icing from fog or air humidity can be distinguished as they start from different capacitance levels: on average, a “fog” icing signal will (after a small dip) increase and then decrease; a “freezing rain” signal will start from its absolute minimum and rise from that point.

Temperature compensation and the impact of signal variances are covered

in Chapters 8 and 9, respectively.

Data evaluation is conducted by means of a least square fit between the temperature compensated, offset-freed measurement data and a data set of thickness versus permittivity for each electrode distance.

Chapter 6

Experimental Environment

This chapter draws on the results from the investigations presented in the previous chapters in order to design a test device. As depicted in Figure 6.1, this device comprises the following parts:

- An energy harvesting system (Section 6.1). The electrical design of the capacitive energy harvesting system is derived from the estimated power demand of the sensor node platform and of the measurement system. The mechanical components are designed to fulfill the requirements with respect to the choice of suitable materials and long-term stability in the given environment.
- A sensor node platform (Section 6.2). In this section, the circuitry is explained comprising microcontroller and data transmission systems. This part transmits the measured data to the host computer.
- A measurement system (Section 6.3). This section gives information on the chosen capacitance icing measurement approach, the solution of the decoupling approach derived in Section 5.3.3 and the required input filters as described in Section 6.3.5.

6.1 Energy Harvesting System

This section describes the development and implementation of an energy harvesting system based on the alternating electrical field of the overhead power

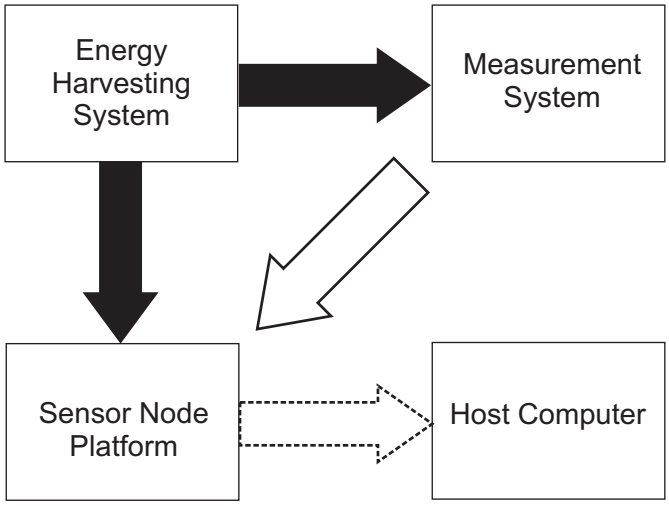

Figure 6.1: Block diagram of the test device environment, comprising the energy harvesting system, measurement system, and sensor node platform, which includes the data transmission circuitry and transmits the data to a base station or a remote host computer. Black arrows indicate energy supply paths while white arrows indicate data paths.

line. First, the electrical design is determined (Section 6.1.1). Then, the design is implemented in hardware for laboratory and/or field use.

In earlier work [19], [130], it could be shown that an energy harvesting system based on the alternating electrical field (i.e., a capacitive voltage divider) can deliver a sufficient amount of power to supply the measurement and data transmission circuitry. This approach could be successfully shown in laboratory experiments. This section describes the development of a test device suitable for outdoor use, mounted at a 220 kV overhead power line.

6.1.1 Electrical Design

In a first step, the power demand of the entire circuitry needs to be evaluated. The design of the energy harvesting circuitry can thus be determined. After

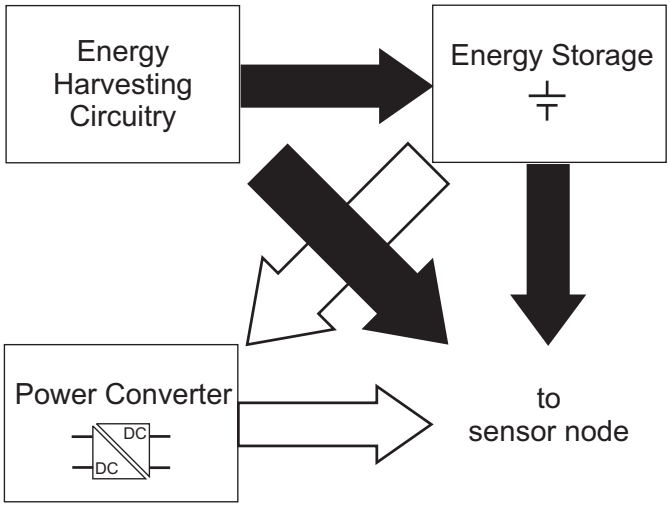

Figure 6.2: Block diagram of the energy harvesting system (black arrows: energy transfers, white arrows: monitoring data paths).

setting the dimensions of the capacitive voltage divider, a suitable transformer needs to be chosen as well as an energy storage system needs to be implemented on the one hand for peak power demands, and on the other hand for bridging periods of shut-down lines. Figure 6.2 depicts an overview of the energy harvesting system's key components: the energy harvesting circuitry, energy storage and the power converter. The sensor node is not only supplied with power from the energy harvesting system but also monitors its status. Besides, a suitable over-voltage protection has to be included in the setup in order to protect the circuitry from voltage spikes due to either nearby lightning strikes, power faults or switching processes at transformer stations.

Power Budget

The main electrical design parameter for the harvesting circuitry is its required power output. For autonomous operation, it is desired to avoid dedicated relay stations between sensor node and host. Therefore, commercial GSM networks

seem to be the most promising way of data transmission. This well-established technology allows for a fully independent operation of the sensor nodes, if necessary.

As the power consumption levels of microcontroller and measurement circuity are negligible compared to the RF output power of up to 2 W of a GSM modem (this level is also due to the required transmission range of up to more than 10 km), the GSM modem is the major energy consumer of the setup. The peak power consumption of the GSM modem therefore amounts to 8 W (current peaks demanded by the transmitter may reach up to 2 A for periods of 5 ms at 3.7–4.2 Volt, compare [134]).

Figure 6.3 depicts the record of a simplified measurement and data transmission cycle including the GSM network log-on. In the first few seconds, only the microcontroller and the measurement circuitry are active, requiring very low power. Then the GSM modem is turned on. After powering up, the GSM modem is in receive mode (checking the network availability), consuming approx. 600 mW. Then, the GSM modem switches to transmission mode for the network log-on process. The power demand rises drastically to more than 2 W (seconds 12-16). Then, the modem switches to idle mode, still remaining connected to the network. The modem is configured by the microcontroller to send a short message and receives the text to be transmitted. The wireless data transfer starting at second 30 causes a high (but pulsed) power demand. At the end of the measurement and transmission sequence, the GSM modem remains idling [4].

The average power consumption of the entire cycle amounts to less than 400 mW. However, this is for an unusually high data transmission duty cycle. Under real-life conditions, data transmission would take place only once every hour, on demand or when trigger levels are reached. In order to cope with repetitive cycles of network log-on and high transmitting power levels, the total power output of the energy harvesting system is designed to this worst-case scenario and therefore needs to deliver a continuous power of 400 mW and additionally provide sufficient energy to recharge the backup battery within a reasonable time. Summarizing this, the output of the harvesting circuitry should range in the area of $>$100 mA at 4 Volt.

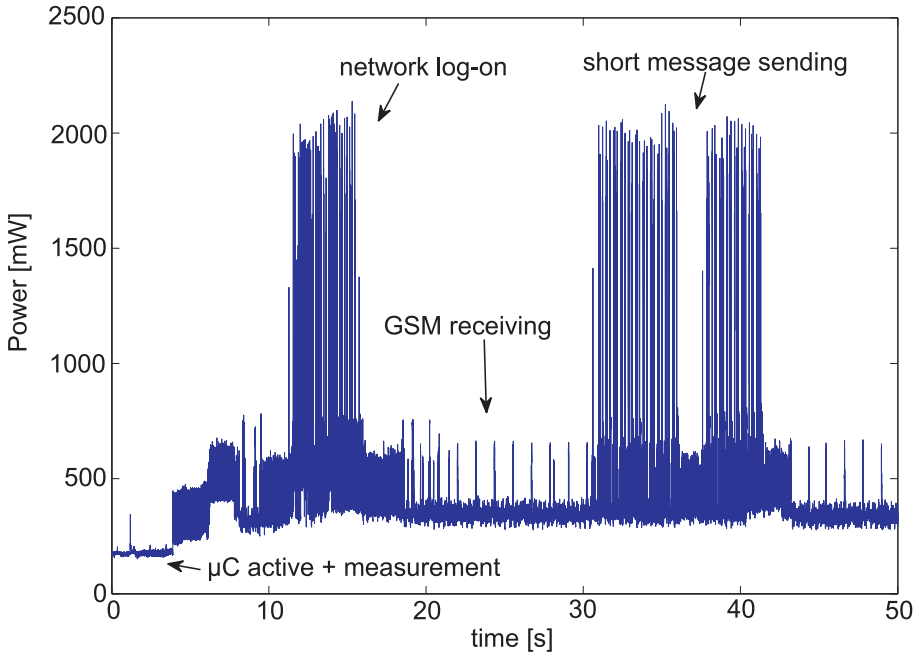

Figure 6.3: Power consumption for a simplified measurement and data transmission cycle [4].

Harvesting Circuitry

The key components of the energy harvesting system are the capacitive voltage divider, the voltage transformer and the shunt regulator. Besides, a bridge rectifier and a storage capacitor are included in the setup. Figure 6.4 depicts a block diagram of the harvesting circuitry.

The conductor can be regarded as a line source with respect to ground. By inserting a conductive hollow cylinder (i.e. the harvester "shell", in the current test device realized by means of aluminium foil on a plastic cylinder), a capacitive voltage divider is formed by the harvester capacitance $C_{co,sh}$ and the harvester ground capacitance $C_{sh,e}$. Both the electric potential of the conductor rope V_{co} (towards the harvester shell) and the potential of the harvester shell (towards earth) V_{sh} are decaying with the natural logarithm of the distance r. For a 220 kV line, this leads to field gradient of several kV within the first few millimeters of distance from the conductor's surface. As the expected currents range around several hundred μA at a voltage of several kV, a transformer is required. A purpose-made 5kV/20V transformer is connected in parallel to the harvester capacitance $C_{co,sh}$. By means of a shunt regulator, the harvester

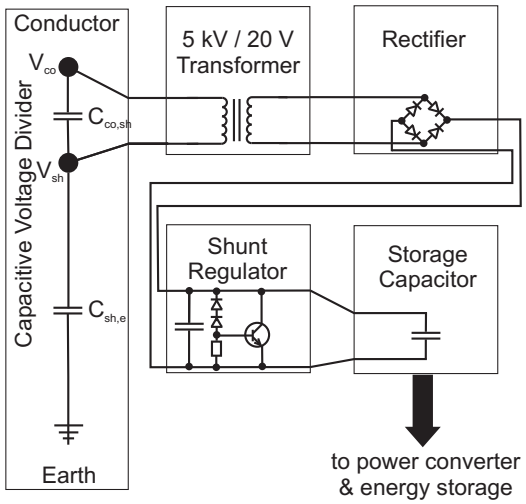

Figure 6.4: Block diagram of the energy harvesting circuitry. A capacitive voltage divider is formed by the harvester capacitance $C_{co,sh}$ and the harvester ground capacitance $C_{sh,e}$ between the conductor rope potential V_{co}, the harvester shell potential V_{sh} and earth.

shell potential is clamped to a maximum of 5 kV with respect to the conductor (this limit is given by the insulation strength of the transformer). Given that, a trapezoid voltage is present between conductor and harvester shell (i.e. on the transformer's primary side). Power can be drawn from the transformer's secondary side as long as the equivalent impedance of the transformer is within the order of magnitude of the capacitance between conductor and harvester shell. After rectifying and smoothing, the harvested energy is fed to energy storage and power converter. For the given power demand of >400 mW, the test device dimensions are well oversized as in laboratory tests the device was already operational at a voltage of 90 kV with respect to ground 7.2.3, while being designed for operation at a line with a nominal voltage of 130 kV.

The harvester shell is based on a warning sphere with a diameter of 60 cm, as it is used for marking ground lines and transmission towers. This sphere is cut in two halves and a cylindric part is inserted in-between. The cylindric part of the conductor shell has a length of 50 cm and the same diameter as the sphere, i.e. 60 cm. The diameter of the aluminium pipe, housing the conductor rope is 50 mm.

The harvester capacitance $C_{co,sh}$ (the inner capacitor) can be approximated as a coaxial cylinder capacitor and calculated the equation 6.1 (with $r_1 = 0.05\ m$, $r_2 = 0.3\ m$, $l = 0.5\ m$), according to [100],

$$C_{co,sh} = \frac{2\pi\epsilon_0\epsilon_r l}{ln(r_2/r_1)} \tag{6.1}$$

which amounts to a nominal capacitance in dry air of 15.5 pF.

The harvester ground capacitance $C_{sh,e}$ (the outer capacitor) can be approximated as a cylinder over an infinite plane and is calculated following equation 6.2 (with $h = 15\ m$, $r = r_2 = 0.3\ m$, $l = 0.5\ m$), according to [100],

$$C_{sh,e} = \frac{2\pi\epsilon_0\epsilon_r l}{acosh(h/r)} \tag{6.2}$$

which amounts to a nominal capacitance in dry air of 6.5 pF at a height of 10 m. Due to the comparatively large distance with respect to its dimensions, a variation of the mounting height (i.e. the distance to ground) only has small impact on the harvester ground capacitance $C_{sh,e}$ (for instance, 6.1 pF at a height of 15 m).

Energy Storage

The electrical power supplied from the output of the harvesting circuitry needs to be properly transformed from the 20 V level in order to supply the sensor node and measurement circuitry. This is achieved by means of a battery management circuitry (charging/discharging the backup battery) and a DC/DC step-down voltage converter, which feeds a second storage capacitor at 4 Volts. This voltage is chosen due to the requirements of the GSM modem, which is designed for 3.7–4.2 Volts operation, i.e. lithium polymer or lithium ion batteries at any state of charge. However, these battery technologies are not suitable for low temperature applications. Since nominal cell voltages of other battery technologies are typically lower, at least two of these cells must be connected in series.

Rechargeable batteries were included in the system to ensure operations over longer periods of power outages or during system maintenance. Two technologies were tested:

- Lithium-Iron-Phosphate ($LiFePO_4$). This is a relatively new technology which (as of 2011) seems to be a stable and durable type of rechargeable lithium batteries. Operating temperatures range down to -20 degrees Celsius, the cells provide good self-discharge characteristics and show good long-term stability. The typical field of application for this battery type are commercial electrical vehicles (EV). In the present application, two cells are connected in series with a nominal capacity of 2 Ah. Difficulties arise from the series connection of cells. Lithium cells typically need a balancing circuitry, which is an additional energy consumer [135].

- Nickel-Cadmium (NiCad). This technology has a comparatively long history and represented the first commercial household battery replacement rechargeable cells in the 1990s (starting with AA and AAA cells). NiCad batteries show good behavior at high discharge currents (for example, in portable electric tools) as well as at low temperatures. Furthermore, they can be trickle charged at a small current without taking damage [136]. However, they suffer from the so-called memory effect and contain cadmium, which is a poisonous heavy metal. Its use in electronics will be further restricted in the immediate future by the guideline on reduction of hazardous substances (RoHS). For the test device setup (which implies that only a small number of cells are used for a limited time), 5 cells in series with a nominal capacity of 1.7 Ah are used.

Both battery types require a suitable charging circuitry and have been successfully tested in laboratory and field tests. Another battery technology, Nickel-Metal Hydride (NiMH), was not taken into account for the tests due to its inferior low-temperature charging performance (with respect to NiCad) and more complicated charging circuitry. As mentioned earlier, NiCad batteries allow for continuous trickle charging while NiMH typically requires triggering the end of the charge cycle via a voltage measurement over time. Nevertheless, NiCad batteries are not suitable for a volume product because of their cadmium content.

The nominal energy capacity of the batteries is 10 and 13 Wh for the NiCad and the LiFePO4 battery, respectively. Assuming a DC-DC conversion efficiency of 90 % and a discharge ratio of 80 %, the energy stored in the batteries

can supply the measurement system for approx. 17 and approx. 20 hours, respectively. However, these times can be enlarged by orders of magnitude if the GSM modem is turned off or measurement intervals are increased. This could be done automatically, as battery voltage, voltage drift between cells and the energy harvesting system's operational parameters are continuously monitored by the sensor node.

Over-Voltage Protection

Over-voltage protection on the primary side of the transformer is necessary as a sudden increase of the power line voltage leads to an increase of the conductor-to-harvester voltage as well and may cause high transient currents. As the high-voltage transformer is designed for a continuous primary voltage of 5000 V, an over-voltage protection needs to work from a voltage very close to this threshold. For a basic test device implementation, a series connection of 25 bidirectional SMP100 Transient Voltage Suppression (TVS) diodes has been implemented. The maximum capacitance of a single diode of 45 pF is divided down to less than 2 pF due to the series connection of 25 elements. This diode chain is connected in parallel to the transformer's primary side. The diodes provide a low leakage current of 2 μA while carrying repetitive peak pulse currents of 100 A.

6.1.2 Mechanical Design and Housing

For the first generation test device [19], a sheet of copper was bent into a cylindric shape and equipped with a voltage and current measurement device. The mounting on the line was established by means of nylon cable ties.

In order to obtain a device suitable for a high voltage laboratory test, it has to fulfill requirements on mechanical stability, follow restrictions on the used materials and be compatible with the high-voltage environment (i.e. high alternating electrical field strength and the exposure to partial discharges). The second generation test device therefore was designed and built by extending a 60 cm diameter warning sphere (as it is used for indicating ground lines) by a cylindric section with a diameter of 60 cm and a length of 50 cm (fabricated by polymer welding). This device is depicted in Figure 6.5 as mounted on a

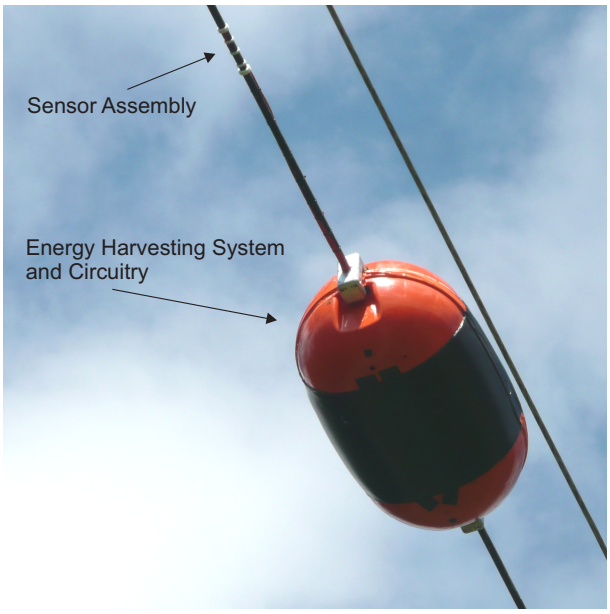

Figure 6.5: Photograph of the test device mounted on a conductor rope.

conductor rope in the field. The cylindrical section is covered with a conductive foil on its inside. As a further mechanical improvement, this foil was fixed with a welded conductive mesh for long-term mechanical stability. For mounting the device onto a conductor rope, high-voltage compatible (i.e. rounded) mounting clamps were made from massive aluminium. In a later re-work, a conductive pipe was introduced in order to ensure exact positioning of the conductor rope within the cylindric section as the position is crucial for reliable operation. Details on the mechanical solution can be found in Figure 6.6.

[19] investigated if icicles, which may form at the surface of the harvester tube, might reduce the harvested power due to partial discharges. By means of welding wires to the harvester shell it could be shown experimentally, that even though there are strong corona effects, no negative impact on the harvester functionality or wireless data transmission could be observed.

6.2 Sensor Node Platform

The sensor node platform is designed to perform the following tasks: control, data processing, acquisition of measurement data regarding the status of the energy harvesting system and measurement data transmission to a

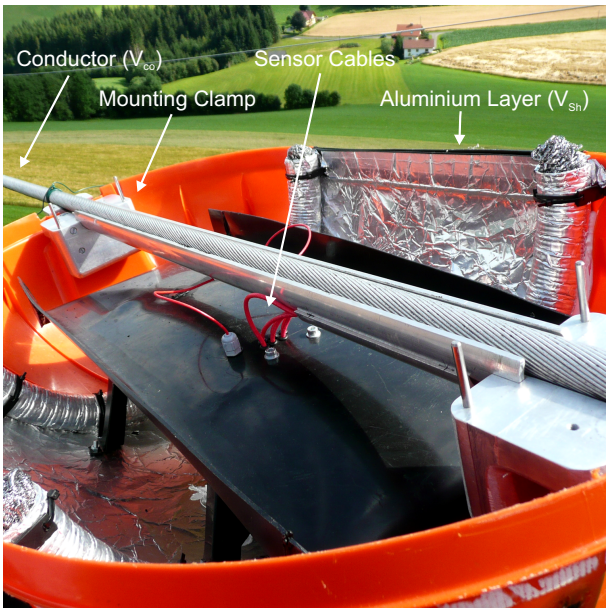

Figure 6.6: Photograph of the lower part of the test device during mounting. The black plastic part below the conductor rope works as a shed to minimize the amount of water dripping or leaking over the circuitry. However, it may occur that the whole device rotates (at least to a certain extent) with the conductor rope due to temperature changes.

host computer. For early (lab, short-term) test setups, very basic platforms (such as battery-powered transmitters, ISM transmitters or third-party sensor nodes [137], [138]) were utilized. For the field tests, a new platform was designed as none of the available platforms had available GSM communication, the required input voltage range nor suitable capacitive measurement circuitry. The data paths of the sensor node are depicted in Figure 6.7: the micro controller (μC) works as a central processing unit. A state machine polls data from the energy harvesting system in order to monitor its operational state as mentioned above, it configures the capacitive icing measurement system and process the measurement data. Via commercial GSM networks, data is sent to a host computer. This data path is bidirectional, which enables remote configuration changes. The second data path uses an ISM transmitter, which acts as a backup communication path.

In order to provide a versatile platform, a laboratory setup based on an ATMEL AT90CAN128 8-bit micro controller was redesigned: the clock frequency was reduced to 8 MHz, thus being also able to reduce the operating voltage

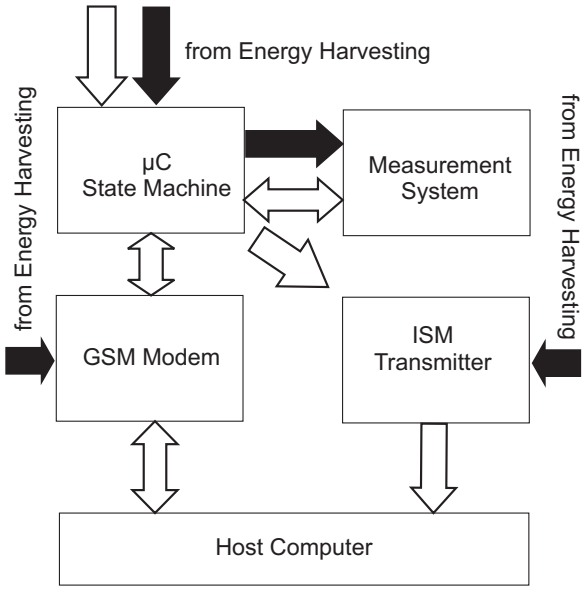

Figure 6.7: Block diagram of the sensor node platform. Black arrows indicate energy transfers (the energy harvesting circuitry powers all components). White arrows indicate data paths (information from harvesting system and measurement circuitry is evaluated and transmitted via GSM (bidirectional) and ISM (unidirectional).

to 3.3 Volt ("μC board)". Furthermore, a stack PCB carrying a GSM modem including the connections to the ISM transmitter was designed and built ("communication board"). On a third PCB, the measurement system (including the capacitive sensor IC) was placed ("measurement board"). Figure 6.8 depicts this PCB stack.

6.2.1 Microcontroller

The following criteria have been taken into account for choosing a suitable micro controller for the given application:

- Low power consumption
- Versatility with respect to different measurands and communication channels
- Computational power and scalability
- Connectivity, I/O functionalities

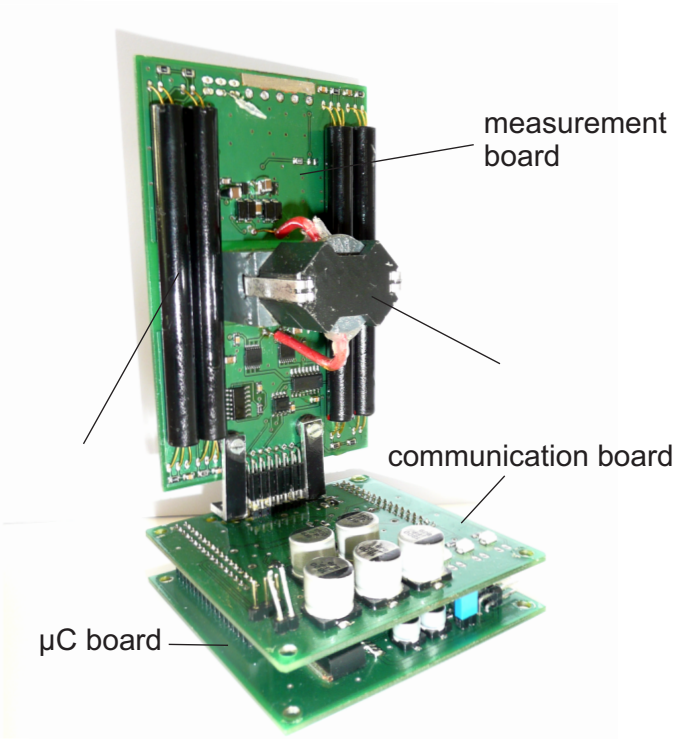

Figure 6.8: Photograph of the complete measurement PCB stack.

- Industrial temperature range (-40 – +85°C)

An ATMEL AT90CAN128 was chosen, as a free development environment is provided and previous good experiences with the IC were available.

6.2.2 Data Transmission

At first, well-developed commercial GSM networks looked most promising as the primary way of data transmission for the following reasons:

- Good area coverage (despite possible blind spots, for instance, in mountainous areas).
- Several providers.
- Off-the-shelf hardware available.
- Expected long future time of operation due to a large number of current subscribers.

- Low costs for data transmission, availability of flat-rate packet data services with permanent network connection.
- No need for further relay stations or repeaters (i.e. no need to power and take care of these devices either).
- No need for further devices or modifications on the transmission line (compared to wire-bound data transmission).

However, as already anticipated in Section 6.1.1, the drawback of GSM is its comparatively high power consumption. The maximum output power of the GSM module [134] is 2 W in the 900 MHz band and 1 W in the 1800 MHz band, respectively. Additionally, due to the time division multiplex character of the transmission (216 slots per second), high power peaks have to be supplied. In idle mode, the required continuous power is almost negligible. However, in terms of energy, the receiver power consumption accounts for the predominant part of the overall energy budget of the circuitry.

The antenna type and shape and its position within the harvester are crucial for a continuous network connection. However, several boundaries are given by available antenna types, gains, directional patterns and physical dimensions as well as allowed mounting positions within the test device due to the electrical field distribution. As the antenna is typically connected to and operating with respect to power ground, it may not be located far from the harvester's outer shell while at the same time the metallic shell might have negative effects on the directional pattern of the antenna or de-tune it. In the half-spherical sections of the outer shell, the field gradient is calculated to be very high, which means that an antenna in this section works as a tip generating partial discharges.

The initial configuration comprised a horizontally mounted, omnidirectional stub antenna at a small distance from conductive part of the harvester shell (compare Figure 6.9). After a redesign, the antenna was mounted within a window in the metallic layer of the outer harvester shell (compare Figure 6.10) during the second field test, which yielded much better network quality measurements.

Besides, the setup was extended by a second data transmission path at UHF ISM frequency (433 MHz) due to difficulties with the GSM network availability during the first field test. The measurement data was transmitted

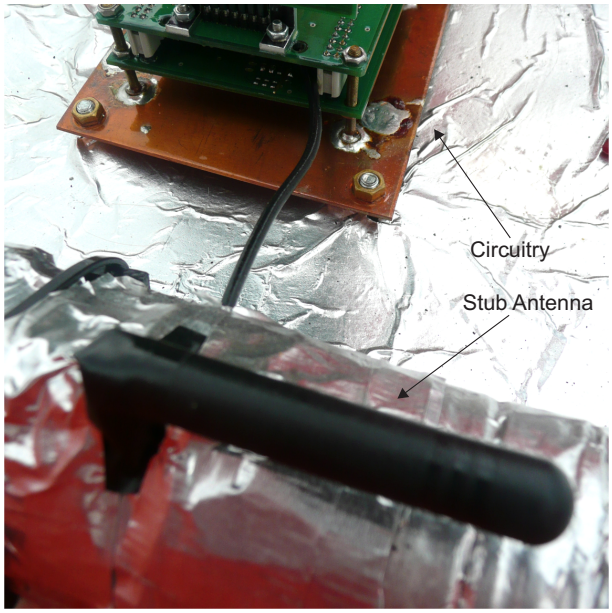

Figure 6.9: Antenna location in the first field test - on the edge of the harvesting metallic layer.

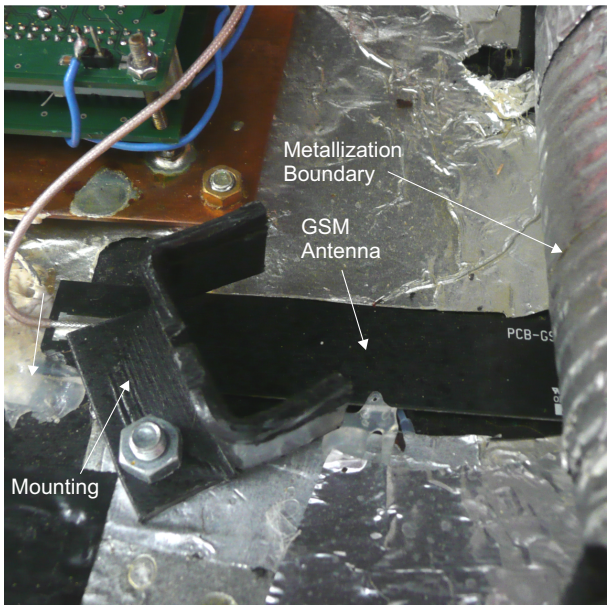

Figure 6.10: Antenna location in the second field test, in a window within the metallic layer of the harvester shell

via a standard Texas Instruments module [139] to a second module connected to the weather station on ground.

6.3 Measurement System

This section covers the components of the measurement system, comprising the following units (compare also Figure 6.11):

- The sensor electrode assembly (comprising the sensor electrodes and the required mounting system for a conductor rope),
- the capacitance measurement circuitry,
- decoupling circuitry between measurement system and sensor node & alignment of components with respect to electrical and magnetic fields,
- input filters of the capacitance measurement,
- EMC considerations with respect to the capacitive sensor front-end and
- conductor temperature measurement & reference measurements.

6.3.1 Sensor Electrode Assembly

In Chapter 5.1.1, two electrode geometries (circular and linear electrodes) were presented. For a field test device, the choice is limited not only by the input ranges of the available capacitance measurement circuitry, but also by the availability of production facilities (both machining and shape forming of PTFE are sophisticated tasks) and by the necessity of a system which can be securely mounted on a conductor surface without big effort. For this reason, linear electrode setups have been realized for the first test device setup.

PTFE cabling and sensor wires were chosen for the first realization attempt due to both their adequate material properties and their commercial availability, for example, for airplane applications. PTFE provides good stability towards environmental conditions (UV radiation, water, ice, high and low temperatures). For the first icing detection experiments, the measurement electrodes were built by a standard coaxial cable with removed (outer)

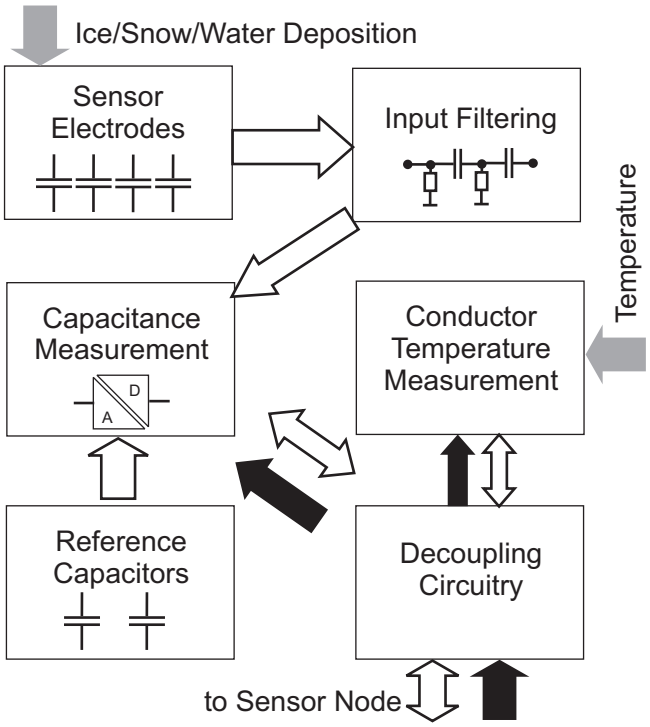

Figure 6.11: Block diagram of the measurement system. Black arrows indicate energy supply paths, white arrows indicate data paths and grey arrows indicate measurands from the environment, i.e. material deposition on the sensor electrodes and conductor temperature.

shielding layer in the sensitive area. This allowed for easy prototyping and modifications during the experiments. A coaxial PTFE cable was used for the first field test in the high voltage environment. Figure 6.12 depicts the sensor as mounted on the conductor line in the first (2009/2010) field test.

In the second (2010/2011) field test, sealed joints were established between sensor cable and sensor electrodes. As a consequence, thinner sensor electrodes could be used allowing to keep a larger amount of conductor surface area open between the electrodes, thus allowing for a sensor behavior closer to the natural environment. The mounting clamps are also made from PTFE and have a very low profile as depicted in Figure 6.13. The first clamp from the left additionally contains and protects the wire joint between sensor cable and sensor electrode wire.

After tearing back the cable into the measurement wire insulation for approx. 1 cm, the insulator ends were sealed against humidity by means of fluo-

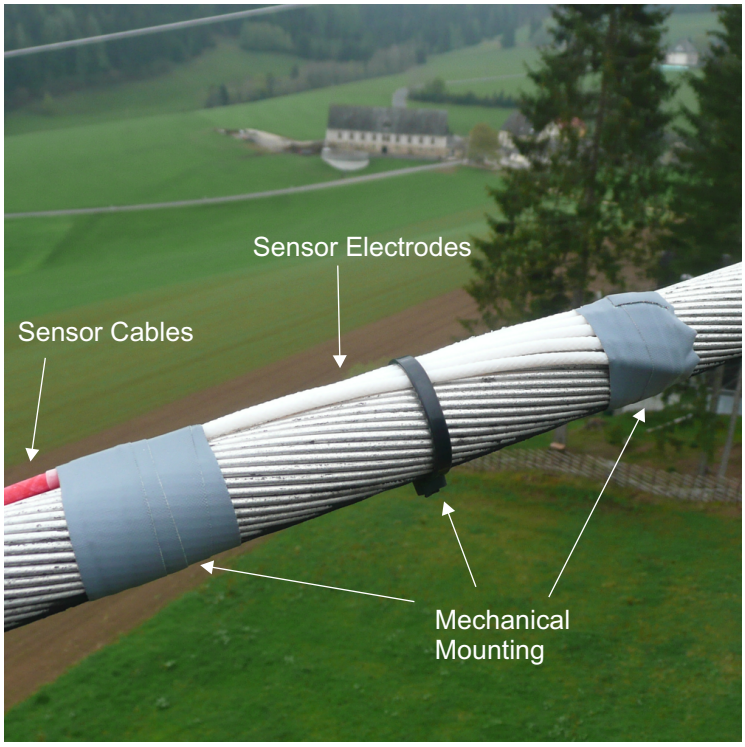

Figure 6.12: Photograph of the first generation field test sensor. Five measurement electrodes (white insulation) are mounted to the conductor rope by means of cable ties and special adhesive tape. The sensor cables (red) connect the electrodes with the measurement circuitry in a distance of approx. 1 m.

ropolymer heat shrink tubes with an inner glue coating. Then, these prepared ends were placed in holes within the rightmost part of the sensor mounting clamps (cf. Figure 6.13).

6.3.2 Capacitance Measurement

There are various technologies available for a reliable measurement of capacitances in the range of few picofarads, differing in their sensitivity towards noise, stray capacity (capacitance towards measurement ground predominantly resulting from the shunt resistances and the availability of bandpass filters:

- DC measurement
- Oscillators (RC, IC, LC)

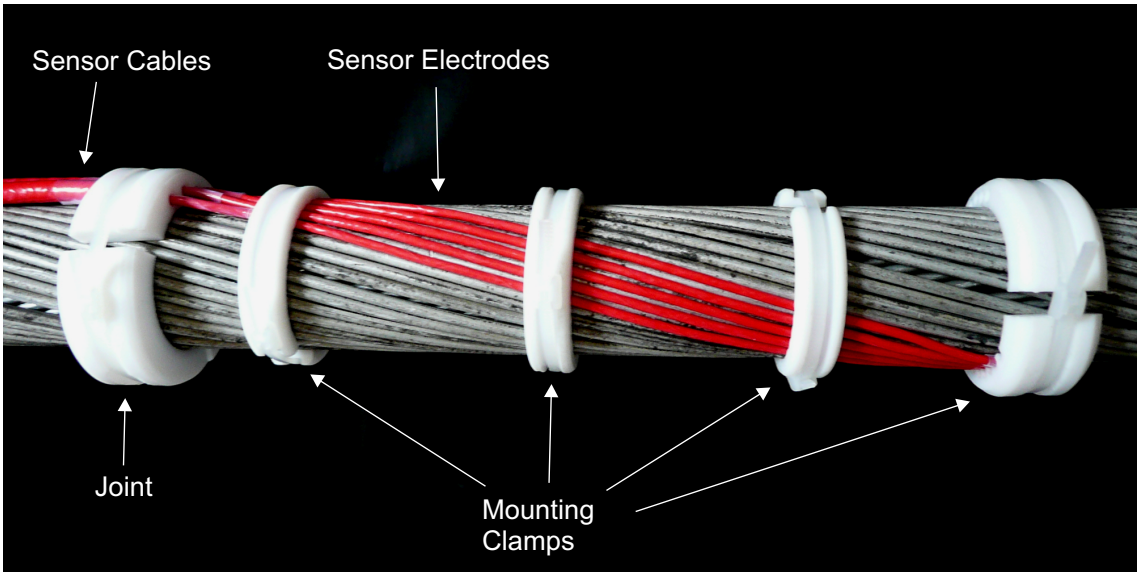

Figure 6.13: Photograph of the second generation field test sensor. The sealed joints between sensor cables and sensor electrodes are housed in the first clamp from the left. The rightmost clamp contains the sealed cable heads.

- Synchronous demodulators (AC signals in the 10kHz – 1MHz range), demodulated by means of High-Z, Low-Z or feedback amplifiers. Sine or square waves are used for excitation, [100].

Commercial capacitance-to-digital converters (CDCs) [140] are used for the present test device setup. These devices can evaluate up to 16 measurement capacitances in the picofarad range with resolutions between 12 and 24 bit. The CDC used for the present test device setup provides 8 input channels, with a capacitance range of 2 pF at a resolution of 16 bit, which is a sub-femtofarad resolution. The excitation source of the CDC operates at a nominal frequency of 240 kHz and is able to drive a maximum output load of 250 pF. This is sufficient for the standard field of application of these ICs, which is capacitive touch controlling for electronic devices. In the present case, it has to be taken into account that the shielded coaxial cable connecting the CDC with the sensor electrodes has a capacitance of 100 pF per meter. The capacitance of the excitation electrode at the conductor surface ranges within the same order of magnitude as the cables are identical. Thus, the maximum distance between CDC and sensor electrodes is limited by the maximum output load as specified by the manufacturer (250 pF between excitation and ground according to [140])

and the allowance of stray capacitances (i.e. less than 40 pF of capacitance between any CDC input and ground). The measurement ICs are controlled and read out via an I^2C bus, which is a 2-wire bidirectional bus also known as Two-Wire Interface (TWI).

6.3.3 Decoupling and Positioning

In this section, the test device implementation of the decoupling approach developed in Section 5.3.3 is described.

Two paths have to be established: an insulated power transmission path and an insulated bidirectional data path. "Insulated" in this context refers to two electrical parameters: on the one hand, dielectric strength and robust operation with respect to a continuous potential difference of 5000 Volt. On the other hand, the capacitance introduced by decoupling has to be as small as possible (below 250 pF to ensure a voltage division ratio of 1:25 (5 kV:125 kV).

Among the two paths, the power path is comparatively easy to establish: as the sensor circuitry only has a total power demand of a few milliwatt, a small isolated transformer operating at a high frequency is a suitable solution.

The bidirectional data transmission path is more challenging to implement: In a first approach, it was investigated if isolating transformers as used for audio applications, network cards or telephone equipment, could be used to transfer the capacitive measurement signals (excitation square waves and receiver signals) between the two different ground levels. These isolation transformers can provide an insulation voltage of 5 kV and introduce only a small additional coupling capacitance of typically 20 pF. Figure 6.14 depicts this decoupling principle, the grey-shaded part in the Figure is referred to the conductor rope potential V_{co}.

Unfortunately, this setup can not be used at the present measurement excitation frequency as the maximum excitation current is exceeded. The coupling capacitances between primary and secondary coil are comparatively large and the insulation voltage as given in the data sheet is not guaranteed for continuous operation.. In fact, the realization of this principle is prevented by the lack of available components.

Consequently, the next evolutionary step was a complete separation of the sensor circuitry (including CDC) from the micro controller. At first, this was

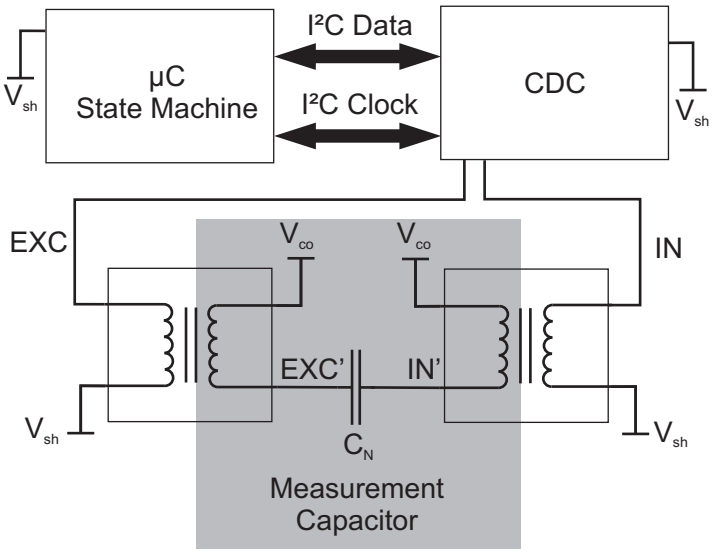

Figure 6.14: Schematic of the decoupling approach by means of isolation transformers. The analog measurement signals are level-shifted via isolation transformers.

achieved by means of bidirectional integrated I^2C bus isolators [141]. These are off-the-shelf components for approx. 800 V continuous isolation voltage, certified to withstand 5 kV for a duration of 1 minute at a temperature of 105°C. These devices were successfully tested at the maximum voltage for several hours. The setup was used for high-voltage icing laboratory measurements as described in Section 7.2.3. The block diagram of this decoupling approach is depicted in Figure 6.15, the grey-shaded part in the figure refers to the conductor rope potential V_{co}.

For long-term use during field tests, data path decoupling was realized by means of bidirectional I^2C bus buffers [142] and optical couplers [143] suited for an isolation voltage of 50 kV. This allows for a long-term stability at a continuous voltage of 5 kV or above. Figure 6.16 depicts the schematic of the discrete circuitry replacing the two I^2C isolators.

Further measures have been implemented in order to ensure a proper lifetime of the circuitry:

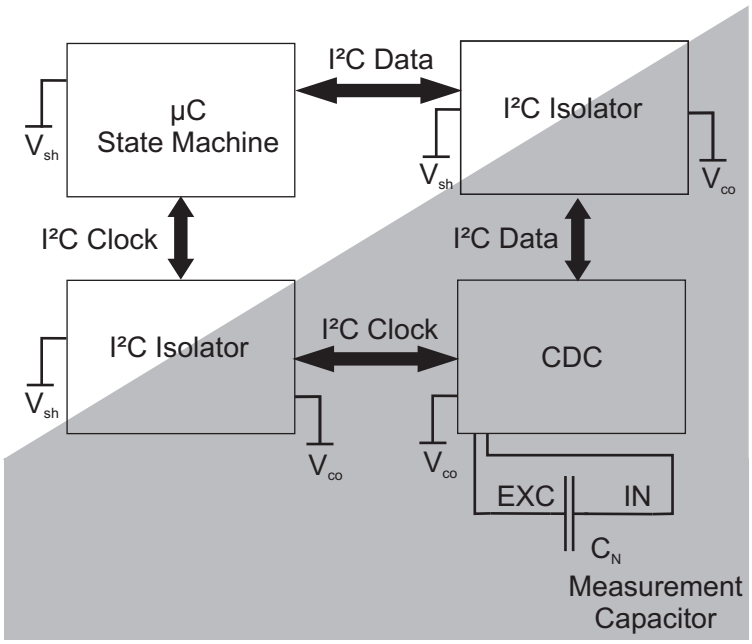

Figure 6.15: Schematic of the decoupling approach using integrated bus isolators. The digital two-wire bus signals are bidirectionally level-shifted by integrated circuits.

- The sensor PCB including the decoupling circuitry is mounted in vertical orientation (i.e. in parallel to the electric field lines) with respect to the rest of the circuity in order to keep additional parasitic capacitances between conductor and harvester shell low.

- The area of the sensor PCB exposed to the alternating magnetic field is minimized in order to avoid effects on the measurement circuitry due to induced voltages. This is achieved by embedding all boards in the plane of the magnetic field of the conductor.

- In high-voltage engineering, minimum distances can be estimated in order to avoid creepage currents. Dry air has a dielectric strength of approx. 3 kV per mm, however, this value is significantly lowered with increasing air humidity. Also, the materials in use (FR4 PCB material, PTFE) provide a high (more than 20 kV per mm) dielectric strength [144]. A problem arises as soon as water is present at any surface due to the high relative permittivity and possible conductivity

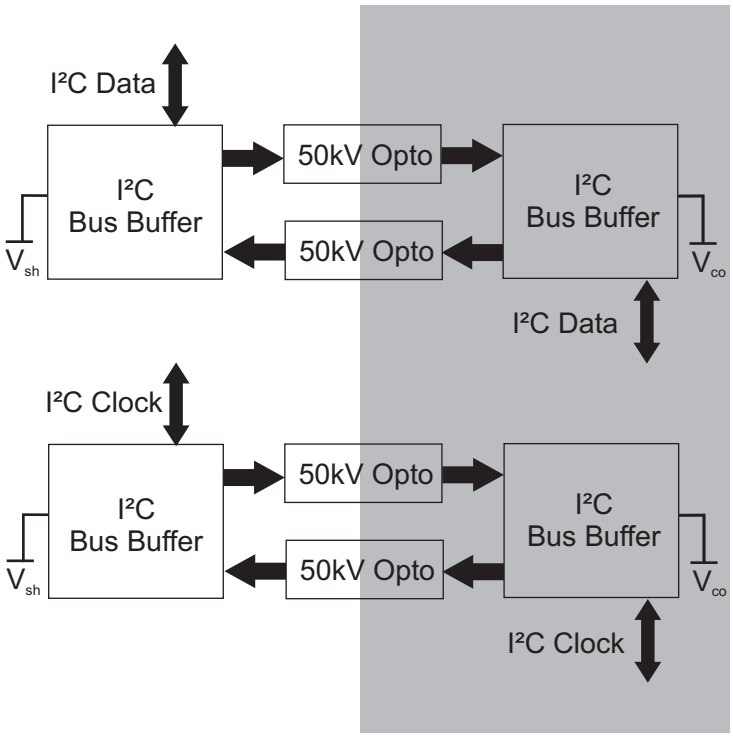

Figure 6.16: Schematic of the I^{2}C isolation using 50 kV optical couplers and bidirectional bus buffers. I^{2}C bus buffers convert the bus wires into two unidirectional data paths, which are level-shifted by means of the optical couplers.

of water. Therefore, in a first approach, a protective film was sprayed, whereas later on, the entire circuitry was sealed in an elastic silicone polymer.

The complete measurement PCB stack with the decoupling solution (but without the sealing polymer) is depicted in Figure 6.17.

6.3.4 Input Filtering

The capacitance-to-digital converter provides an internal 50 Hz filter to avoid disturbances, i.e. a lowered signal-to-noise ratio from power cables and other sources which emit the grid AC frequency. However, additional input filtering is required in order to protect the circuitry as the maximum input current of the receiver channels is limited to 10 mA per channel [140] and an AC voltage of several kV at a frequency of 50 Hz is present between these channels and measurement ground (i.e. the conductor rope potential V_{co}). This occurs

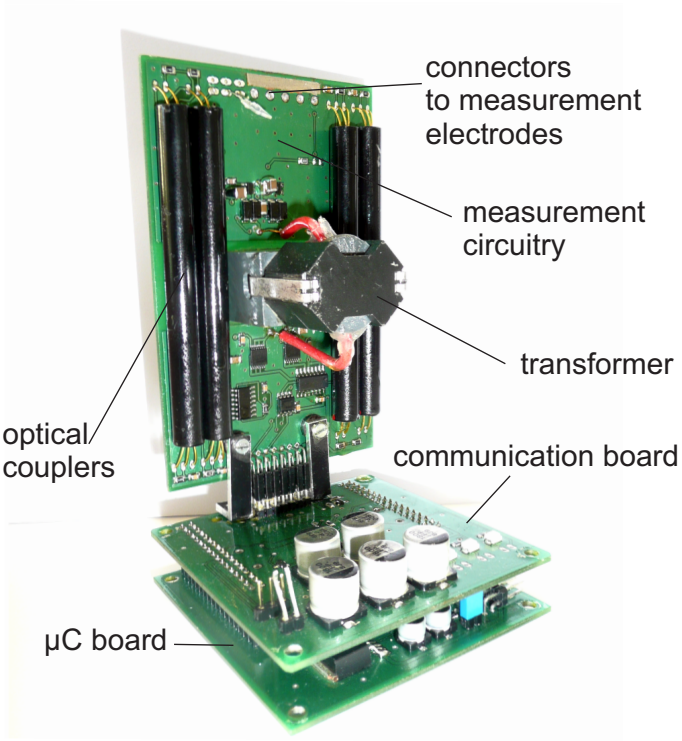

Figure 6.17: Photograph of the complete measurement PCB stack with the decoupling solution using 50 kV optical couplers.

on each channel due to the non-zero distance between the measurement electrodes and the conductor surface, positioned within the area of the highest field gradient. In order to protect the inputs, this 50 Hz input currents need to be minimized. This is achieved by means of input filters, which separate the 50 Hz disturber from the 240 kHz measurement carrier frequency (as specified in the CDC data sheet [140]). The input circuitry as depicted in Figure 6.18 was experimentally found. In the schematic, V1 is the sweep source. C_{cab} represents the given parasitic capacitance of the coaxial sensor cables $C_{p,sc}$. The dedicated filter elements comprise R_1, C_f and R_2.

Figure 6.19 depicts the frequency response of the filter circuitry. For the desired input frequency, both amplitude and phase remain nearly unchanged while both low and high frequencies are cut by 20 dB per decade.

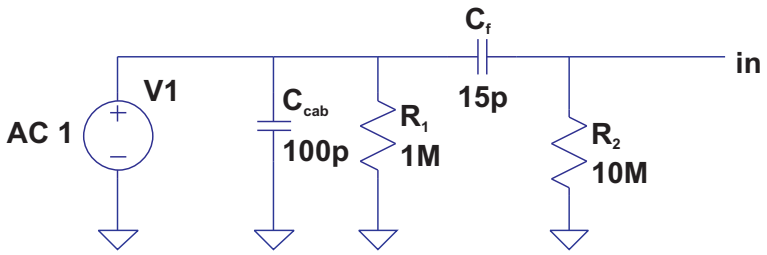

Figure 6.18: Schematic of the external input filters of the CDC capacitive inputs. $V1$ is the sweep source, C_{cab} represents the parasitic sensor cable capacitance $C_{p,sc}$.

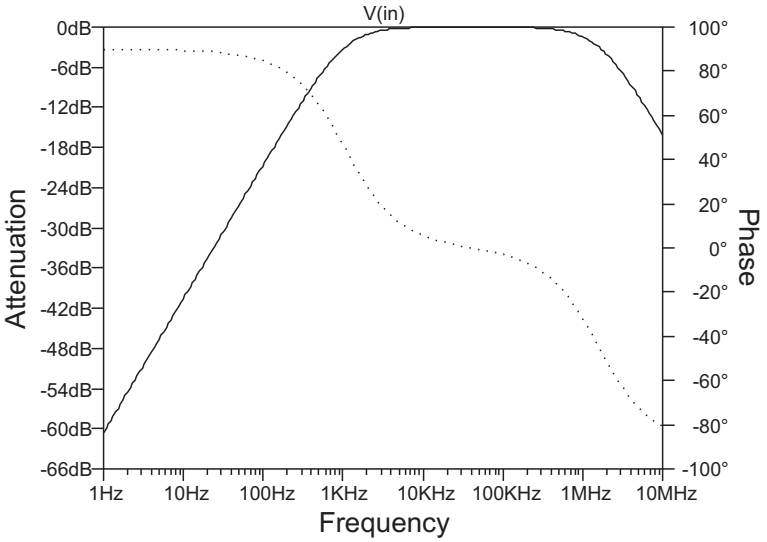

Figure 6.19: Frequency response characteristic of the input filter between 1 Hz and 10 MHz. The solid line represents the amplitude while the dotted line represents the phase of the signal.

6.3.5 Electromagnetic Compatibility Considerations

Though following the restrictions discussed in Sections 5.2.2 and 5.2.1, electromagnetic compatibility (EMC) might be one further issue to be dealt with. The sensor front-end may be exposed to various sources of electromagnetic disturbers and at the same time, the circuitry (capacitive sensor front-end, GSM and ISM communication) may act as a disturber towards other devices.

The following incoming EMC sources have been considered regarding the test device setup:

- Disturbers originating from partial discharges at the conductor surface: this can occur due to water, ice or dust at the conductor surface, especially in the vicinity of the sensor electrodes or in the area of the mounting clamps. Immunity towards these disturbers is achieved by means of the capacitive input filtering concept (compare Section 6.3.3).

- Disturbers originating from partial discharges at the harvester shell surface. The reasons may be, for instance, icicles or bird droppings. If located in the immediate vicinity of a data transmission antenna, these effects may disturb the network communication. However, it is unlikely to disturb both data transmission paths at once.

- Disturbers from lightning strikes hitting the conductor carrying the test device, other conductors or other objects in the vicinity: the surge protection diodes will take the additional transient current resulting from an over-voltage on the harvester capacitance $C_{co,sh}$.

- Disturbers originating from power switching processes: these will have characteristics similar to lightning strikes but with a much lower amplitude. The surge protection diodes can protect the circuitry from these disturbers.

- Disturbers originating from the alternating magnetic field: compare Section “Decoupling and Positioning” (6.3.3).

As mentioned earlier, the test device has been tested for compliance with the listed EMC disturbers. Measures have been implemented to ensure continuous operation.

The test device acts as EMC source in the following ways:

- GSM communication (900 MHz, 1800 MHz) has a peak power output of 2 W or 1 W, respectively.
- ISM communication (433 MHz) has a maximum output power of 10 mW.
- The Capacitance-to-Digital converter radiates the square wave excitation signal at 240 kHz at a very low power level given the total power consumption of the IC, which is approx. 3 mW [140].

All the mentioned signals are not critical to the operation of the power line or communication systems.

6.3.6 Conductor Temperature Measurement & Reference Capacitances

The following measurands have been added in the test device:

- Conductor temperature. Temperature measurement has been implemented by means of a measurement IC, which evaluates the temperature depencence of a diode's forward voltage. This measurement channel has two advantages: it gives an additional option to exclude the presence of ice (if the temperature exceeds the defined limit), and it is used to compensate for a possible temperature dependence of the capacitive icing sensor assembly.
- Reference capacitances within the capacitive icing detection setup. Capacitive elements in pi-configuration have been implemented as reference capacitors in order to be able to compensate for temperature or aging drifts of the CDC as well as compensation for the input filters, as the input filters are also included in the reference channels. Both reference capacitances are in the range of a dry or iced conductor.

Summarizing, the reference measurements allow for compensation of temperature effects, detection of high humidity levels and provide additional information on the overhead power line status.

Chapter 7

Laboratory Setups and Experimental Results

Preceding tests under real-world conditions, experiments with the test device under laboratory conditions were carried out. This chapter is divided into two major parts: Section 7.1 reports the results of experiments regarding the capacitive icing measurement, whereas Section 7.2 is reports on tests which were carried out with a complete system setup comprising energy harvesting, icing detection and data transmission.

7.1 Icing Test Setups

In this section, test setups for icing experiments are described and measurement results are shown and discussed. This section is structured into a description of the experimental setups (see Sections 7.1.1, 7.1.2 and 7.1.3), followed by experimental results (Section 7.1.4).

7.1.1 Natural Environment

As a first approach to obtain icing measurement data, it seemed to be possible to observe natural icing processes at low air temperatures also in urban areas, for instance, during snow fall or when fog is present at low temperatures. Even though the opportunity was taken to install an example measurement assembly on the rooftop of a university building, nothing else than occasional rain showers could be observed during the test phase. This is mainly due to

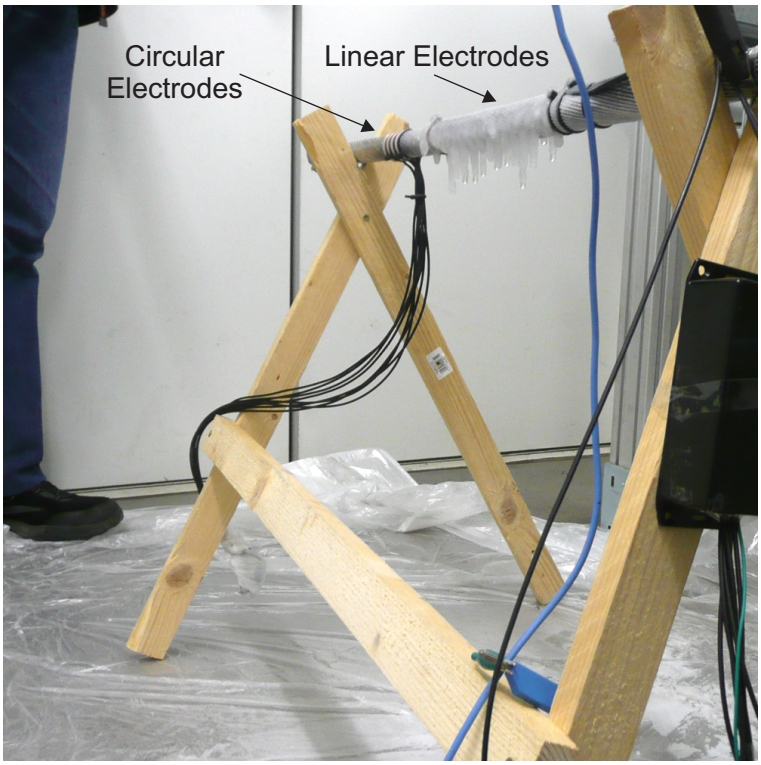

Figure 7.1: Photograph of the climate chamber icing test setup.

the improper climate conditions in Graz (low altitude, high incidence rate of inversions).

7.1.2 Climate Chamber

Consequently, further experiments have been conducted in a climate chamber (at Virtual Vehicle GmbH). The entire setup was brought to a temperature of -10°C and tests with freezing water drops were conducted. Thick layers of clear ice with a small air content could be achieved. However, those experiments consumed a lot of time and thus also a high amount of energy which makes the procedure both time- and cost-intensive. Figure 7.1 depicts the measurement setup during experiments in the climate chamber, testing both circular and linear electrodes setups at the same time (for electrode setups: compare Section 5.1.1, for example results: compare Section 7.1.4.

7.1.3 Laboratory Icing Setup

In order to be able to imitate atmospheric phenomena (i.e. various types of icing, compare Section 2.2), a stationary laboratory environment to achieve icing under known conditions was designed and built. Therefore, a copper pipe replacing the steel core of a power line is streamed by a coolant at a temperature of -40°C, leading to an adjustable conductor surface temperature below zero. The coolant is supplied by a pump in a reservoir which is placed inside a cold chamber which carries out the necessary heat transfer. In order to replicate a surface similar to a power line, the conducting aluminium layers were mounted on top of the copper pipe. The experimental area is comparatively small yet sufficient for icing investigations.

A schematic of the measurement setup is depicted in Figure 7.2. The maximum ice layer thickness is given by the environmental air temperature, but layers with a thickness of up to several centimeters could be achieved. Additionally, an air fan, an ultrasonic fogger and a dropping pipe with a water pump complete that simple yet effective icing setup which can be used to generate various forms of icing.

In order to be able to imitate atmospheric phenomena (i.e. various types of icing, compare Section 2.2), a stationary laboratory environment to achieve icing under known conditions was designed and built. Therefore, a copper pipe replacing the steel core of a power line is streamed by a coolant at a temperature of -40°C, leading to an adjustable conductor surface temperature below zero. The coolant is supplied by a pump in a reservoir which is placed inside a cold chamber which carries out the necessary heat transfer. In order to replicate a surface similar to a power line, the conducting aluminium layers were mounted on top of the copper pipe. The experimental area is comparatively small yet sufficient for icing investigations.

The following varieties of ice qualities could be produced and have been investigated with the laboratory icing setup:

- Icing originating from air humidity. This process is similar to natural rime icing, as it will mainly occur with low air temperature and high air

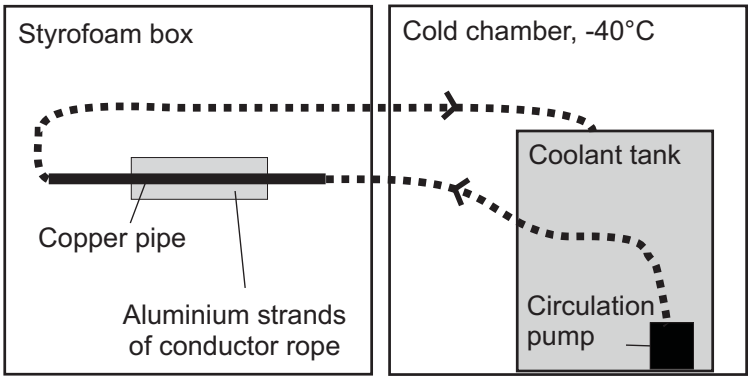

Figure 7.2: Schematic of the laboratory icing setup. A circulation pump supplies coolant from a tank in a cold chamber that is kept at -40°C to the isolated experimental area. There, a copper pipe is streamed by the coolant, replacing the steel core of a conductor rope sample.

humidity while no precipitation occurs.

- Icing originating from fog from an ultrasonic fogger. This process is comparable to natural in-cloud icing and characterized by the presence of a high amount of small water droplets in the air. This process can lead to the growth of thick ice layers within comparatively short periods of time. In the experiments, rime layers of several centimeters could be obtained.

- Icing originating from freezing water drops. This process is referred to as “freezing rain conditions”, when cold or super-cooled droplets hit a cold surface and freeze immediately. This phenomenon can also lead to a thick ice layer deposition within rather short time. In the laboratory icing setup, the limited cooling power of the setup was limiting the ice accretion rate.

Further ice qualities can occur in a natural environment and comprise dry and wet snow as well as all kinds of state transitions including melting snow, sublimation, and melting ice layers. When a line is thermally de-iced, for instance, water may be present in the core while the outer shell is still frozen.

7.1.4 Example Results of Icing Experiments

In this section, example measurement results of icing experiments are presented, using different measurement electrode setups and different ice qualities. These experiments focused on investigations on distinguishing different ice qualities from the capacitance signals over time.

Icing by means of air humidity leads to a white, light, fragile and opaque layer of ice. The slow growth process results from the high air content and poor heat transfer within the layer. An example measurement signal trace of freezing air humidity is depicted in Figure 7.3. Two measurement capacitances C_1 and C_2 at two distances formed by 10 cm electrodes were used for this experiment.

It can be seen that for this electrode configuration, the capacitance C_1 between the two nearest electrodes is decreasing at the beginning, then rises to a maximum and decreases again (black graph). Below, the grey graph of originates from measurement capacitance C_2 having three times the inter-electrode distance of C_1. For C_2, the signal swing is smaller compared to C_1 and the maximum of the measured capacitance occurs at a higher thickness. Both measurement capacitances show the same behavior when water is present: the values drop below the "dry" levels.

A picture set of the same measurement run is shown in Figure 7.4. The stills have been taken 15 minutes, 1 hour, 4 hours and 6 hours after turning on the coolant pump, respectively.

It was found that the first ice crystals form at the most exposed points of the surface. Soon, a homogeneous layer with a high air content covers the entire surface.

Icing by means of fog from an ultrasonic fogger is similar to air humidity icing. However, in comparison to Figure 7.3, the presence of small

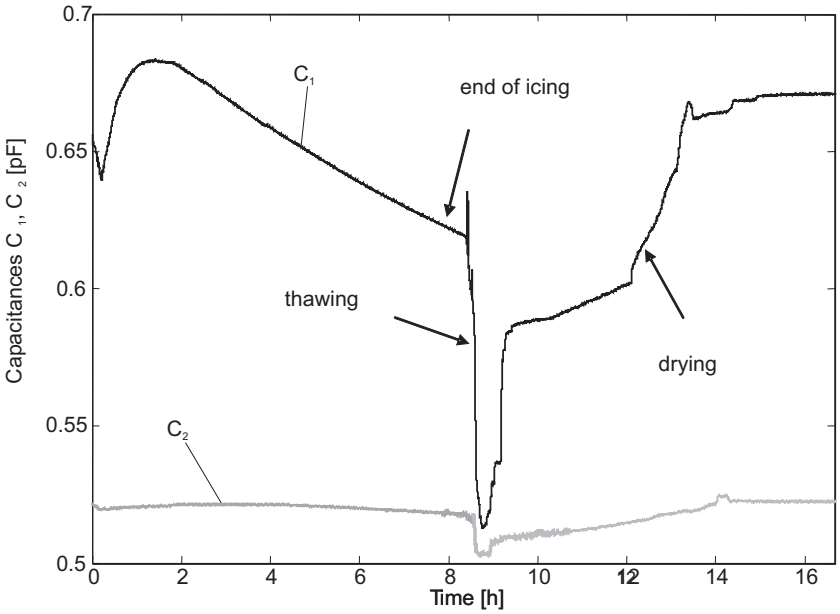

Figure 7.3: 2 measurement capacitances C_1 and C_2 over time for a laboratory air humidity icing experiment [2]. The grey graph of measurement capacitance C_2 originates from a measurement capacitance having two times the inter-electrode distance of measurement capacitance C_1 (compare Figure 5.8).

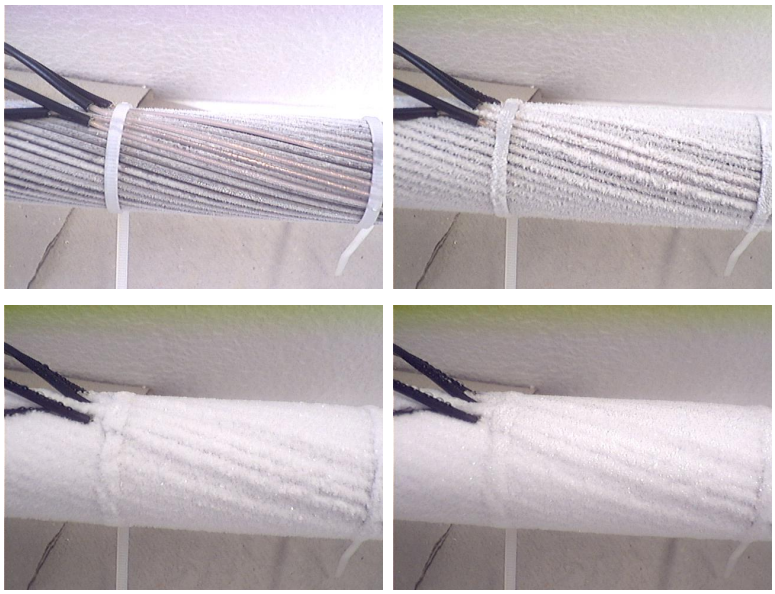

Figure 7.4: Captures of icing originating from air humidity (after 15 min, 1 h, 4 h and 6 h)

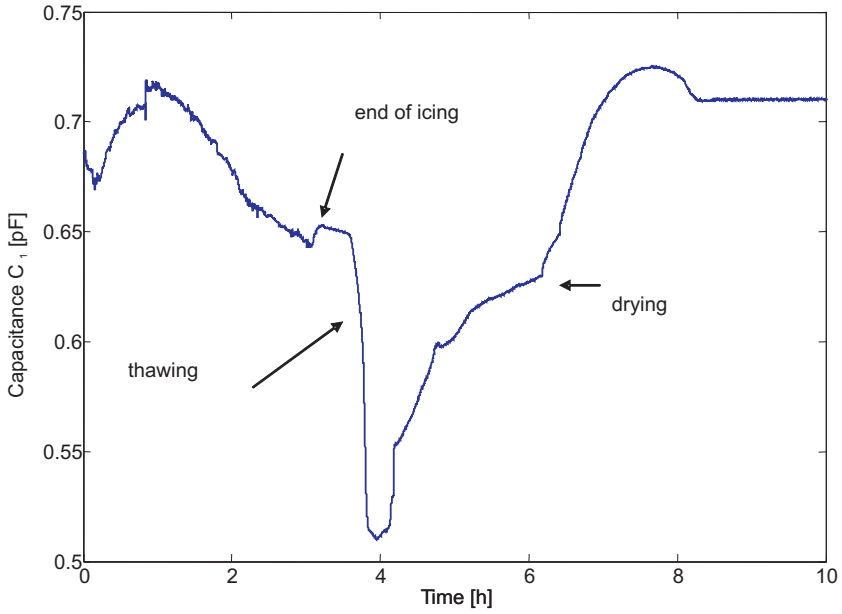

Figure 7.5: Measurement capacitance C_1 (compare Figure 5.8) over time during a fog icing experiment [2]. The main difference compared to Figure 7.3 is the increased noise level on the capacitance over time signal during the icing phase (0...3 h).

liquid water droplets leads to a higher measurement noise, while keeping the characteristics of the measurement electrode signal over time similar. This is most probably caused by the attaching water droplets causing rapid changes in permittivity.

Figure 7.5 depicts a measurement signal trace using two 10 cm electrodes. The additional noise component is visible especially at the beginning of the measurement.

A picture set of the measurement run depicted in Figure 7.5 is shown in Figure 7.6. The stills have been taken 15 minutes, 1 hour, 4 hours and 6 hours after turning on the cold fluid circulation pump, respectively. The images may seem comparable to Figure 7.4, however, the density of the ice layer is much higher and has qualities which range from frozen wet snow to hard rime ice. The latter is comparable to what happens when a cloud supplies large amounts of water to a cold surface.

Icing by means of freezing water drops is usually referred to as "freezing rain". In a natural environment, super-cooled water droplets hitting a surface will entirely freeze. In the laboratory setup, cooled liquid water drops (at

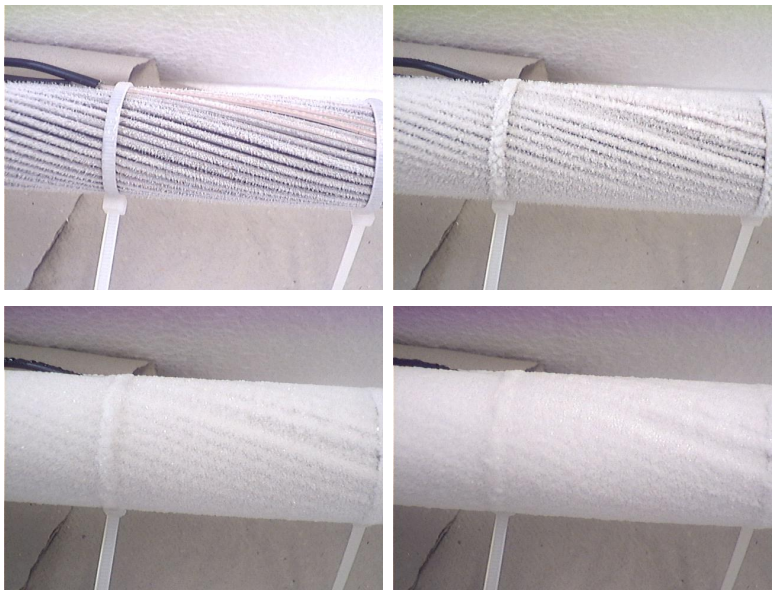

Figure 7.6: Icing photos originating from fog produced by an ultrasonic fogger (after 15 min, 1 h, 4 h and 6 h).

a temperature still above 0°C) hit a cold surface and freeze partially, while the excess water will drop off. The resulting layer consists of high-density, transparent, clear ice, having a negligible air content.

Figure 7.7 depicts a measurement signal trace using 10 cm electrodes (two measurement capacitances). It can be seen that the presence of water on top of the ice layer has a strong effect on the measurement signal. The steep descents in the signal are caused by the pouring of water, while the slow signal increases represent the growth of the ice film.

A picture set of a water drops measurement run in the climate chamber setup is depicted in Figure 7.8. The pictures have been taken 5 minutes, 1 hour and 2 hours after the beginning of the experiment, respectively.

It could be shown that in the various setups, different ice qualities cause distinguishable measurement signals as expected and explained in Chapter 5.

7.2 Complete System Tests

The complete test device consisting of energy harvesting, sensor node platform (including the data transmission circuitry) and the decoupled front-end including the icing detection was tested under various laboratory conditions

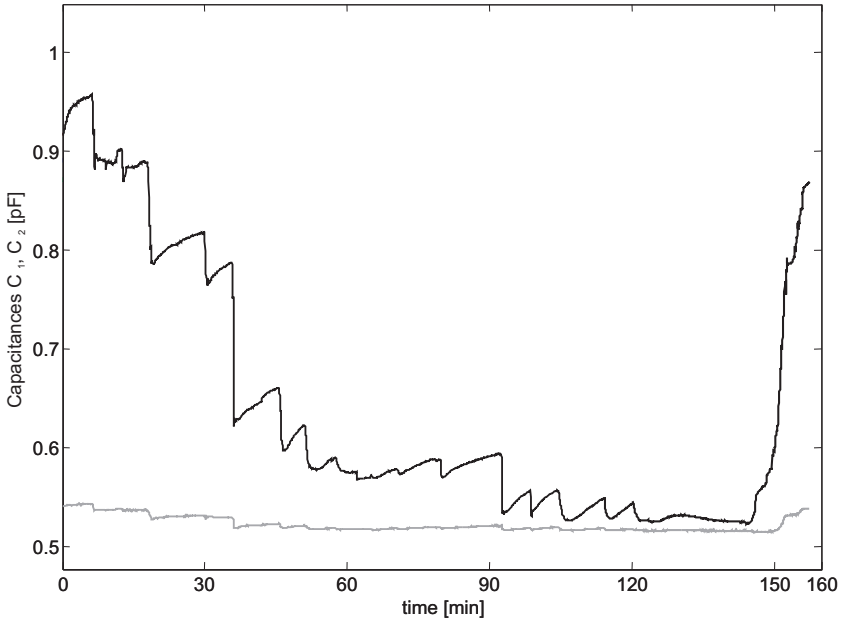

Figure 7.7: Capacitance over time signals of measurement capacitances C_1 and C_2 (compare Figure 5.8) over time for a water droplet icing experiment [2]. The grey graph of C_2 originates from a measurement capacitance having two times the inter-electrode distance of C_1. It can be seen that the presence of water on top of the ice layer has a strong effect on the measurement signal. The steep descents in the signal are caused by the pouring of water, while the slow signal increases represent the growth of the ice film.

in order to test the system's robustness prior to a field test. The tests were carried out several times at the beginning and repeated after each design iteration during later optimizations. The test chain comprises the simulation of an alternating current comparable to the vicinity of a high voltage conductor (see Section 7.2.1), high voltage compatibility tests with a HV supply using a high voltage transformer (see Section 7.2.2) and a system test including an ice layer on a conductor line in the high-voltage laboratory (see Section 7.2.3). The latter setup is comparable to the situation in the field, except for environmental conditions such as solar radiation and precipitation. As mentioned above, the various tests were carried out in order to ensure operation in the expected harsh environment.

Before the first electrical test, the test device was sprayed with water from all sides in order to detect points of eventual water entry. Furthermore, the system was mounted on a conductor line sample on the roof platform of the

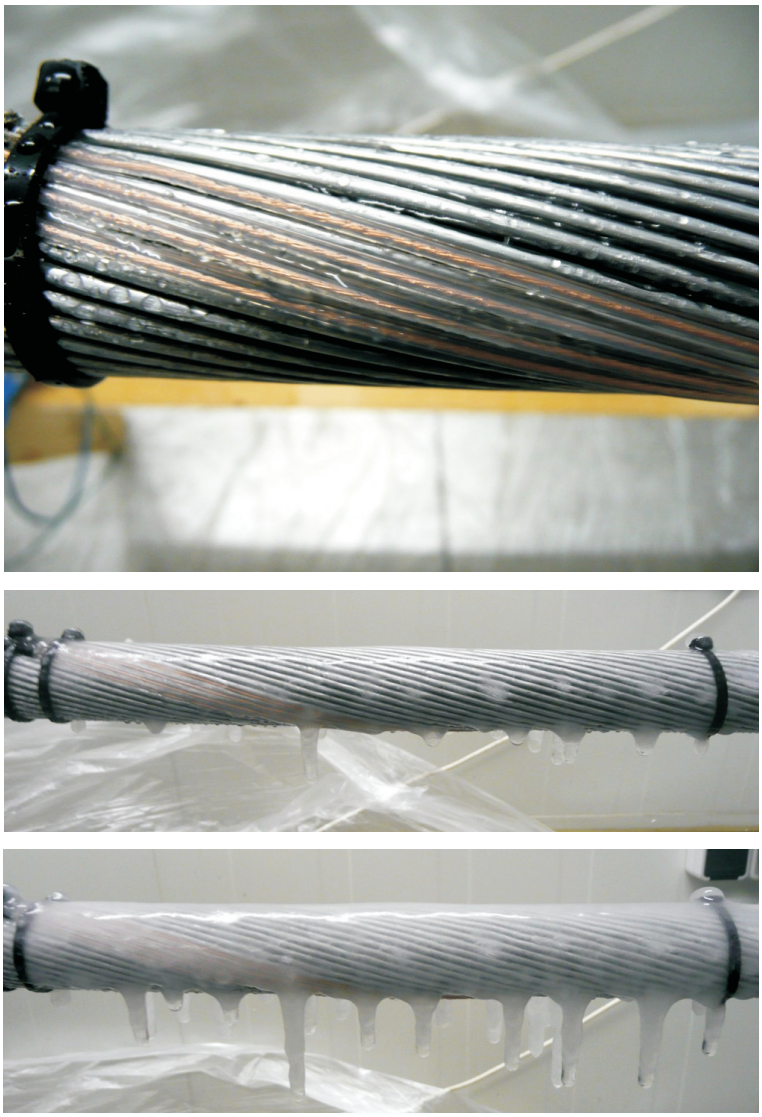

Figure 7.8: Icing photos originating from freezing water drops (after 5 min, 1 h and 2 h).

institute, exposed to sun, wind and rain. Thereby, optimum positions for water draining holes could be determined. This is of high importance as water films inside the harvester may lead to short-circuits between conductor and harvester shell and thereby disturb the harvesting circuitry's operation.

7.2.1 High Current Tests

Preliminary to high voltage tests, the complete system was exposed to high currents (i.e. strong magnetic fields caused by high currents) as they are present on a power transmission line and may have effects on the measurement circuitry due to induced voltages within parts of the circuitry. For the laboratory measurement, a power transformer capable of providing a secondary current of approx. 190 A was used. By inserting eight windings through a hollow pipe replacing the conductor in the setup, an effective current of approx. 1500 Ampere could be reached. By comparison of the measured capacitance values of a dry conductor (i.e. nominal capacitance values) with and without the application of the current, it could be shown that there is no sensitivity of the measurement circuity towards high currents. Figure 7.9 depicts the schematic of the test setup.

7.2.2 Laboratory High Voltage Test

In order to test the circuitry regarding its behavior in a high voltage environment, two laboratory high voltage tests have been conducted, both using a neon lamp stray transformer generating a maximum output voltage of 6 kV:

- Application of high voltage onto the terminals of the harvester capacitance $C_{co,sh}$. This test does not only evaluate the correct function of the energy harvesting circuitry, but also the over-voltage protection system can be tested easily and under known conditions. Also, the stability of the decoupling circuitry was tested. A schematic of the test setup is depicted in Figure 7.10.

- Application of a strong electrical field across the measurement electrodes. This setup applies a potential difference between measurement electrodes and measurement ground (i.e. conductor potential) as it is caused by the

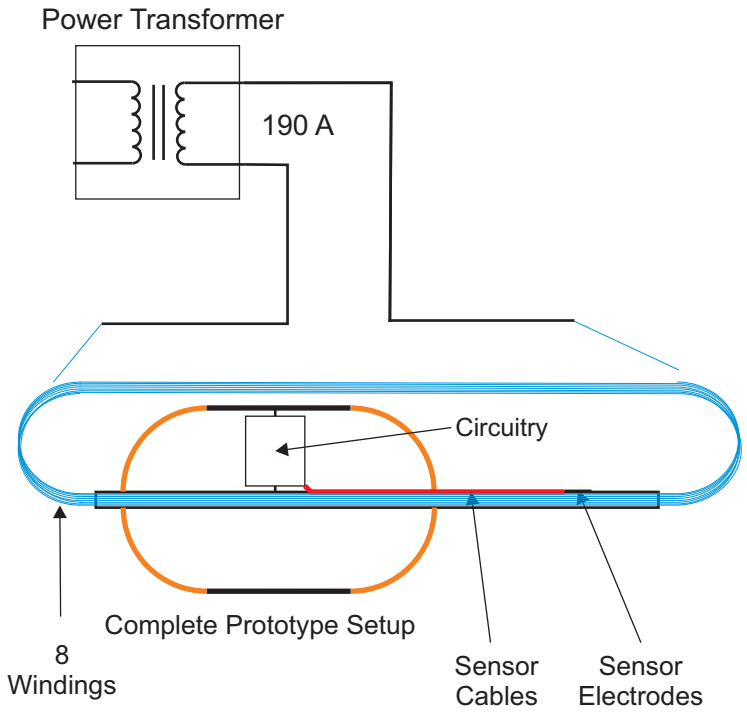

Figure 7.9: Schematic of the laboratory high current test

electric field gradient when mounted onto a conductor in the field. This test is used to evaluate the input filter circuitry of the capacitive icing measurement system. The two outputs of the transformer are connected to the conductor and to a metallic shell around the measurement electrodes, respectively. For this test, power supply of the sensor node and the measurement system was established by means of the backup battery. In order to generate partial discharges, a sheet of absorbent paper was wrapped around the conductor sample piece in the area of the sensor electrodes. After recording the dry (i.e. the nominal) capacitance of the setup, water was dropped on the paper cloth, thus keeping a water film in the vicinity of the sensor electrodes. The resulting measurement values could be recorded as expected (i.e. a decrease of the recorded capacitances values could be recorded) while the standard deviation (i.e. the SNR) of the measurement rises due to the presence of both 50 Hz disturbers and partial discharge events. It could be shown that the filter structure operates sufficiently well. A schematic of the test setup is depicted in Figure 7.11.

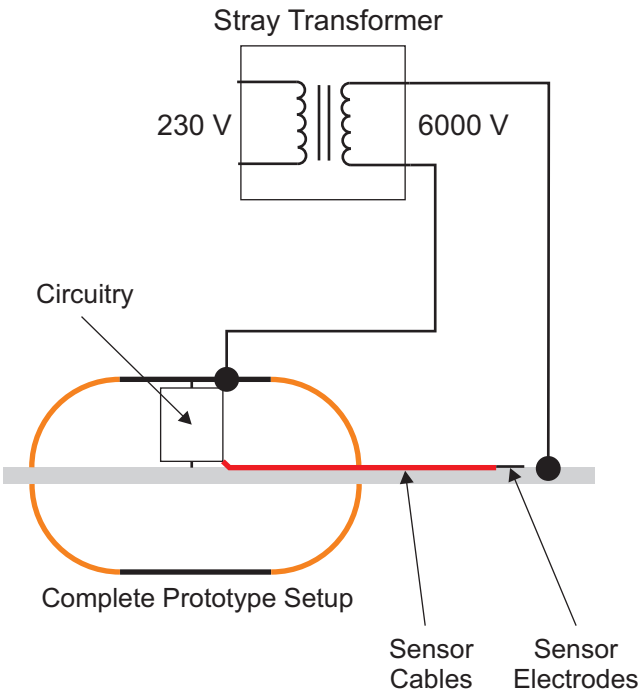

Figure 7.10: Schematic of the laboratory high voltage setup for harvesting, overvoltage and decoupling tests

7.2.3 High Voltage Laboratory Icing Test

After successfully passing the previous tests including iterations of redesigns, the test device was evaluated at the high-voltage laboratory at Graz University of Technology. Since conductor icing can not be achieved in that environment, the presence of ice was ensured by means of freezing an ice shell with a thickness of approx. 50 mm around a sample of a conductor line, being then part of the measurement setup. This pre-fabricated ice shell was used to observe both presence and melting of an ice layer. It has to be noted that the ice quality in this experiment differs from a typical real-world ice quality as usually clear ice layers of the fabricated thickness are not likely to occur: in most occurrences of natural icing, the overall air content of the accreted ice will be higher. Figure 7.12 depicts the measurement setup: The test device is mounted to a steel pipe carrying the harvester test device. A short iced conductor line

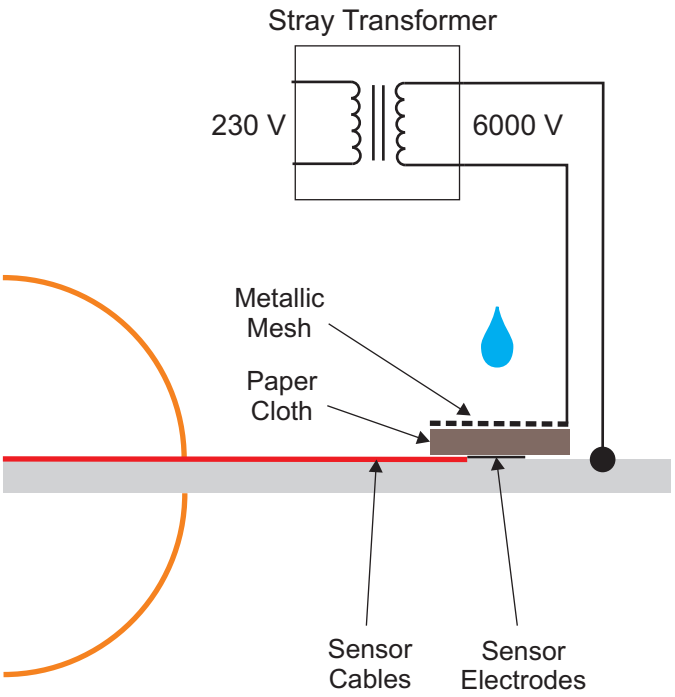

Figure 7.11: Schematic of the laboratory high voltage setup for input filter tests

sample is joint to the pipe, carrying the electrode assembly and the ice layer. For the experiment, the steel pipe was then lifted to a height of approx. 10 m (compare Figure 7.13) and connected to an adjustable high voltage source. The voltage level and was continuously increased (starting from 0 Volt) towards the specified system voltage. The system started its operation at approx. 90 kV phase voltage, equivalent to a system voltage of 153 kV line-to-line, which is a good indicator for the adequate design of the harvester circuitry. The device was fully operational and provided measurement results in the expected range for an iced conductor (compare Figure 7.14).

7.3 Summary on Laboratory Experiments

After successfully testing the functionality of the icing measurement circuitry in various icing setups, the measurement circuitry had to undergo tests concerning its operation under high-voltage and high-current conditions. Finally, the setup was successfully tested under conditions comparable to the real

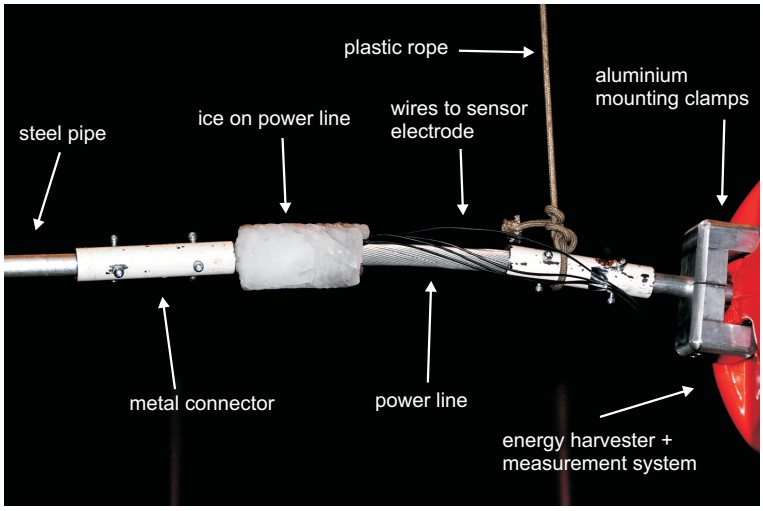

Figure 7.12: Measurement electrodes and ice block on a conductor line sample during the measurement at a high voltage conductor at the high-voltage laboratory [4]

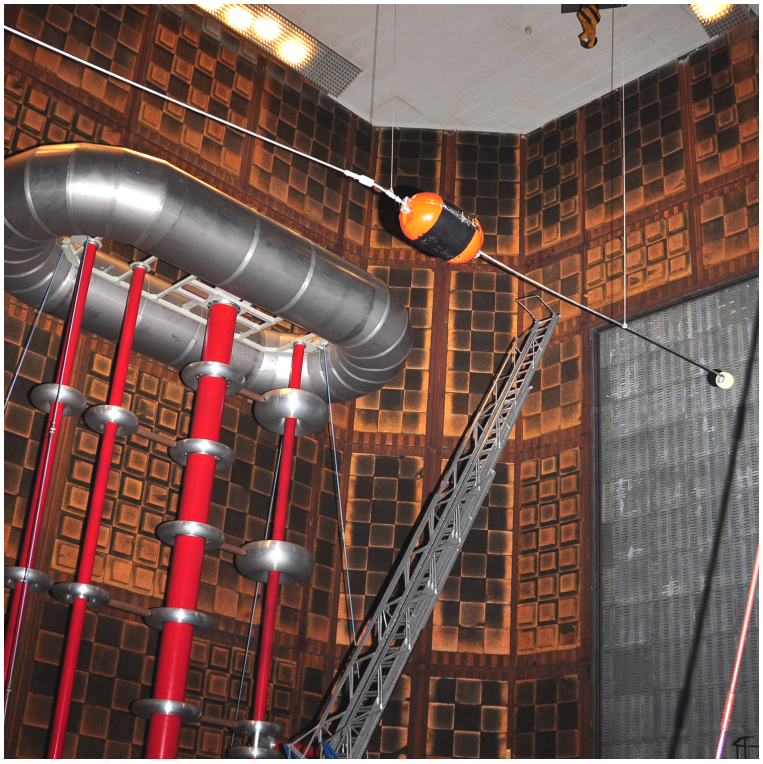

Figure 7.13: Photograph of the setup mounted on a steel pipe during the laboratory high-voltage icing test

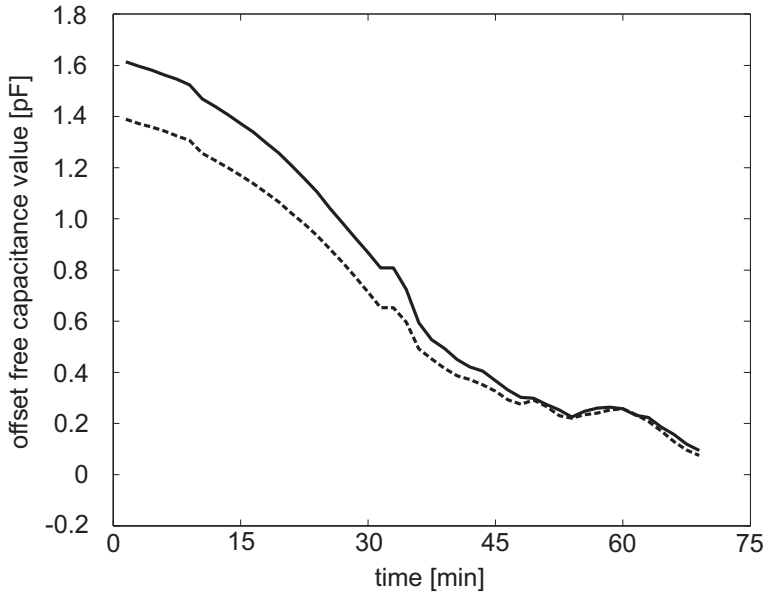

Figure 7.14: Capacitance over time signals of the final measurement at an iced high voltage conductor at the high-voltage laboratory. The conductor line is covered with ice, the ice layer thickness is decreasing (melting) [4]. The two measurement capacitances (solid line and dashed line) have a similar inter-electrode distance, the difference in the measurement signals may be caused by undesired motion of the electrodes during the freezing process of the sample.

world.

In the next chapter, the experiences and results from two winter seasons' field tests are reported.

Chapter 8

Field Test Setups and Experimental Results

This chapter describes the experiences and the results of field tests with the device deployed on a 220 kV system voltage overhead line of the largest Austrian transmission system operator, Austrian Power Grid (APG).

In the winter season 2009/2010, the test device was mounted and successfully operated for the very first time. Examples of icing events are given and explained in Section 8.1. A second field test was conducted with an improved test device in the winter season 2010/2011. Results, measurement data and information on icing events are depicted and explained in Section 8.2.

8.1 Field Test 2009-2010

In this section, experiences with the very first field test 2009-2010 are reported. In Section 8.1.1, the measurement environment and parameters are described. Section 8.1.2 briefly presents the base station designed for autonomous operation and weather data collection. Thereafter, Section 8.1.3 reports about detected icing events. Finally, Section 8.1.4 summarizes the results of the field test.

8.1.1 Environment

On February 22, 2010, the test device was mounted in the vicinity of transmission tower No. 158 of APG's line No. 285 on Obdacher Sattel in the Austrian

Alps. The location is situated on a hilltop at an altitude of approx. 1000 m a.s.l. Icing events had been observed there before.

By means of a truck-mounted crane, the test device was lifted and fixed onto the conductor rope. Measurement electrodes were attached to the conductor rope using low-profile cable clips and an appropriate adhesive tape.

Measurement data transmission at this location was established by means of GSM short messages (SMS) using a SIM card of an Austrian network provider. Measurement data were acquired continuously, averaged and stored by the microcontroller. Once in 48 minutes (equaling approx. 1000 messages per month), a short message was transmitted including the following data set:

- one measurement of 4 capacitive channels every 5 minutes plus a standard deviation value per channel
- one temperature measurement value
- two reference capacitance values plus a standard deviation value
- one energy harvesting circuitry output voltage measurement plus a standard deviation value

These data set was packed into an alphanumerical text code. First, the text message was sent to a host computer via an SMS-to-email gateway service. Turning out to be less reliable than assumed, it was decided to transmit the message to a dedicated cell phone connected to a host computer.

Figure 8.1 depicts the mounting process, where the two half-cylinders are joint together and mounted onto the line; Figure 8.2 shows the entire setup on the line, including the sensor cables and electrode assembly, while Figure 8.3 depicts a detailed view of the first field version of the electrode assembly. Four measurement capacitances are formed by a common transmitter and four receiver electrodes. The electrode length amounts to 15 cm, the total electrode diameter is 3 mm (including approx. 2 mm of insulation). The sensitive area is located in a distance of approx. 1 m from the harvester shell. The diameter of the conductor rope amounts to 28 mm.

Figure 8.4 shows the setup viewing towards the transmission tower.

Figure 8.1: Mounting the test device onto the conductor rope, February 2010.

Figure 8.2: Test device on conductor rope, February 2010.

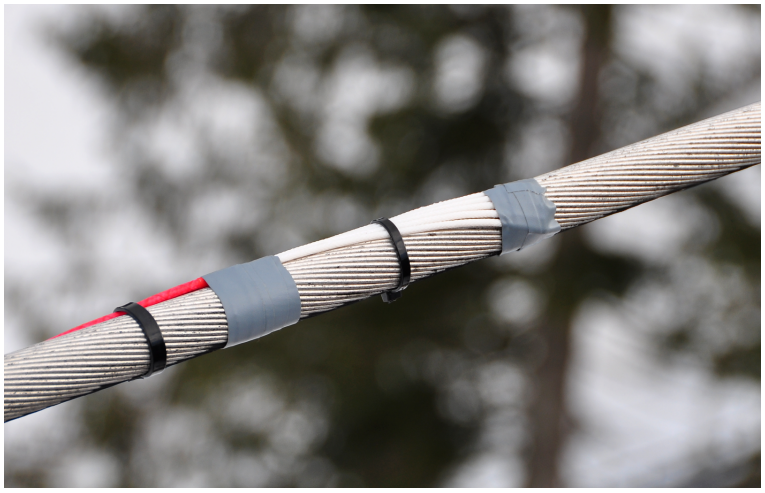

Figure 8.3: Electrodes assembly details, February 2010 [3]. Five measurement electrodes (white insulation) are mounted to the conductor rope by means of cable ties and special adhesive tape. The sensor cables (red) connect the electrodes with the measurement circuitry in a distance of approx. 1 m.

Figure 8.4: Test device on conductor rope, February 2010.

8.1.2 Base Station

For reference data collection, a reliable weather monitoring system was desirable. As the location is rather remote, the next continuously inhabited house is several hundred meters away, so there is no mains power available in the vicinity of the transmission tower. Therefore, it was decided to rely on a lead-acid battery-powered solution. Capacity was designed so that a battery exchange once in two weeks would be more than sufficient. This was also the time interval for data collection from the weather monitoring system.

The following weather parameters were recorded in this field test:

- Air temperature
- Relative air humidity
- Precipitation rate
- Wind speed and direction

Furthermore, a camera was installed, taking images of the scene in regular intervals with the weather data inserted in the images. Figure 8.5 depicts the complete station with camera, meteorological sensors mounted on the transmission tower and a battery container.

8.1.3 Example Events 2009-2010

The period between March 2 and March 11, 2010, is analyzed in more detail concerning example icing events. Figure 8.6 shows the conductor temperature signal of the entire period.

Figure 8.7 depicts the capacitive icing measurement data for the same period of time. One suspected icing event seems to have occurred on and around March 3. This event is referred to as Event 1 and is most probably a growing ice layer. The period of four days between March 7 and March 11 is also an icing event (referred to as Event 2) and is mostly due to accumulating snow layers and probably hoarfrost icing.

Figure 8.5: Overview of the base station, containing weather camera and meteorological sensors on the transmission tower and a battery container (green/orange).

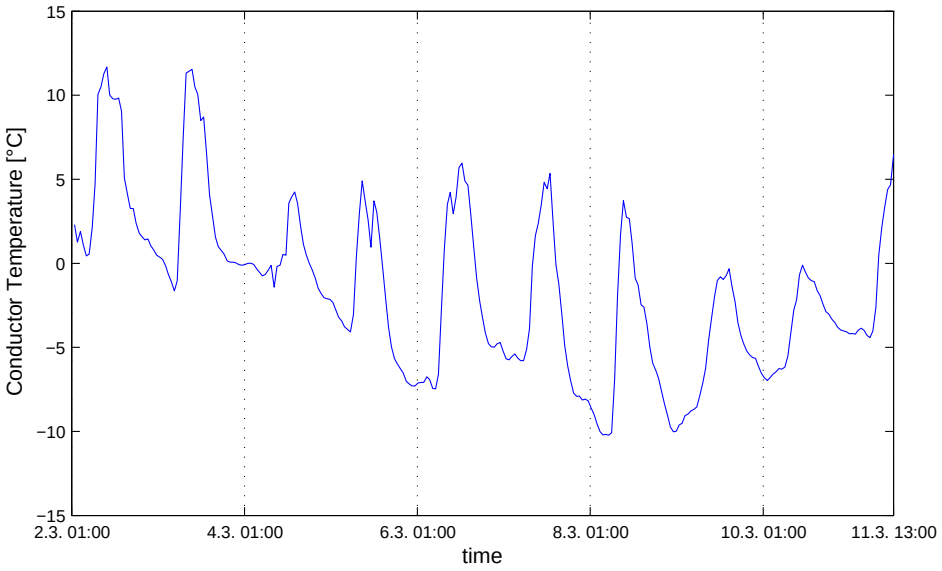

Figure 8.6: 2009-10: Conductor temperature over time between March 2, 2010, 01:00 and March 11, 2010, 13:00 [8]. On nearly every day within that period, both positive and negative temperatures occur.

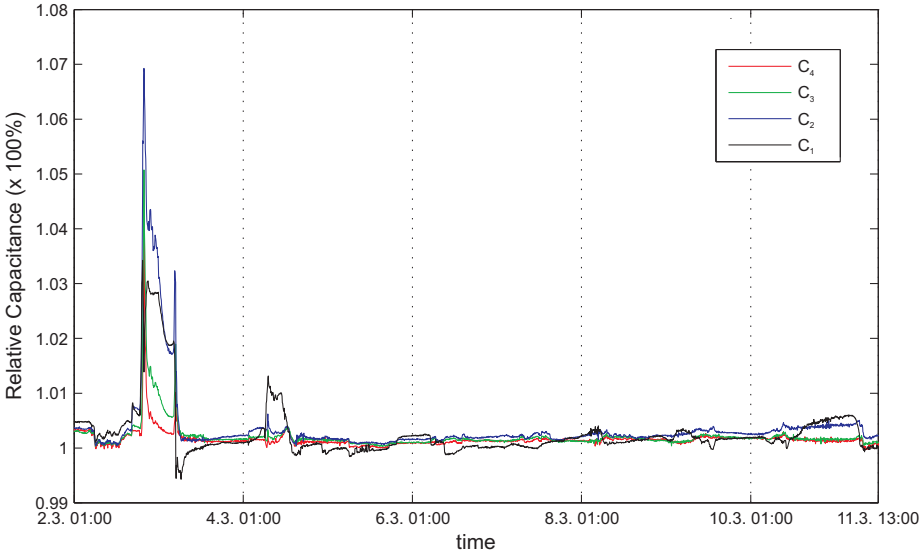

Figure 8.7: 2009-10: Capacitances over time between March 2, 01:00 and March 11, 13:00 [8]. Capacitances C_1 to C_4 are depicted over time. It can be seen that the signal range is smallest for the largest inter-electrode distance (C_4, red line)

Example Event 1

An icing event and its detection by the capacitive measurement system are described. The duration of the event is approx. 36 hours and it was caused by low temperatures, high air humidity and snow accretion. Capacitive measurement data are compared with other measurands such as conductor temperature, relative air humidity, variance of the capacitance measurement and wind speed.

Figure 8.8 compares the measurement signals of the conductor temperature and the capacitance readout C_1 between the transmitter and the neighboring receiver electrode. Starting on March 10, 2010, 12:00, the icing event has a duration of approx. 36 hours. As the temperature is below 0°C, the measured capacitance increases as ice and snow are accumulating at the conductor surface, and therefore also on the sensor. After approximately 20 hours, a melting process starts and the measured capacitance decreases below the nominal value. The conductor temperature is not yet above 0°C at this moment. This is most likely due to the fact that the mounting location of the temperature sensor is not optimal. Concerning the temperature measurement, air and conductor

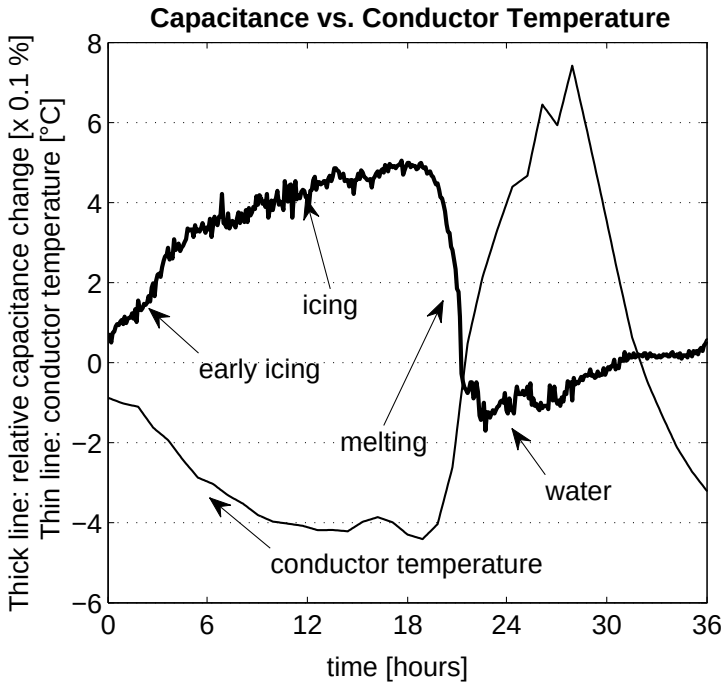

Figure 8.8: Event 1: Conductor temperature and capacitance change over time [3]. At the beginning, the temperature is below 0°C and the measured capacitance increases as ice and snow are accumulating at the conductor surface. After 20 hours a melting process starts and the measured capacitance decreases below the nominal value.

temperature differ by several degrees. This is due to the height (and wind speed) difference (conductor rope in a height of approx. 20 meters and and the base station's temperature sensor approx. 2 m above ground). Furthermore, the enclosure of the temperature sensor inside the harvester shell and its exposure to solar radiation lead to a positive temperature offset. Other impacts (such as thermal losses of the conductor due to the load current) could not be observed during the field test. Over the whole period of the field test, the average load of the transmission line was at a relatively low level. Referring to the load data provided by APG, the electrical load never exceeded 15 % of the nominal load of the transmission line. This results in only a few watts of dissipated power per meter of the conductor rope, and therefore, this is a negligible effect.

Figure 8.9 depicts the variance signal of the capacitance measurement trace

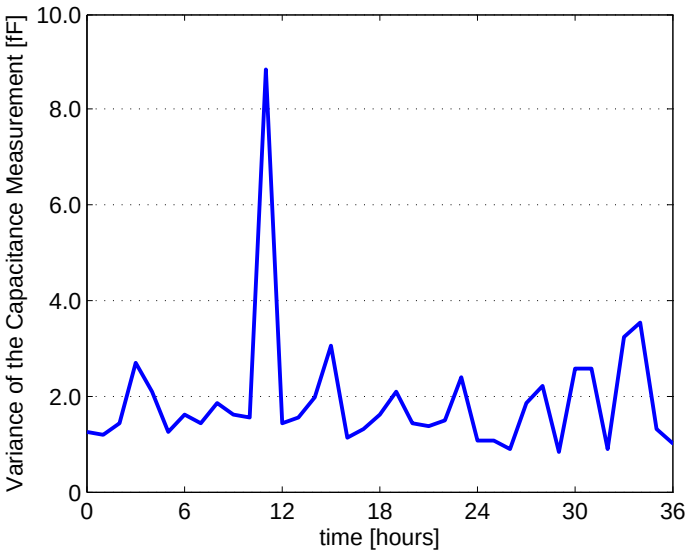

Figure 8.9: Event 1: Variance of the capacitive icing signal over time [3]. High variance values seem to correspond with elevated surface activity, i.e. rapid melting, freezing, snow flake accumulation and especially the presence of water droplets.

for the event. It is obvious that there is no correlation of the variance signal with the occurrence of wind. High variance values seem to correspond with elevated surface activity, i.e. rapid melting, freezing, snow flake accumulation and especially the presence of water droplets causing very fast signal changes. If wind were the reason of a high variance, it could be derived that the sensor geometry (especially the distance between sensor wires and conductor) would change due to the external forces. This is apparently not the case.

The obtained measurement trace in Figure 8.8 shows a similar trend to the measurements obtained in the laboratory experiment. By the use of multiple measurement capacitances (here, capacitance measurements of measurement capacitances C_1 and C_2 are used), ambiguities especially in transition regions can be minimized (compare Figure 8.10). A low pass filter is applied to the raw data. The icing event follows the graph over time in counter-clockwise direction.

Figure 8.11 depicts a weather camera image when there is snowfall. It can be seen that the test device is already covered with snow.

Figure 8.12 depicts both the recorded wind speed and air humidity measurement data. Air humidity naturally corresponds with air temperature. High

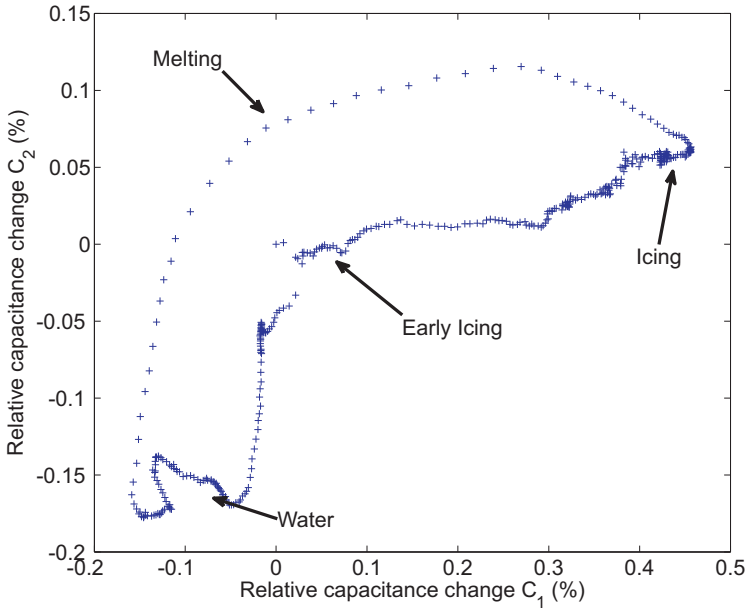

Figure 8.10: Event 1: Measurement capacitance C_1 over measurement capacitance C_2 [3]. It can be seen that by evaluation of two measurement capacitances, possible ambiguities between icing/drying and melting can be resolved.

Figure 8.11: Event 1: Weather camera image from March 10, 2010, 3 p.m. [3]. Snow falls and deposits on the test device.

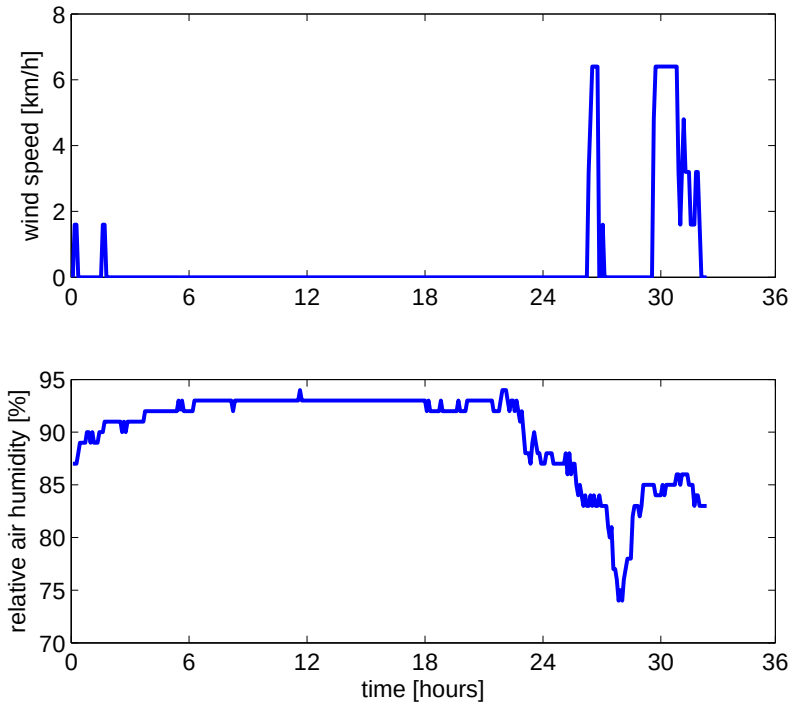

Figure 8.12: Event 1: Wind speed and air humidity at ground level [3].

relative air humidity can be observed during the nights, while a lower relative air humidity is measured during the day due to the temperature change. However, this correspondence is altered when there are clouds and precipitation. Then, the relative air humidity typically remains at a constant high level and other processes than just warming up and cooling down of the "same" air mass occur. Obviously, this is the case here. Concerning the wind speed, it can be seen that hardly any wind occurs during the icing event. Little wind leads to a lower supply with humidity, which would be necessary to form thicker ice layers (such as rime icing). Summing up the weather information, most of the capacitive measurement signal change seems to be caused by snow accretion.

Example Event 2

A second, potentially heavy icing event was detected in the night from March 2 to March 3 of March, 2010. However, the base station was out of power at that time due to a defective battery cell. Weather data prior to the failure were as follows:

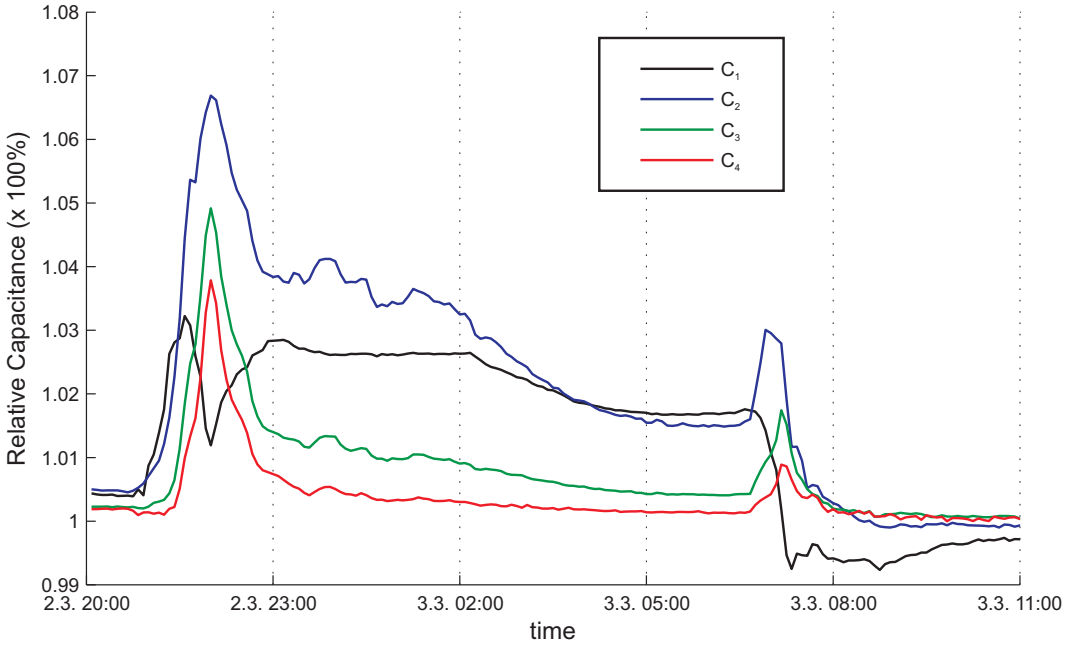

Figure 8.13: Event 2: Capacitive icing detector data of all measurement channels [8]. The time signal of the measurement capacitances are comparable to what has been recorded during artificial icing events in laboratory experiments (compare Figure 7.3 in Section 7.1.4).

- Zero wind
- High air humidity (94 % and above)
- Air temperature close 0°C (i.e. between +2°C and -3°C)

These conditions are what is typically known as icing conditions. Figure 8.13 depicts the capacitance measurement data, Figure 8.14 depicts the temperature data for the same period of time. The time signal of the measurement capacitances are comparable to what has been recorded during artificial icing events in laboratory experiments.

8.1.4 Results 2009-2010

It could be shown that both icing detection and energy harvesting can be successfully operated in a 220 kV overhead line environment. Several icing events of different qualities and durations could be observed with a behavior

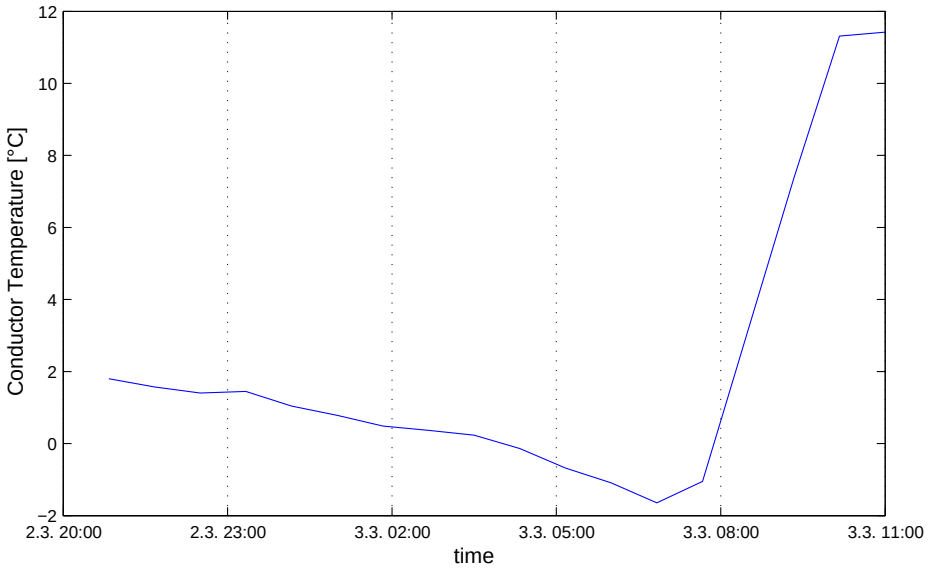

Figure 8.14: Event 2: Temperature data [8].

similar to laboratory experiments. However, several tasks for improvement arose during the test:

- Electrode assembly: electrodes need to be even thinner than initially in order to have less 50 Hz disturbances, and more free conductor surface in-between the electrodes) + mounting clamps to facilitate mounting.
- Temperature measurement: sensor position needs to be outside the harvester shell.
- Creepage currents: over the long period of the field test, creepage currents along PCB surfaces could be traced. Better humidity protection was implemented as a consequence.
- Flash-overs at the harvesting transformer: this component was entirely sealed in silicone.
- Lithium batteries suffered from low temperatures and unbalancing: replacement by nickel-based cells.
- GSM connection was repeatedly lost. After tests with a GSM repeater and a detailed evaluation of the available networks in August 2010 showing continuously changing coverage conditions for different providers, an

international SIM card was used in order to improve the situation. Furthermore, an ISM radio link to the base station needed to be implemented.

- Base station relying on battery power only was impractical: grid connection was aimed at

More information on the test device and its modifications can be found in Chapter 6.

The first field test was concluded by un-mounting the field test device from the conductor line on May 4, 2010.

8.2 Field Test 2010-2011

Fortunately, the field test could be continued in the following winter season. Given the difficulties that were found as the outcome of the first season, various measures were implemented in order to improve the overall reliability of the system. Section 8.2.1 shortly introduces the second version of the base station. Thereafter, Section 8.2.2 reports about some recorded icing events. Finally, Section 8.2.3 summarizes the outcome of the second field test.

Soon after the initial installation on October 5, 2010, problems with creeping currents (most probably caused by water entrance during the mounting procedure) were experienced, leading to the replacement of optical couplers and further encapsulation of the circuitry with a special silicone grouting elastomer. After a test in the high-voltage lab, water spraying and a continuous test in the lab, the test device was mounted again in the field on January 17, 2011 and remained operational until the end of the field test in April 2011.

8.2.1 Base Station

On September 29, 2010, the weather monitoring system was moved to a nearby house, making batteries obsolete and allowing for the operation of equipment with an increased power demand due to a mains connection. A PC was installed not only for weather data and image storage, but also in order to receive data via the backup ISM radio channel. Each short message was therefore sent

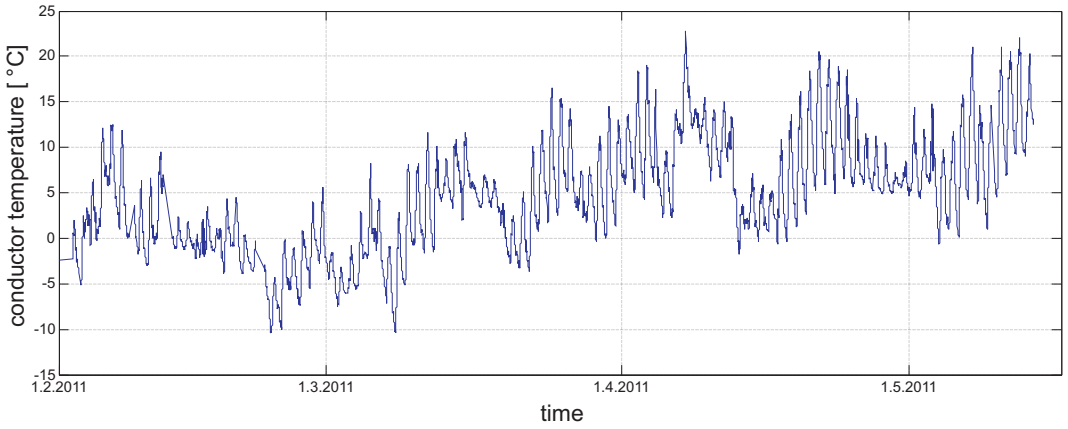

Figure 8.15: 2010-11: Air temperature between February 1 and May 15, 2011 [9].

not only via the GSM link to the host computer, but also via the ISM channel and stored locally.

8.2.2 Example Events 2010-2011

Figure 8.15 shows the air temperature at the base station from February 1 until May 15, 2011. It can be seen that only few times temperatures remained below zero for more than a day.

Example Event 3

This event was observed on February 18, 2011 and is characterized by a thin layer of rime ice. Figure 8.16 depicts the relative capacitance of the electrode pair with the smallest inter-electrode distance and the conductor temperature. The capacitance signal increases while the measured temperature approaches zero during night. Though the temperature measurement value remains above zero, it can be assumed that this is due to the thermal capacitance of the mounting clamps resulting in a thermal delay of the temperature measurement. Figure 8.17 shows corresponding images from the weather camera, indicating suitable icing conditions.

Example Event 4

Four minor events occurred between January 28 and February 1. Figure 8.18 depicts the relative capacitance of the electrode pair with the smallest inter-

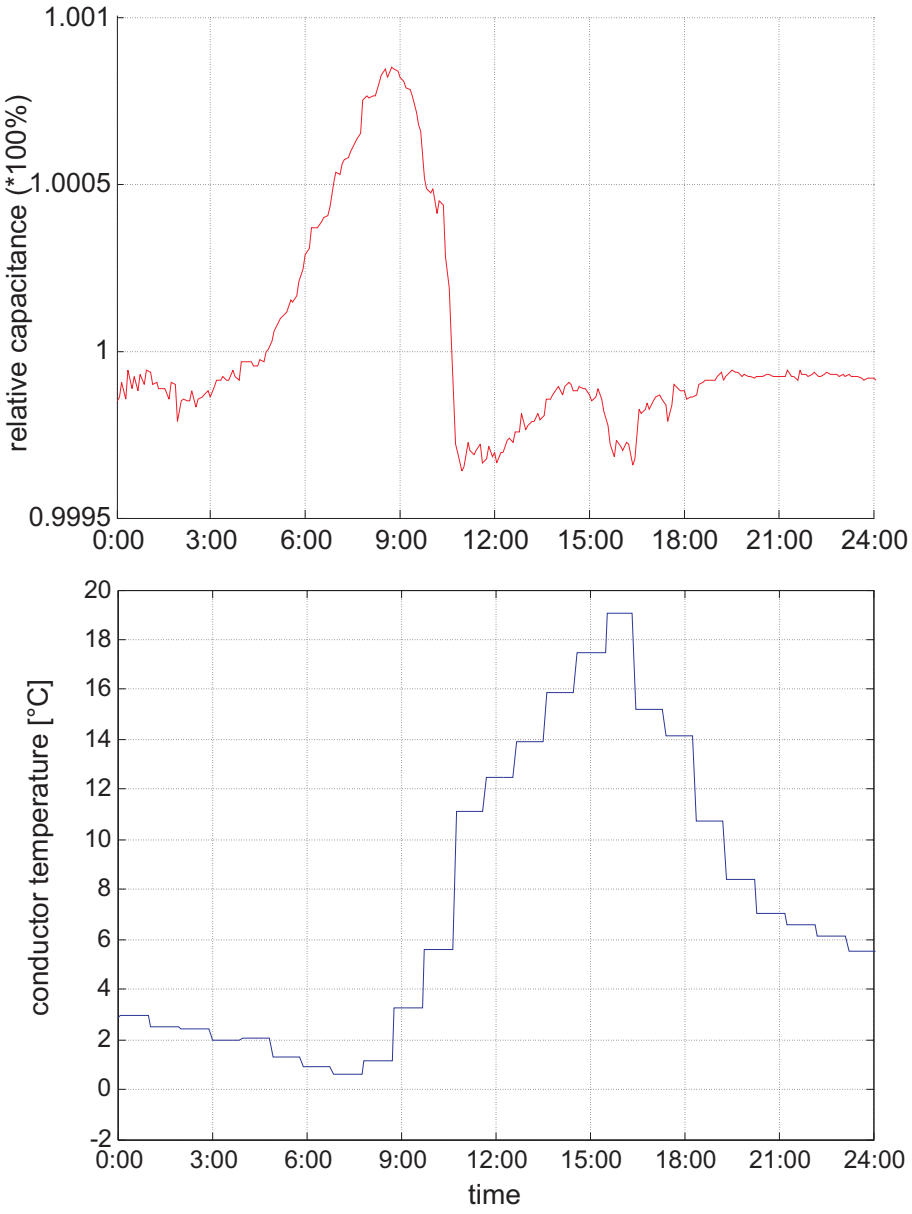

Figure 8.16: Event 3: Capacitive measurement data of measurement capacitance C_1 and conductor temperature on February 18, 2011 [9]. The capacitance is rising as a thin layer of ice accumulates (3h...9h). The absence of a strong signal decrease during the melting phase may be due to the minimal amount of water.

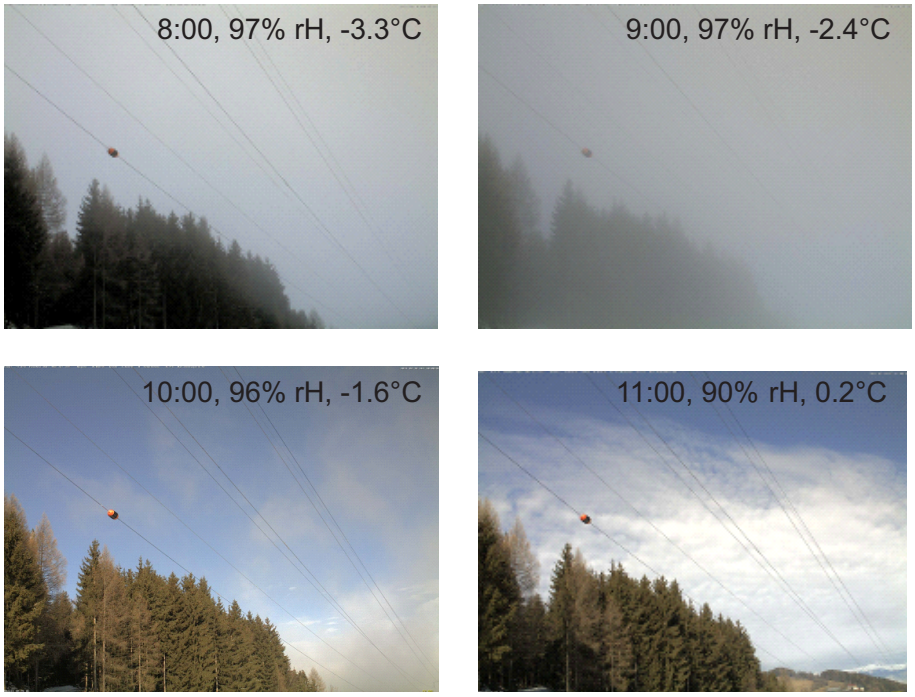

Figure 8.17: Event 3: Weather camera images on February 18, 2011 [9]. Icing conditions are present between the early morning and approx. 10 a.m.

electrode distance and the corresponding signal variances, which reach their maxima during phases of high surface activity. Furthermore, it seems that melting periods result in the highest variance levels due to fast permittivity and capacitance changes.

Figure 8.19 depicts the conductor temperatures and load status of the line in the same time period.

Example Event 5

Event 5 is an example for a wet, then drying conductor. Different amounts of water (films and/or droplets) were present at the conductor surface (compare Figure 8.20). In the evening of March 18, water dried off completely, most likely due to wind.

Figure 8.21 depicts the corresponding conductor temperatures of the line. Only positive temperatures have been recorded.

Figures 8.22 and 8.23 depict weather camera images on March 16 (12 p.m., precipitation rate of 5 mm per hour) and March 17 (12 p.m., high air humidity not detected as rain by the rain sensor), respectively.

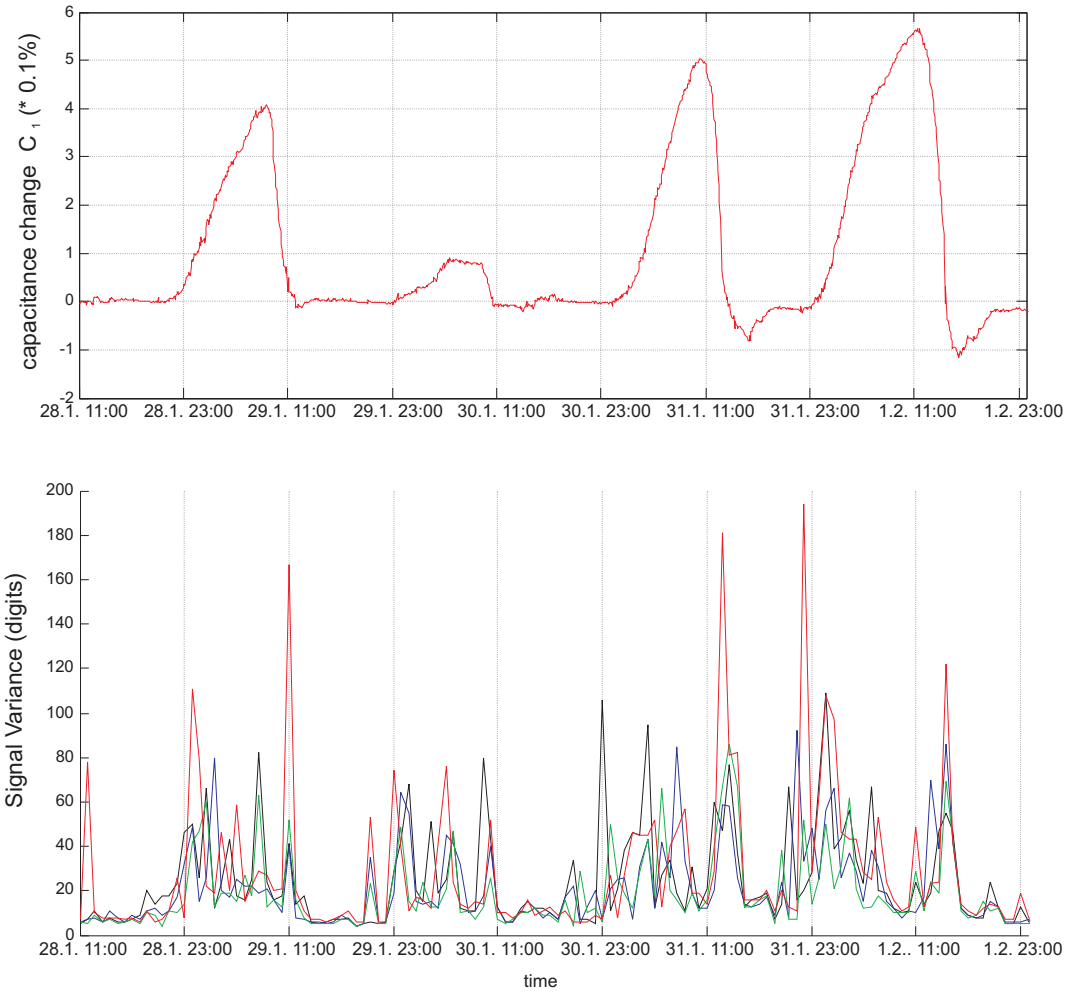

Figure 8.18: Event 4: Capacitive measurement data (measurement capacitance C_1) and signal variances (for measurement capacitance C_1 (red), C_2 (green), C_3 (blue), C_4 (black)) between January 28 and February 1, 2011 [9]. Phases of ice accumulation and melting most often show high signal variance due to an increased surface activity, see January 28 23:00–January 29 11:00.

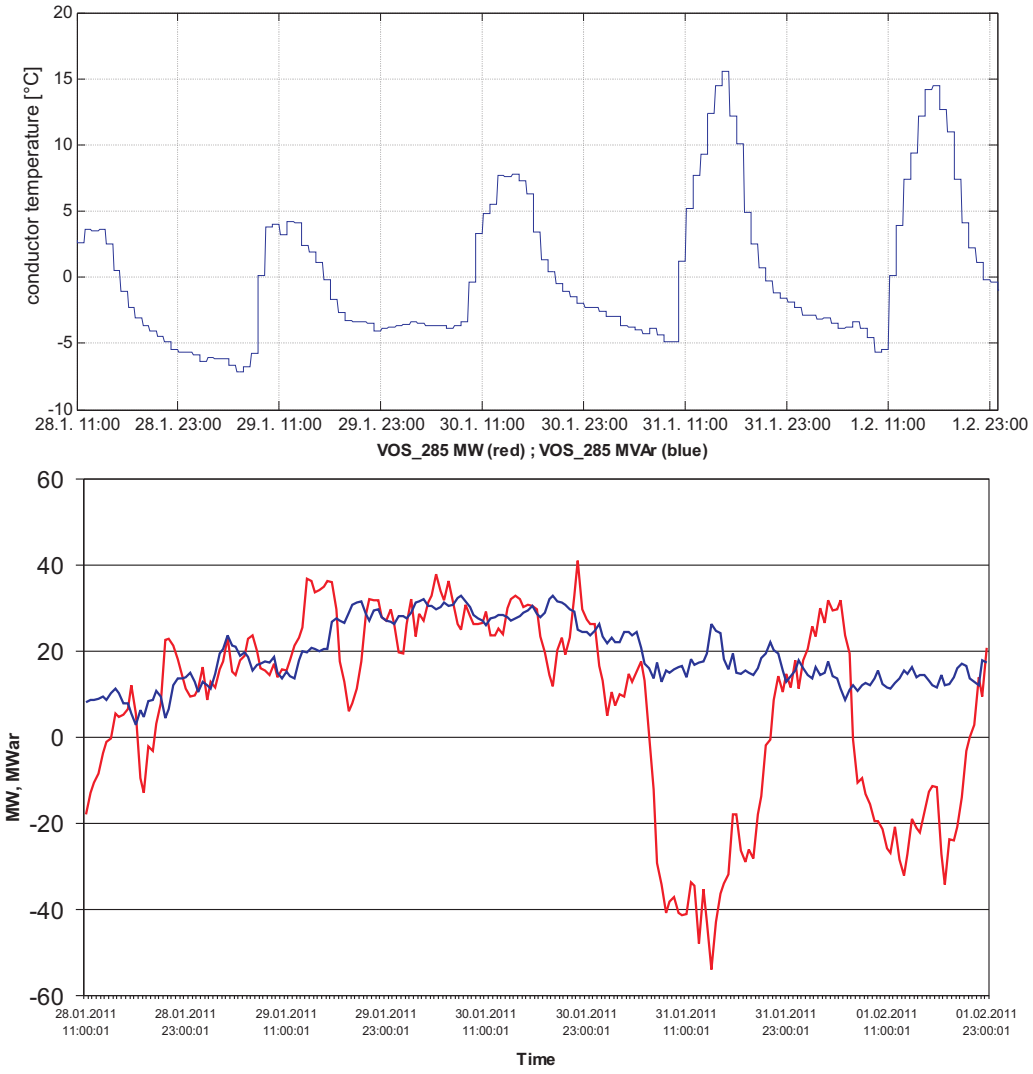

Figure 8.19: Event 4: Conductor temperature and power load [9]. As depicted earlier, temperatures below zero lead to icing. The power load, however, has an insignificant impact on the conductor rope temperature. This is most probably due to the comparatively low power levels in the observed period of time.

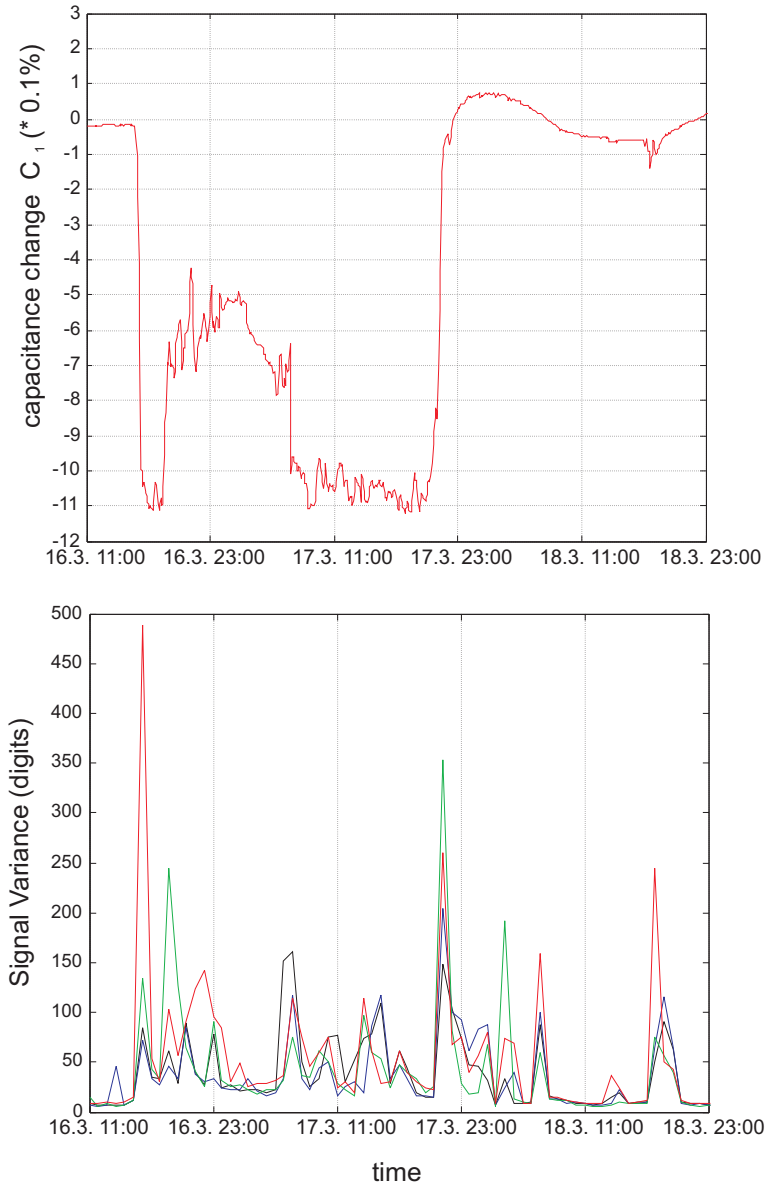

Figure 8.20: Event 5: Capacitive measurement data (measurement capacitance C_1) and signal variances (for measurement capacitance C_1 (red), C_2 (green), C_3 (blue), C_4 (black)) between March 16 and 18, 2011 [9]. High signal variance can be seen due to the presence of water drops on the surface. Furthermore, the capacitance values for a wet surface are always lower than for a dry conductor with an exception due to, for instance, droplets during the drying process.

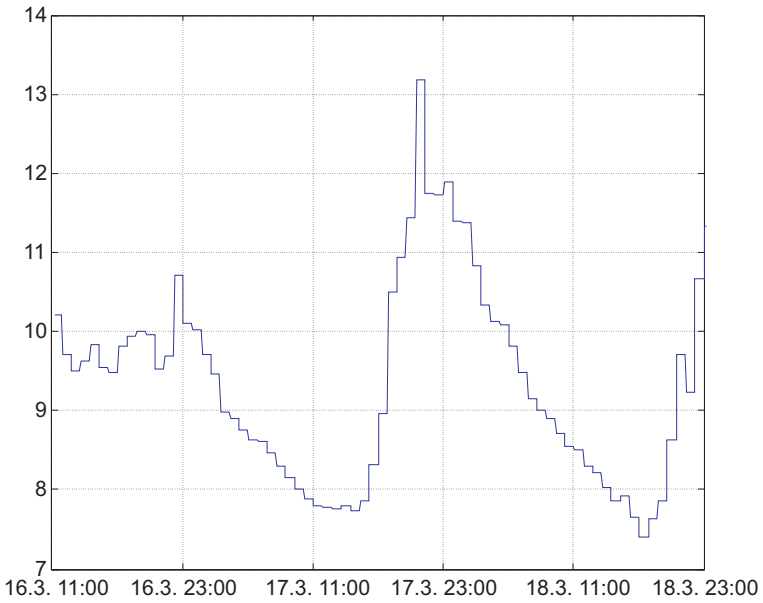

Figure 8.21: Event 5: Conductor temperature [9], always positive during this event.

Figure 8.22: Event 5: Weather camera image on March 16, 12 p.m. [9], dry weather.

Figure 8.23: Event 5: Weather camera image on March 17, 12 p.m. [9], rainy weather.

8.2.3 Results 2010-2011

Though no critical icing events could be recorded in the second field test, it could be shown that the test device could be kept operational for several months on a 220 kV line. Various improvements had been implemented based on the findings of the earlier tests. By means of comparison with weather data, several minor icing events could be identified. The presence of ice and water can be clearly distinguished from each other and from a dry conductor. Besides, ice thickness can be estimated to a certain extent already from the signal amplitude of the first measurement capacitance. At this point, an outlook could be given as follows:

- More reference data should be collected in suitable environment and in the field in order to match measurement data with the actual icing status
- The circuitry needs re-design in order to obtain series product level
- Electrode mounting is easier than before, but still tricky to be mounted by a worker.

- Camera images can not reliably deliver information on conductor icing status due to the typically large distance.

At this point, the project ended but an industry partner showed interest in industrialization of the measurement principle. Chapter 9 gives information on the respective investigation on suitable material systems, design and the actual realization as well as icing tests in a climate tunnel.

Chapter 9

Industrialization

In this chapter, an overview is given on efforts made on the implementation of the capacitive icing detection principle for an industrial system to be applied on high-voltage overhead lines. In the experimental test device approach described in Chapter 6, especially the sensor mounting process is time consuming and critical to the sensor characteristics as the electrode positions may vary due to the complicated mounting procedure. Furthermore, the longevity and robustness of the manufactured components may be questionable. For this reason, a mechanically robust solution, providing an expected lifetime of more than 10 years, is desired.

The industry partner had a framework available for conductor rope temperature monitoring. It looked promising to implement the capacitive icing detection front-end in the existing, proven framework offering suitable housing, mounting, data transmission circuitry and battery power supply. Due to the available power source, the energy harvesting approach was not implemented at this stage in order to minimize costs and risks of development as well as the time-to-market of a small series. Hence, the focus in this chapter is put on the development of a durable electrode assembly, where the choice of materials and material processing technologies is crucial.

Section 9.1 gives information on several investigated materials suitable for the environment in which to operate the equipment, including summaries on processing technologies. Also, the suitability of the material solutions is evaluated with respect to the design of an icing sensor front-end. In Section 9.1.6, the different approaches are compared and possible solution approaches, which

in part have been realized as laboratory test devices during the design process of the industrial electrode assembly, are presented. Section 9.2 informs on design and realization of the series device and first results of icing tests in a climate tunnel.

9.1 Material Systems

For an industrial electrode assembly, various material systems were investigated beforehand. Though the best solution seems to be a purpose-made PTFE sinter part or a string ribbon cable with a geometry comparable to the field test device setup, this approach is not feasible due to the high costs. Therefore, further material systems with comparable material properties were investigated in order to design and build an industrial electrode assembly.

Sections 6.3.1 and 5.2.2 provide information on the realization of the sensor front-end of the test device setup. It was found that an electrode assembly design using cables with an insulation made from polytetrafluoroethylene (PTFE), which is a comparatively robust polymer, provided good stability through its material properties, given as follows:

- Wide operational temperature range: -200°C -> +200°C
- High UV stability as a native material property
- Desirable mechanical properties: low friction, rigid
- Virtually no water absorption
- Good dielectric properties (low $\varepsilon_r = 2$, corona resistant)
- Surface quality: most of the conductor surface is available between the measurement electrodes, i.e. changes in the icing behavior due to the application of the sensor are minimized

Generally speaking, the structure that needs to be realized consists of layers of conductive structures with non-conductive matter in-between and around them, insulating them from the environment. At the same time, the overall thickness must be kept as small as possible (i.e. below a few millimeters) in

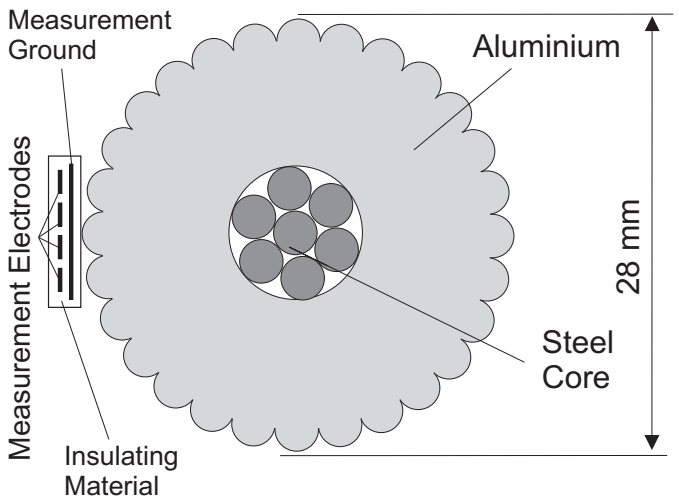

Figure 9.1: Sketch of the required measurement electrode assembly structure.

order to avoid high voltages between measurement electrodes on the one side and in order to minimize aerodynamical alterations on the other. Conductive interconnections between the conductive planes need to be manufactured. Towards the environment, the structure needs to be enclosed by nonconductive material except at specified terminals serving as ports towards the measurement circuitry. Figure 9.1 shows a cross section of this structure.

For a small series, several readily available material systems were taken into consideration. The following material systems deliver the best fit to the given requirements and were investigated more in detail:

- Printed Circuit Board (PCB) + Fluoropolymer Coating
- Printed Circuit Board + Polyurethane (PU) Coating
- Printed Circuit Board + Silicone Coating
- Metal Inlays in Polymer Rapid Prototyping Processes
- Layered Ceramics (for example, Low Temperature Cofired Ceramics, LTCC)

All technologies fulfill the requirements given above to a certain extent and are known and established technologies. The denoted material systems are described in detail in the following sections, while at the end of the chapter, a comparison is given. In total, four of the mentioned material systems have been tested in laboratory setups.

9.1.1 Printed Circuit Board + Fluoropolymer Coating

A printed circuit board is a standard product, typically consisting of two layers of photolithographically formed conductive structures and an electrically isolating carrier material in-between. It can also be manufactured as a multi-layer structure with numerous layers. Printed circuit board manufacturing typically starts with a raw material consisting of conductive and non-conductive layers already glued together. After drilling and through-connecting of drill holes where necessary, the conductive layers are covered with a photo-resistive film, exposed to light according to lithography data, a protective polymer serves as a cover or the part is laminated together with further layers. Typically, the core material is so-called FR4, i.e. a glass fiber reinforced epoxy resin. Other materials such as polyamides, PTFE and polyimide are commercially available. Furthermore, aluminium can be used as a carrier material with laminated thin polymer-based multi-layer substrates. Epoxy resins need to be protected from UV radiation and FR4 has a tendency to absorb water (up to a few per cent), which is due to the glass fibers running through the material, increasing the surface available for water absorption. For this reason, a robust coating is necessary, as water absorption can radically change the dielectric properties and may also lead to cracks, fractures etc.

One manufacturer tried to apply a thin layer of a fluoropolymer on an aluminium based PCB using an electrostatic lacquering process. The resulting layer had a thickness between 30 to 50 micrometers, which is far from the minimum thickness required for mechanical stability. Figure 9.2 depicts a test device of an electrode assembly in this technology.

The major drawback of this material system is due to the non-stick nature of fluoropolymers in combination with other materials. Adhesion to the PCB carrier material was good, however, very poor adhesion was achieved between the coating and the electrode surfaces making the coating unsuitable for a

Figure 9.2: Photo of a sensor electrode setup (aluminium based PCB with fluoropolymer coating).

harsh environment. In addition to that, the quality of the coating itself turned out poor. Field tests with this setup showed a very high sensitivity towards increasing or decreasing air humidity at temperatures well above zero. The devices were tested in a potentiostat at the Institute of Materials Physics, Graz University of Technology, revealing a non-negligible DC conductivity of the layer. The most probable cause may have been porosities in the layer. Therefore, this material system was not investigated further when it had became obvious that layers of the originally desired thickness (approx. 0.5 to 2 mm) could not be manufactured in a sufficiently high quality.

9.1.2 Printed Circuit Board + Polyurethane Coating

In search of better coating materials, polyurethanes were investigated. Polyurethanes (PU) are polymers, which result from polycondensation of an isocyanate and a polyalcohol. The choice of raw materials leads to a wide range of resulting material properties from soft foams (for instance, used for thermal insulation or car seats) to highly robust parts (for example, protective aprons for snowcats). Polyurethanes are typically used within the industrial temperature range and (-40 to +85°C) can be protected from UV radiation by means of additives. Mechanical properties can be set so that there is almost no abrasive wear. Water absorption is reasonable (in the range of 0.5 %). Relative permittivity varies between 3 and 6 at frequencies below 1 MHz. Good surface qualities can

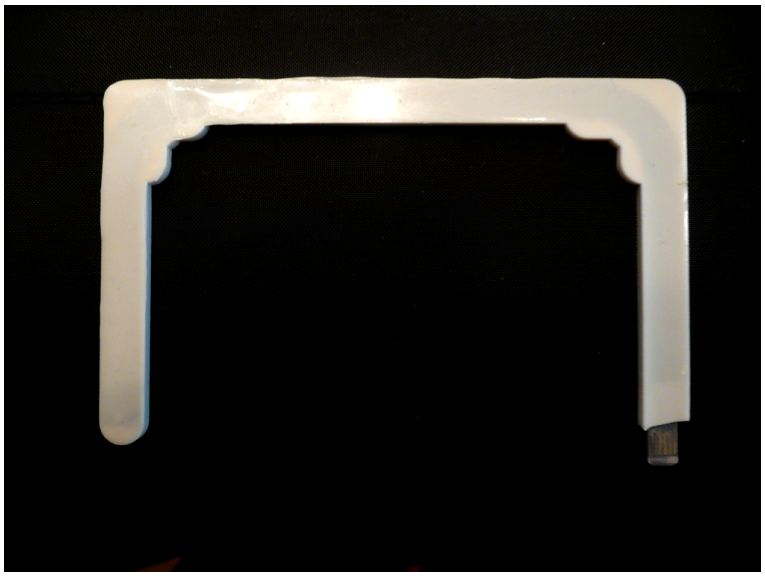

Figure 9.3: Photo of a sensor electrode setup (aluminium based PCB with a white polyurethane coating).

be achieved depending on the manufacturing technique. Dielectric breakdown voltage typically exceeds 20 kV per millimeter [145].

Coating with polyurethane can be established by means of cold molding (for example, reaction molding) or by injection molding (typically with thermoplastic resins). This is a complex procedure as the part to be coated needs to be kept at the correct position during the molding process (for instance, by means of removable pins). A simple test device has been manufactured using cold molding around an aluminium PCB, yielding a coating layer thickness between 1 and 2 millimeters, enclosing the entire sensor electrodes PCB. Figure 9.3 depicts a test device of an aluminium based PCB with a polyurethane coating.

Preliminary measurements revealed good results. However, none of the available small-series manufacturers was able to guarantee mechanical, UV and high-voltage properties at PU layer thicknesses below 5 mm. It turned out that the risk of delaminations or damages due to environmental conditions was too high.

9.1.3 Printed Circuit Board + Silicone Coating

As a further material system, silicones have been investigated as a coating material for PCBs. Being one of few anorganic materials in electrical and electronic engineering, silicones are used in high-voltage engineering applications for insulation purposes. Similarly to polyurethanes, silicones are available in a wide variety of different mechanical properties. Silicones can typically withstand elevated temperatures even exceeding 200°C. As they do not originate from hydrocarbons but derive from silicon compounds, they are typically fireproof. Silicones can be made UV stable by means of additives. Water absorption is typically below 0.1 %. Relative permittivity ranges from 2 to 4 at frequencies below 1 MHz. Polymerization of silicones can be triggered, for example, by air humidity or elevated temperatures. Typically, side products such as water, alcohols or acetic acid are released during the polymerization, but special mixtures are available for casting and sealing electronic circuitry which do not release by-products that are harmful to electronic circuitry. Dielectric breakdown voltage typically is in the range of 20 kV per millimeter [146].

Similar to polyurethanes, coating with silicone is typically a cold molding process. For increased reaction speed, heat-curable silicones are available. The drawback of silicone coatings is the problem they share with other polymers: achieving thin yet stable layers is a sophisticated task.

Generally, adhesion between PCB and the coating polymer is a critical issue. It has to be ensured that the coating polymer sticks well to the surface (for instance, by its chemical properties) or that the coating is kept in position by mechanical means (for example, coating-filled drill holes or especially prepared surface structures, etching etc.) One further issue which disadvantages polymer coatings is obviously a certain minimum layer thickness in order to ensure mechanical stability. On the other hand, there are coatings which due to their application process only allow layer thicknesses which are too thin to be mechanically stable over the lifetime of the device.

Consequently, other processing technologies which in the first instance would not rely on coating or molding processes were searched in order to minimize costs and risks before a series production.

9.1.4 Metal Inlays in Polymers - Rapid Prototyping

So-called rapid prototyping processes seemed to be a suitable manufacturing technology for a fast and cost-efficient evaluation of material systems. Compared to molding, similar materials can be made use of, but different manufacturing techniques (such as layer-per-layer deposition) are used: complex three-dimensional structures can be made from polymers which are, for example, heat- or light-cured. The approach looks promising as the achievable manufacturing resolution is high while keeping the costs comparatively low. Conductive (metal) parts can also be inserted, thus reliably enclosing them during manufacturing. However, the technology is young, available material systems are limited and especially, silicones and fluoropolymers were not available at the time of request.

9.1.5 Layered Ceramics - Low Temperature Co-fired Ceramics

Ceramics are a widely used material in high voltage engineering. Especially for high-voltage insulating elements (power transmission line insulators, transformer insulators and also smaller parts such as fuse holders) and can be made, for example, from alumina or porcelain-type base materials. Besides electrical insulation, the main advantages of this non-organic material are its very high resistance against mechanical stress (pressure, traction) and at the same time its robustness against creeping currents. Ceramic insulators are typically manufactured in a process similar to the fabrication of china ceramics - raw materials are blended with water and additives, the workpieces are shaped, glazed and fired.

Layered ceramics are a hybrid, thick-film technology for the production of small, accurate ceramic objects such as microfluidic reactors [147] or electronic components. Low temperature co-fired ceramics (LTCC) are sintered (cofired) at a temperature up to 1000°C, according to the manufacturers specification. Due to its ceramic character, the objects' operational temperature range exceeds all limits which inhere in organic materials. UV stability is easily achieved (for example, titanium dioxide itself is a commercial sun blocker). Water absorption is negligible (below 0.1 %). Thermal expansion is also small

(below 6 ppm/°C). Compared to metals, the fired material is brittle (flexural strength 320 MPa, young's modulus 120 GPa). Conductive structures (e.g. made from an 8 micron layer of silver paste) can be included in a layered structure. Capacitors, resistors and via connections can be printed on inner and outer layers, which allows also for complete devices integrated in the material [148]. The dielectric constant of ceramic materials is typically higher than of polymers, equaling 7.8 for a DuPont 951 material. The typical resolution for conductive structures and cuttings is 100 microns. Concerning high-voltage operation, the breakdown voltage exceeds 40 kV per millimeter [149], [145].

The raw material of LTCC components are so-called "green tapes" (microdispersed ceramic particles in a polymer matrix) and conductive pastes (typically silver, gold or palladium). For each layer, a piece of green tape is cut out (using a knife, an infrared laser or a hot-knife) and the conductive structures are deposited, for example, by means of sieve printing. Via connections are established by means of cutting holes in the green tape, which are then filled with a conductive paste. The layers are stacked and aligned one over the other and the layer compound is laminated by means of high pressure (typical values are 3000 psi, 70°C). The following sintering process removes the polymer matrix, sinters the ceramic particles together and thereby yields the end product. Typically, more than 100 layers can be stacked and a line resolution of 100 μm can be achieved [150].

Concerning the production process of LTCC, several limitations need to be respected:

- Shrinkage during firing. The laminated substrates shrink between 10 and 20 % in x, y and z axis, most often anisotropically [151].

- Conductive plane fill densities. Ceramics adhering to ceramics provide good mechanical stability, whereas the bond between metal and ceramics is a potentially weak point. Therefore, a 50 % conductive fill of a layer is standard while a solid fill (100 %) may lead to mechanical instabilities.

- Maximum part sizes. Due to size limitations of raw materials and limitations of working areas of laser cutters and mechanical presses, the typical maximum part size (after firing) is 96 mm x 96 mm, which is already

large compared to what LTCC is typically used for (for instance, SAW filters, chip antennas etc.).

- Non-rectangular objects tend to deform during sintering, therefore they need to be separated after the firing process requiring highly sophisticated technologies (diamond saws or high-power lasers).

However, the thermal stability and excellent hermiticity with virtually no water absorption highly qualifies LTCC parts for use in harsh environments such as high voltage over-head power lines.

9.1.6 Comparison of Material Systems

Table 9.1 compares the investigated material systems regarding the relevant parameters. Concerning the costs, PCBs with coatings are most affordable as standard mass production processes can be used. Rapid prototyping and LTCC processes require more expensive equipment such as printing sieves or complex molding forms. A purpose-made teflon cable or teflon sinter part is the most expensive solution.

With respect to water absorption, ceramics, silicone and PTFE show the best behavior (0.5 % or less), while spray-on fluoropolymer coatings showed porosities and water absorption of polyurethanes highly depends on the actually used ingredients.

Good UV resistivity can be achieved for PTFE, fluoropolymers and ceramics, while all other materials must be made UV resistant by means of additives.

PTFE, fluoropolymers, silicones and ceramics have a very wide operational temperature range. Moreover, they can withstand partial discharges for a long time, while this may be more challenging for other polymers like, for example, polyurethanes.

The lowest permittivity (approx. $\varepsilon_r = 2$) can be achieved for PTFE. Other polymers range between 2 and 6, while typical LTCC material systems range between 7 and 10.

Good mechanical properties include sufficient resistance against abrasive wear, uniform and smooth surfaces while providing a surface, which is comparable to the conductor line in terms of wetting and accretion behavior. Thin fluoropolymer coatings revealed a weak mechanical stability while polyurethane

	Material Parameters						
	Costs	Water	UV	Temp.	Corona	Permitt.	Mech.
Teflon Cable	-	+	+	+	+	+	+
PCB+Fluoropolymer	+	o	+	+	+	+	-
PCB+Polyurethane	+	o	o	o	o	+	o
PCB+Silicone	+	+	o	+	+	+	o
Rapid Prototyping	o	o	o	o	o	+	o
Ceramics (LTCC)	o	+	+	+	+	o	+

Table 9.1: Comparison of material systems for an industrial electrode assembly on high-voltage power lines. "+" denotes low costs, low water absorption, high UV stability, wide operational temperature range, good resistance towards partial (corona) discharges, low permittivity, good surface properties and high mechanical stability. "−" denotes the opposite, "*o*" denotes properties in-between.

and silicone coatings have hydrophobic surface properties. Therefore, these polymers tend to accrete ice later than the conductor itself. The teflon cable can be managed to offer enough conductor surface so that the icing behavior is not altered too much. Ceramics (which are typically oxides) show an ice accretion behavior which is comparable to the conductor line surface, which is also an oxide - i.e. aluminium oxide.

Comparing the available technologies, a PTFE cable or PTFE sinter part on the one hand and a ceramic part on the other hand seem to be most promising. Both methods are costly and have long lead times. Under the aspect of costs and lead time, the ceramic solution has an advantage as there are production facilities available for both small and large series.

9.2 Realization

Given a lot size of less than 50 devices in a first batch, low-temperature co-fired ceramics were the material system of choice. Due to the fact that the data communication and energy management system were readily available from a power line temperature monitoring probe, the electrode assembly and sensor front-end was designed to fit to the existing system framework.

In Section 9.2.1, details on the electrode assembly and its integration into

Figure 9.4: Photo of the Micca temperature probe.

the existing framework is reported. Section 9.2.2 presents icing experiments with test devices, conducted at the CIGELE Atmospheric Icing Research Wind Tunnel (CAIRWT) at the University of Québec at Chicoutimi, Canada, in December 2012. Finally, Section 9.2.3 explains the extraction of icing data from the achieved experimental measurement data.

9.2.1 Design and Integration

Micca Informationstechnologie GmbH is a company providing solutions to overhead line operators especially in the field of conductor temperature measurement and measurement of meteorological parameters. The product line "Enhanced Monitoring Overhead Transmission" was chosen as a framework for a novel icing detection device based on the measurement principle as described in Chapter 5.

The framework is a conductor temperature measurement device for so-called "thermal rating". A photo of this device is depicted in Figure 9.4.

This device is operated by a battery and can transmit measurement data to a base station over a wireless connection. This base station collects the data and transfers it to a database via GSM networks. More than 100 sensors are in operation worldwide.

One of the main challenges concerning the electrode assembly design was to minimize effects on the icing behavior due to the presence of the sensor itself with respect to the given mechanical structure of the probe framework. According to aerodynamical considerations, it was tried to keep a minimum

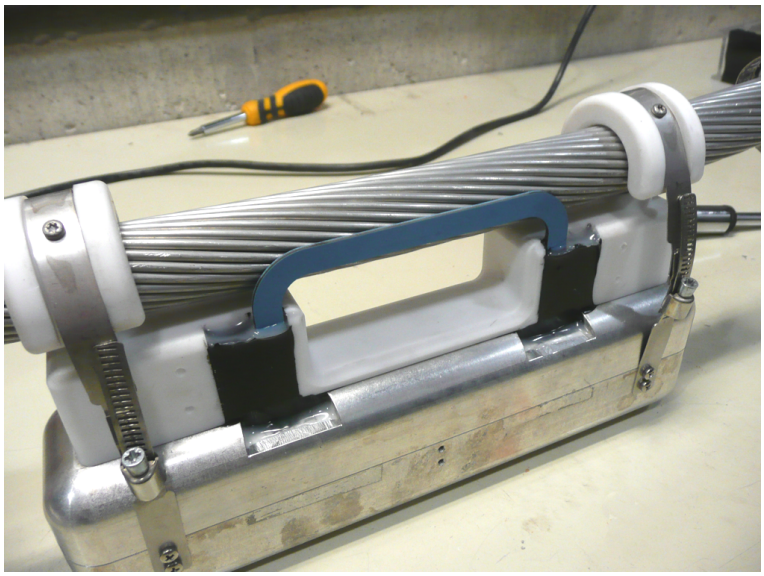

Figure 9.5: Assembled probe before mounting in wind tunnel.

area open all around the conductor in the sensor area. These deliberations together with high-voltage issues (compare Section 5.2) led to the design as depicted in Figure 9.5. It shows an assembled probe before undergoing tests in an icing climate channel.

The major part of the capacity inside the housing is occupied by the battery, as a standard lifetime of 10 years is guaranteed by the manufacturer. Therefore, the capacitance measurement circuitry together with input filters as described in Section 6.3.4 was included in the current measurement board inside the device. Following the results of Section 9.1.6 and the insights gained from failed tests with simpler technologies, an LTCC electrode assembly could be manufactured after a lead time of approx. half a year. These parts were connected to the measurement circuitry with flexible prints, after which the openings of the device was sealed.

The left and right LTCC electrode assemblies are mirrored with respect to each other. Each sensor contains a transmitter electrode, four receiver electrodes as well as two reference capacitors and have a total thickness of less than 2 mm. As described in Section 9.1.5, separation of non-rectangular parts after the sintering process requires diamond saws or high-power lasers. For this purpose, laser cutting was used. The resulting edge roughness was measured with a Diavite surface roughness meter (compare Figure 9.6).

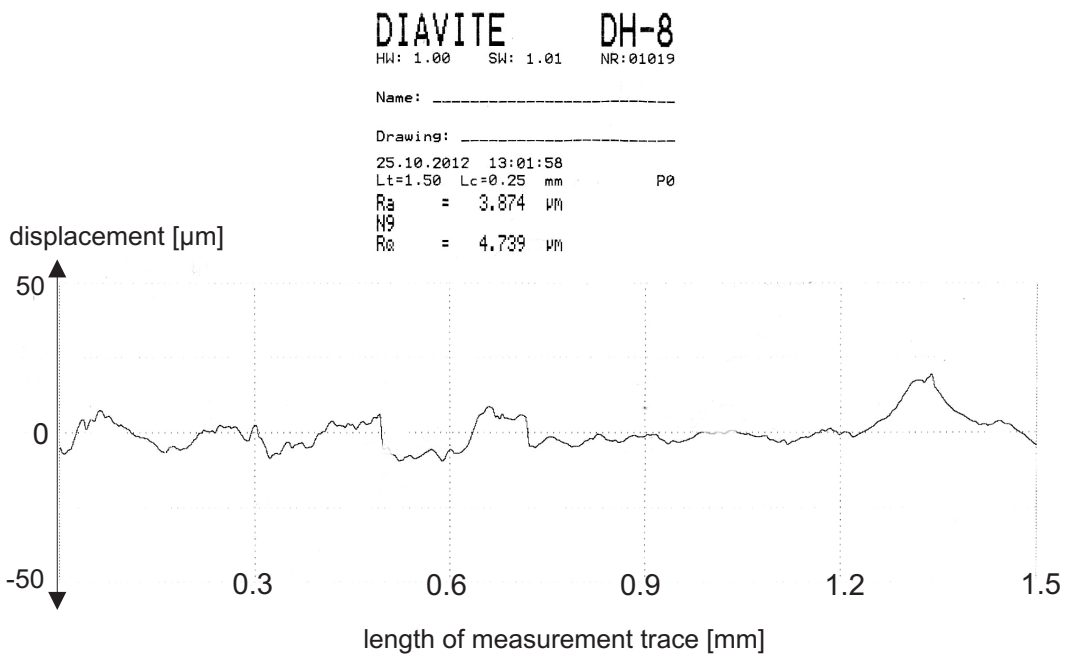

Figure 9.6: Roughness measurement record of the laser-cutted electrode assembly edge. The roughness arithmetic mean R_a amounts to approx. 3.8μm, the roughness quadratic mean R_Q amounts to approx. 4.7μm

Figure 9.6 shows a roughness scan of the laser-cutted edge of the sensor. The laser cutting process of the sintered LTCC part causes a higher surface roughness, but the surface quality appears to be sufficiently smooth.

9.2.2 Atmospheric Icing Research Wind Tunnel Tests

In December 2012, the first available icing probes were tested at the CIGELE Atmospheric Icing Research Wind Tunnel (CAIRWT) at UQAC/CIGELE in Chicoutimi, Québec, Canada together with the working group of Prof. Masoud Farzaneh. Various different ice qualities and layer thicknesses could be created and deposited on the probe. Parameters which can be set are

- Air temperature,
- Wind speed, and
- Water amount and droplet size (LWC, MVD).

Figure 9.7: Overview of CIGELE Atmospheric Icing Research Wind Tunnel [10].

Figure 9.7 shows the entire wind tunnel system, where the container at floor level contains the test section.

Air temperature at CAIRWT can be set down to -30°C at wind speeds up to 29 m/s. At the same time, water can be inserted in the air stream by means of heated spray nozzles. Through controlling water pressure, the total liquid water content (LWC) and mean volume diameter of the droplets (MVD) can be varied within certain limits, exceeding 8 g of water per cubic metre of air [10]. Through modification of these parameters, ice quality and air content of the produced ice can be varied. It can be defined if water droplets should freeze in the air stream already or if they get supercooled and freezes when impacting on the surface. By further increasing the amount of water at the same wind speed and temperature (or decreasing wind speed and increasing temperature at the same amount of water), water films can form at the surface, leading to the formation of ice qualities such as curtain glaze or icicles. Figure 9.8 shows the formation of glaze ice on the probe, while Figure 9.9 depicts the formation of icicles due to an increased water content.

Further common ice types (as described in Section 2.2) are soft and hard rime. Figure 9.10 depicts an early stage of soft rime icing, while Figure 9.11 shows a cross section of a setup where several centimeters of soft rime have

Figure 9.8: Probe in icing tunnel, glaze ice.

Figure 9.9: Probe in icing tunnel, glaze ice and icicles.

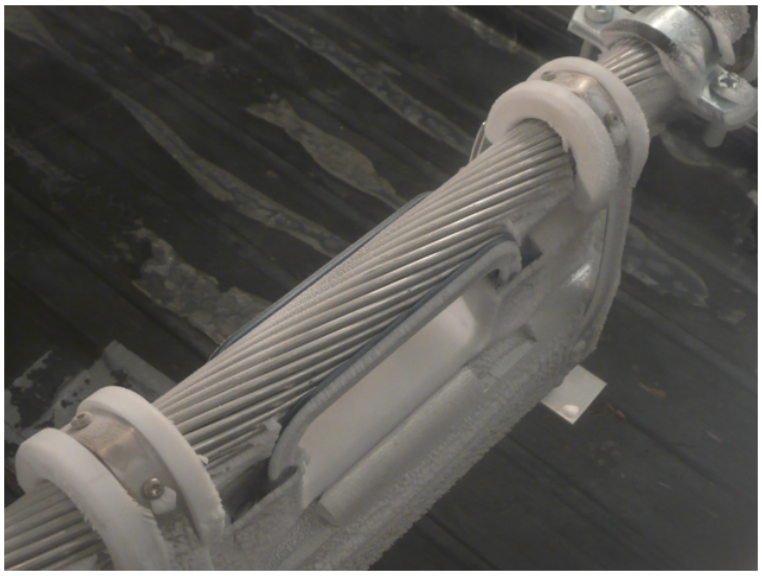

Figure 9.10: Probe in icing tunnel, thin soft rime.

accreted.

Hard rime contains less air, has a higher density and is therefore more relevant in conductor icing. Figure 9.12 shows an approx. 1 cm thick layer of hard rime on the electrode assembly, while Figure 9.13 shows a cross-section of a setup where several centimeres of hard rime have accreted. Comparison of Figure 9.11 and Figure 9.13 clearly shows the different properties of the two types of rime ice.

Furthermore, an ice quality similar to snow could be produced. The result is depicted in Figure 9.14.

Measurement data have been recorded for all events together with photos and still images from a video camera. Information on preliminary evaluation is given in Section 9.2.3.

9.2.3 Evaluation and Preliminary Results

The resulting data from the CAIRWT tests were used to design an algorithm to indicate the icing status of the sensor's surfaces. It turned out that both probes used in the tests suffered from problems at the soldered junctions between PCB and LTCC parts, leading to loose contacts opening and closing depending on mounting position and temperature. Furthermore, a PCB design error was discovered at the measurement PCB layout, causing parasitic capacitances to

Figure 9.11: Probe in icing tunnel, thick soft rime.

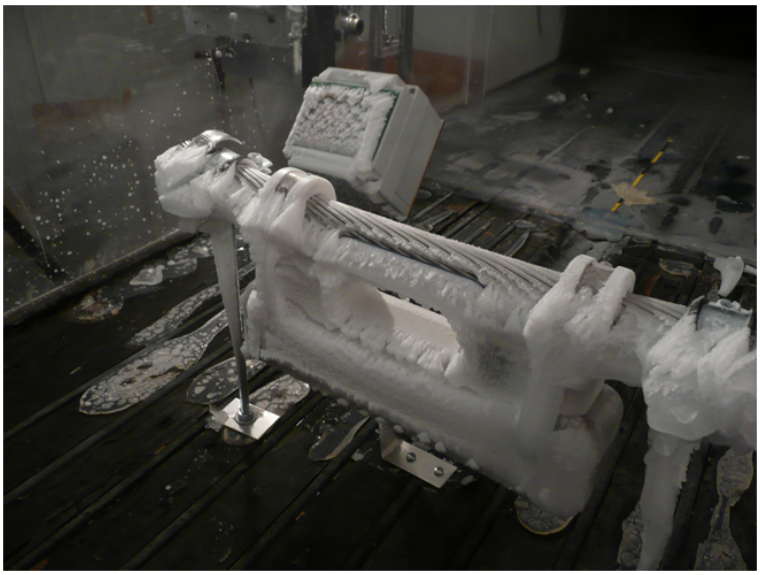

Figure 9.12: Probe in icing tunnel, thin hard rime.

Figure 9.13: Probe in icing tunnel, thick hard rime.

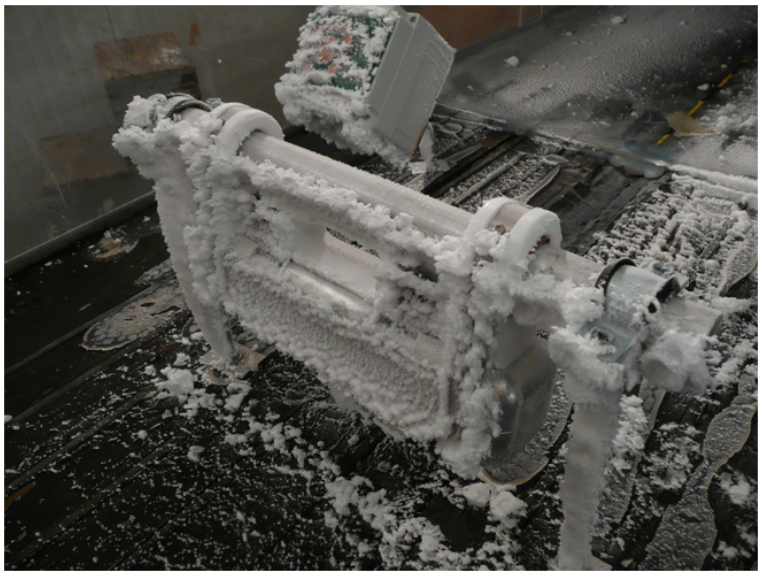

Figure 9.14: Probe in icing tunnel, snow-like icing.

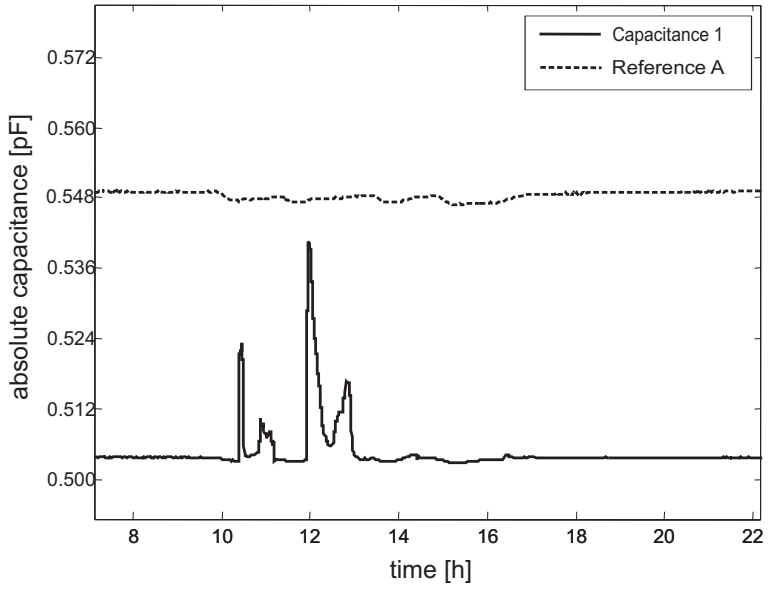

Figure 9.15: Example data from a glaze icing event at CAIRWT. Reference A is a reference capacitor inside the LTCC electrode assembly used for temperature compensation, which is shielded by ground layers. Capacitance 1 is formed by the electrode pair with the largest inter-electrode distance.

at least one measurement channel per side.

Figure 9.15 depicts raw data from two glaze icing events. The plot shows one of the reference capacitances ("Reference A"), which changes due to temperature and increased load on the transmitter electrode. Signal "Long" shows the behavior of the capacitance signal of the measurement capacitor with the largest inter-electrode distance. It can be seen that the capacitance increases during the presence of water (two steep rises in the signal at the beginning of the event and two slower signal rises during the melting process, while due to the low permittivity of ice only, the signal is comparatively small due to the large distance between transmitter and receiver.

The conducted tests led to the following conclusions:

- Aside from data losses due to hardware/design issues, the measurement capacitance signals behaved as expected.

- Further collection of reference data (from both climate chamber and "natural" field data) is necessary in order to cover as many icing scenarios as possible.

- Maximum signal changes occur at early stages of icing and with the presence of water, which is a key feature of the icing probe. Consequently, resolution decreases with increasing ice layer thickness. This is acceptable as the main purpose of the sensor is icing detection and indicating an icing status trend.
- Different ice qualities yield different signals. This allows for a classification of icing events.

Based on this conclusions, data evaluation will be conducted as follows (work still in progress):

1. Raw data (four 16 bit values representing the four measurement capacitances per side) are transmitted via the radio link.
2. Offset values (recorded in a calibrated environment and stored, for instance, in the base station) are subtracted.
3. Temperature compensation is done by means of 2-point calibration using the reference capacitors embedded in the LTCC sensors. Additionally, further reference channels could be implemented in the measurement PCB.
4. Field simulation by means of the finite element method (FEM) delivers distributions of capacitance values over ranges of both layer thicknesses and permittivities.
5. A Maximum Likelihood Estimator (MLE) is then used to find the thickness/permittivity value pair best fitting to the measured data set.

Several further improvements to this evaluation can enhance the performance of the data evaluation. For instance, there are physical limitations such as maximum speeds at which accretion and melting can occur. Also, temperature can not change stepwise. Taking into account the signal variance as a good indicator for surface activity can further refine the evaluation.

Chapter 10

Conclusion and Outlook

In section 10.1, the author draws conclusions on his work in the field of atmospheric icing and its detection while section 10.2 provides an outlook on future perspectives of the presented approach.

10.1 Conclusion

In this PhD thesis, first, a design for an autonomous icing detection device on high-voltage overhead power lines was developed. After defining the problem and setting the boundaries for an experimental realization, icing detection principles and energy harvesting methods were investigated.

An icing sensor front-end for operation close to the surface of a high-voltage overhead power line conductor rope was designed and tested. Within the progress of this thesis, aims and goals which have been set in the beginning needed to be revised and adapted, mainly due to new boundary conditions coming from the coincidence of different research fields such as electrical measurement, high-voltage technology, material science and atmospheric icing.

Energy harvesting from the alternating electric field was implemented and a circuitry design was found to operate both capacitive energy harvesting and capacitive measurement in parallel. In the course of this PhD thesis, several test devices were realized and evaluated both in laboratory setups and in field tests for two winter seasons. Both, energy harvesting from the alternating electric field and icing detection by means of capacitive sensing proved their feasibility in the field on a 220 kV overhead power transmission line. During the two

winter seasons' field tests, several icing events could be successfully detected. Furthermore, steps towards a successful industrialization of the measurement principle were taken.

10.2 Outlook

In the author's opinion, the developed design may play a significant role in the so-called smart grid in the future - an electricity distribution grid which is equipped with automated measurement and communication devices collecting data for higher efficiency and improved reliability. As described in chapter 9, commercial deploy of the icing measurement principle is in progress and shows positive results in the field and high interest from the relevant market. It is desirable that endangered sections of the worldwide power distribution grid will be equipped with a system as presented in this work or with similar systems. The number of fatal accidents due to icing can be decreased or at least the effects can be mitigated if there is early knowledge about a deteriorating icing status. For example, people can be evacuated, lines can be shut down in advance or even early de-icing measures can be deployed.

Own Publications and Reports

[1] M. J. Moser, H. Zangl, T. Bretterklieber, and G. Brasseur, "An Autonomous Sensor System for Monitoring of High Voltage Overhead Power Supply Lines," *e&i - Elektrotechnik und Informationstechnik*, vol. 126, no. 5, pp. 214–219, May 2009.

[2] M. J. Moser, H. Zangl, and G. Brasseur, "Icing Detector for Overhead Power Transmission Lines," in *Proceedings of the 2009 IEEE Instrumentation and Measurement Technology Conference*, Singapore, 2009, pp. 1105–1109.

[3] M. J. Moser, T. Bretterklieber, H. Zangl, and G. Brasseur, "Capacitive Icing Measurement in a 220 kV Overhead Power Line Environment," in *Proceedings of the 2010 IEEE International Conference on Sensors, Waikoloa, HI, USA*, 2010, pp. 1754–1757.

[4] M. J. Moser, T. Bretterklieber, H. Zangl, and G. Brasseur, "Strong and Weak Electric Fields Interfering: Capacitive Icing Detection and Capacitive Energy Harvesting on a 220 kV High-Voltage Overhead Power Line," *IEEE Transactions on Industrial Electronics*, vol. 7, no. 7, pp. 2597–2604, 2011.

[5] M. J. Moser, "Capacitive Icing Detection and Capacitive Energy Harvesting on a 220kV HV Overhead Power Line," in *Proceedings of the ARGE Sensorik PhD Summit 2011*, B. Jakoby, Ed., no. 978-3-9502856-1-1 (ISBN). ARGE Sensorik, June 2011.

[6] M. J. Moser and H. Zangl, "Rotor Blade Icing Detection by Means of Capacitive Sensing," in *Winterwind 2012 Book of Abstracts*, 2011.

[7] M. J. Moser, M. Brandner, and H. Zangl, "Sensor Fusion for a Blade Surface-Mount Icing Detector for Wind Turbines," in *Winterwind 2012 Book of Abstracts*, 2012.

[8] M. J. Moser, T. Bretterklieber, H. Zangl, and G. Brasseur, "Field Test of a Capacitive Icing Detection and Conductor Temperature Measurement System on a 220 kV Overhead Power Line," Internal Technical Report, June 2010.

[9] M. J. Moser, H. Zangl, T. Bretterklieber, and G. Brasseur, "A Capacitive Icing Detection and Conductor Temperature Measurement System, Field Test 2010-2011," Internal Technical Report, June 2011.

Bibliography

[10] H. Banitalebi-Dehkordi, L. Kollar, M. Farzaneh, P. Camirand, and C. Damours, "Introduction, Instrumentation and Calibration of CIGELE Atmospheric Icing Research Wind Tunnel (CAIRWT)," NSERC/Hydro-Québec/UQAC Industrial Chair on Atmospheric Icing of Power Network Equipment (CIGELE) and the Canada Research Chair on Engineering of Power Network Atmospheric Icing (INGIVRE), University of Québec at Chicoutimi, Tech. Rep., 2010.

[11] M. Lacroix, L. Brouillette, and A. Blais, "Hydro Quebecs De-icing System: Automated Overhead Line Monitoring and De-icing System," in *Proceedings of the 2008 Cigre Session, B2-211*, Paris, France, 2008, pp. 1–7.

[12] M. Huneault, C. Langheit, R. St.-Arnaud, J. Benny, J. Audet, and J.-C. Richard, "A Dynamic Programming Methodology to Develop De-Icing Strategies During Ice Storms by Channeling Load Currents in Transmission Networks," *IEEE Transactions on Power Delivery*, vol. 20, no. 2, pp. 1604 – 1610, April 2005.

[13] X. Jiang, J. Zhao, B. Luo, J. Zhang, and C. Huang, "Survey and Analysis of Ice Accidents of Early 2008 in Southern China," in *Proceedings of IWAIS XIII, Andermatt, Switzerland*, 2009, pp. 1–5.

[14] L. Makkonen and B. Wichura, "Simulating Wet Snow Loads on Power Line Cables by a Simple Model," *Cold Regions Science and Technology*, vol. 61, pp. 73–81, 2010.

[15] B. Zemljaric, P. Zabukovec, Z. Jovanovic, and M. Starasinic, "Phase Conductor Break Caused by Snow Accretion on 110 kV Overhead Power

Line," in *Proceedings of IWAIS XIII, Andermatt, Switzerland*, 2009, pp. 1–6.

[16] X. Jiang, S. Fan, Z. Zhang, C. Sun, and L. Shu, "Simulation and Experimental Investigation of DC Ice-Melting Process on an Iced Conductor," *IEEE Transactions on Power Delivery*, vol. 25, no. 2, pp. 919–929, April 2010.

[17] K. Bakic, F. Jakl, and B. Debenjak, "The First Experiences with Ice-Monitoring System for Transmission Network in Slovenia," in *Proceedings of IWAIS XIII, Andermatt, Switzerland*, 2009, pp. 1–6.

[18] P. Dyke, D. Havard, and A. Laneville, *Atmospheric Icing of Power Networks*. Springer, 2008, ch. Effect of Ice and Snow on the Dynamics of Transmission Line Conductors, pp. 171–225.

[19] H. Zangl, T. Bretterklieber, and G. Brasseur, "Energy Harvesting for Online Condition Monitoring of High Voltage Overhead Power Lines," in *Proceedings of the IEEE International Instrumentation and Measurement Technology Conference*, Vancouver Island, Canada, May 15-20 2008, pp. 1364–1369.

[20] S. Fikke, J. Kristjánsson, and B. Nygaard, *Atmospheric Icing of Power Networks*. Springer, 2008, ch. Modern Meteorology and Atmospheric Icing, pp. 1–27.

[21] "Guidelines for Meteorological Icing Models, Statistical Methods and Topographical Effects." CIGRÉ Working Group B2.16, Tech. Rep. 291, 2006.

[22] "Systems for Prediction and Monitoring of Ice Shedding, Anti-Icing and De-Icing for Power Line Conductors and Ground Wires," CIGRÉ Working Group B2.29, Tech. Rep. 438, December 2010.

[23] H. Zangl, A. Fuchs, T. Bretterklieber, M. Moser, and G. Holler, "Wireless Communication and Power Supply Strategy for Sensor Applications Within Closed Metal Walls," *IEEE Transactions on Instrumentation and Measurement*, vol. 59, no. 6, pp. 1686 – 1692, 2010.

[24] R. Fischer and F. Kießling, *Freileitungen*, 3rd ed. Springer, 1989.

[25] L. Makkonen, "Models for the Growth of Rime, Glaze, Icicles and Wet Snow Deposits on Structures." *Philosophical Transactions A*, vol. 358(1776), pp. 2913–2940, 2000.

[26] M. Homola, P. Nicklasson, and P. Sundsbo, "Ice Sensors for Wind Turbines," *Cold Regions Science and Technology*, vol. 46, pp. 125–131, 2006.

[27] L. Makkonen, "A Model of Hoarfrost Formation on a Cable," *Cold Regions Science and Technology*, vol. 85, pp. 256–260, 2013.

[28] C. Ahrens, *Meteorology Today*, 9th ed. Brooks/Cole, 2009.

[29] P. Admirat, *Atmospheric Icing of Power Networks*. Springer, 2008, ch. Wet Snow Accretion on Overhead Lines, pp. 119–166.

[30] Y. Sakamoto, "Snow Accretion on Overhead Wires," *Philosophical Transactions of the Royal Society*, vol. 358, pp. 2941–2970, 2000.

[31] M. Farzaneh and K. Savadjiev, *Atmospheric Icing of Power Networks*. Sprin, 2008, ch. Statistical Analysis of Icing Event Data for Transmission Line Design Purposes, pp. 31–80.

[32] K. Fujii and T. Takahashi, "Observation of Natural Snow Accretion on Test Conductors," in *Proceedings of IWAIS XIII, Andermatt, Switzerland*, 2009.

[33] L. Makkonen, "Modelling Power Line Icing in Freezing Precipitation," *Atmospheric Research*, vol. 46, pp. 131–142, 1998.

[34] M. Farzaneh, C. Volat, and A. Leblond, *Atmospheric Icing of Power Networks*. Springer, 2008, ch. Anti-icing and De-icing Techniques for Overhead Lines, pp. 229–265.

[35] R. Menini and M. Farzaneh, "PTFE-Coated Anodized Aluminum Alloy 6061 With Icephobic Properties," in *Proceedings of IWAIS XIII, Andermatt, Switzerland*, 2009.

[36] F.Arianpour, M. Farzaneh, and S. Kulinich, "Ice Adhesion and Hydrophobic Properties of Coatings Based on Doped RTV Silicone Rubber," in *Proceedings of IWAIS XIII, Andermatt, Switzerland*, 2009.

[37] C. Laforte, J. Carriere, and J. Laforte, "How a Solid Coating Can Reduce the Adhesion of Ice on a Structure," in *Proceedings of the Tenth International Workshop on Atmospheric Icing of Structures, Brno, Czech Republic*, 2002.

[38] L. Makkonen, "Ice Adhesion - Theory, Measurements and Countermeasures." *Journal of Adhesion Science and Technology*, vol. 26(4), pp. 413–445, 2012.

[39] R. Hefny, L. Kollár, M. Farzaneh, and C. Peyrard, "Adhesion of Wet Snow to Different Cable Surfaces," in *Proceedings of IWAIS XIII, Andermatt, Switzerland*, 2009.

[40] J. Petrovic, "Mechanical Properties of Ice and Snow," *Journal of Materials Science*, vol. 38, pp. 1–6, 2003.

[41] S. Montambault and J. Cote, "Remotely Operated Vehicle for Inspection and Intervention of a Live Line," US Patent 6 494 141, 2002.

[42] A. Leblond, B. Lamarche, D. Bouchard, B. Panaroni, and M. Hamel, "Development of a Portable De-Icing Device for Overhead Ground Wires," in *Proceedings of the 11th International Workshop on the Atmospheric Icing of Structures (IWAIS 2005), Montreal, Canada*, 2005.

[43] R. Egbert, R. Scharag, W. Bernhart, G. Zumwalt, and T. Kendrew, "An Investigation of Power Line De-Icing by Electro-Impulse Methods," *IEEE Transactions on Power Delivery*, vol. 4, no. 3, 1989.

[44] M. Landery, R. Beauchemin, and A. Venne, "De-Icing EHV Overhead Transmission Lines using Electromagnetic Forces Generated by Moderate Short-Circuit Currents," *IEEE Canadian Review*, pp. 10–14, Spring 2001.

[45] A. Nourai and R. Hayes, "Power Line Ice-Shedder," US Patent 6 660 934, 2003.

[46] A. Leblond, Y. Asano, and M. Isozaki, "Performance Study of LC-Spiral Rods Under Icing Conditions," in *Proceedings of IWAIS XIII, Andermatt, Switzerland*, 2009.

[47] J. Bruchu, R. Cloutier, and A. Bergeron, "On-Load Network De-Icer for HV Transmission Lines," in *Proceedings of the 11th International Workshop on the Atmospheric Icing of Structures (IWAIS 2005), Montreal, Canada*, 2005.

[48] R. Cloutier, A. Bergeron, and J. Brochu, "On-Load Network De-Icer Specification for a Large Transmission Network," *Transactions on Power Delivery*, vol. 22, no. 3, pp. 1947–1955, July 2007.

[49] P. Couture, "Switching Modules for the Extraction/Injection of Power From a Bundled HV Line," *IEEE Transactions on Power Delivery*, vol. 19, no. 3, pp. 1259–1266, 2004.

[50] C. Guanghui, S. Sheng, L. Mingming, and C. Daifeng, "Novel Deicing Approach of Overhead Bundled Conductors of EHV Transmission Systems," *IEEE Transactions on Power Delivery*, vol. 24, no. 3, pp. 1745–1747, July 2009.

[51] J. D. McCurdy, C. R. Sullivan, and V. F. Petrenko, "Using Dielectric Losses to De-Ice Power Transmission Lines with 100 kHz High-Voltage Excitation," in *Proceedings of the IEEE Industry Applications Conference 2001. Thirty-Sixth IAS Annual Meeting*, vol. 4, October 2001, pp. 2515–2519.

[52] T. Kendrew, "An Investigation of Power Line De-Icing by Electroimpulse Methods," *IEEE Transactions on Power Delivery*, vol. 4, no. 3, pp. 1855–1861, July 1989.

[53] V. Petrenko, M. Higa, M. Starostin, and L. Deresh, "Pulse Electrothermal De-Icing," in *Proceedings of the International Offshore and Polar Engineering Conference, Honolulu, HI, USA*, 2003.

[54] B. Nygaard, S. Fikke, L. Elvertro, and K. Harstveit, "Modeling Icing in Exposed Mountain Terrain," in *Proceedings of the 12th International*

Workshop on Atmospheric Icing of Structures (IWAIS2007), Yokohama, Japan, 2007.

[55] B. Nygaard, "Evaluations of Icing Simulations for the COST727 Icing Test Sites in Europe," in *Proceedings of the 13th International Workshop on Atmospheric Icing of Structures (IWAIS2009), Andermatt*, 2009.

[56] L. Makkonen and E. P. Lozowski, *Atmospheric Icing of Power Networks*. Springer, 2008, ch. Numerical Modelling of Icing on Power Network Equipment, pp. 83–110.

[57] S. Fikke, G. Ronsten, A. Heimo, S. Kunz, M. Ostrozlik, P.-E. Persson, J. Sabata, B. Wareing, B. Wichura, J. Chum, T. Laakso, K. Säntti, and L. Makkonen, "COST-727, Atmospheric Icing on Structures: 2006, Measurements and Data Collection on Icing: State of the Art," *Publication of MeteoSwiss*, vol. 75, p. 110 pp, 2007.

[58] H.-J. Draeger, D. Hussels, and R. Puffer, "Experiences with the Weather Parameter Method for the Use in Overhead Line Monitoring Systems," in *Proceedings of the 2008 Cigre Session, B2-107*, Paris, France, 2008, pp. 1–8.

[59] K. Savadjiev and M. Farzaneh, "Modeling of Icing and Ice Shedding on Overhead Power Lines Based on Statistical Analysis of Meteorological Data," *IEEE Transactions on Power Delivery*, vol. 19, no. 2, pp. 715–722, April 2004.

[60] M. Muhr, S. Pack, S. Jaufer, W. Haimbl, and A. Messner, "Development and Implementation of a Monitoring-System to Increase the Capacity of Overhead Lines," in *Proceedings of the 2008 Cigre Session, B2-101*, Paris, France, 2008, pp. 1–6.

[61] T. Seppa, "Accurate Ampacity Determination: Temperature-Sag Model for Operational Real Time Ratings," *IEEE Transactions on Power Delivery*, vol. 10, no. 3, pp. 1460–1470, 1995.

[62] B. Tammelin, "Wind Turbine in Icing Environment: Improvement of Tools for Sitting, Certification and Operation," NEW ICETOOLS, Finnish Meteorological Institute, p. 127, Tech. Rep., 2005.

[63] A. Eliasson, P. Gunnlaugsson, and E. Thorsteins, "Ice Accumulation at Measuring Site Hallormstadahals," in *Proceedings of IWAIS XIII, Andermatt, Switzerland*, 2009.

[64] *ISO 12494: Atmospheric Icing of Structures. ISO/TC 98/SC 3, 2000-07-20*, ISO Std.

[65] The Ice Load Surveillance Sensor IceMonitor. Combitech. http://rwis.net/res/pdffiles/IceMonitor_Product_Sheet.pdf, downloaded 7/8/2013.

[66] J. Chum, J. Vojta, and J. Hosek. Automated Measurement of Icing on the West of the Czech Republic. Institute of Atmospheric Physics. http://www.ufa.cas.cz/html/upperatm/chum/namraza/Icingmeasczech2.pdf, downloaded 4/9/2013.

[67] "Guide for Selection of Weather Parameters for Bare Overhead Conductor Ratings," CIGRÉ Working Group B2.12, Tech. Rep. 299, August 2006.

[68] R. Hackmeister, "Icing Detector for Aircraft," US Patent 6 010 095, January 4, 2000.

[69] M. Frant, "Icing Indicator System," US Patent 3 229 271, January 11, 1966.

[70] J. Kim, "Fiber Optic Ice Detector," US Patent 5 748 091, May 5, 1998.

[71] A. Ikiades, "Direct Ice Detection Based on Fiber Optic Sensor Architecture," *Applied Physics Letters*, vol. 91/10, p. 104, September 2007.

[72] W. Li, J. Zhang, L. Ye, and H. Zhang, "A Fiber-Optic Solution to Aircraft Icing Detection and Measurement Problem," in *Proceedings of the International Conference on Information Technology and Computer Science*, July 2009, p. 357.

[73] M. Anderson, "Electro-Optic Ice Detection Device," US Patent 6 425 286, July 30, 2002.

[74] J. Vivekanandan, "Ice Detection Using Radiometers," US Patent 5 777 481, July 7, 1998.

[75] B. Magenheim, "Microwave Ice Detector," US Patent 4 054 255, October 18, 1977.

[76] C. Bassey and G. Simpson, "Aircraft Ice Detection using Time Domain Reflectometry with Coplanar Sensors," in *Proceedings of the 2007 IEEE Aerospace Conference*, 2007.

[77] M. Luukkala, "Detector for Indicating Ice Formation on the Wing of an Aircraft," US Patent 5 467 944, November 21, 1995.

[78] H. Gao and J. Rose, "Ice Detection and Classification on an Aircraft Wing with Ultrasonic Shear Horizontal Guided Waves," *IEEE Transactions on Ultrasonics, Ferroelectrics and Frequency Control*, vol. 56, no. 2, pp. 334–344, February 2009.

[79] J. R. Chamuel, "Ultrasonic Aircraft Ice Detector Using Flexural Waves," US Patent 4 461 178, July 24, 1984.

[80] R. Johansson, P. Wetzer, and J. Makinen, "Method for Identification of Different States of Water, and Sensor Arrangement for Use in the Method," US Patent 5 585 551, December 17, 1996.

[81] R. Watkins, A. Gillespie, M. Deighton, R. Pike, and C. Scott-Kestin, "Ice Detector," US Patent 4 604 612, August 5, 1986.

[82] H.-G. Bruchmüller, "Sensor for Monitoring the Deposition of Frozen Fog and/or Ice on Surfaces," US Patent 4 532 806, August 6, 1985.

[83] M. J. Vellekoop, B. Jakoby, and J. Bastemeijer, "A Love-Wave Ice Detector," in *Proceedings of the IEEE Ultrasonics Symposium 1999*, Caesars Tahoe, Nevada, USA, October 1999, pp. 453–456.

[84] M. Kirby and R. Hansman, "Method and Apparatus for Measurement of Ice Thickness Employing Ultra-Sonic Pulse Echo Technique," US Patent 4 628 736, December 16, 1986.

[85] N. Goto, "Frost Sensor," US Patent 4 404 852, September 20, 1983.

[86] C. Barre, D. Lapeyronnie, and G. Salaun, "Ice Detection Assembly Installed on an Aircraft," US Patent 7 000 871, February 21, 2006.

[87] J. Hughes, "Ice Detectors," US Patent 3 541 540, November 17, 1970.

[88] F. Werner and E. Grindheim, "Ice Detector," US Patent 3 341 835, September 12, 1967.

[89] N. Weinberg, "Ice Detecting Apparatus," US Patent 32 700 330, August 30, 1966.

[90] R. Wilfred, "Ice Detector," US Patent 3 240 054, March 15, 1966.

[91] M. Koosmann, "Membrane Type Non-Intrusive Ice Detector," US Patent 4 611 492, September 16, 1986.

[92] T. Kamiyama and K. Miyamoto, "Frost Detector," US Patent 4 176 524, December 4, 1979.

[93] D. Cronin, D. Jackson, and D. Owens, "Ice Detector Configuration for Improved Ice Detection at Near Freezing Conditions," US Patent 6 320 511, November 20, 2001.

[94] M. Lustenberger, "Process for Detecting the Likelihood of Ice Formation, Ice Warning System for Carrying out the Process and Utilization thereof," US Patent 4 570 881, February 18, 1986.

[95] S. Roy, R. DeAnna, A. Izad, and M. Mehregany, "Miniature Ice Detection Sensor Systems for Aerospace Applications," in *Proceedings of the Eleventh Annual International Workshop on Micro Electro Mechanical Systems (MEMS)*, January 1998, p. 75.

[96] X. Li, W. Shih, J. Vartuli, D. Milius, R. Prudhomme, I. Aksay, and W.-H. Shih, "Detection of Water-Ice Transition Using a Lead Zirconate Titanate/Brass Transducer," *Journal of Applied Physics*, vol. 92, no. 1, pp. 106–111, 2002.

[97] K. Claffey, K. Jones, and C. Ryerson, "Use and Calibration of Rosemount Ice Detectors for Meteorological Research," *Atmospheric Research*, vol. 36(3-4), pp. 277–286, 1995.

[98] *Goodrich Sensor Systems: Model 0871LH1 Ice Detector, Specifications Sheet, 2006.*

[99] M. Farzaneh and K. Savadjiev, "Statistical Analysis of Field Data for Precipitation Icing Accretion on Overhead Power Lines," *IEEE Transactions on Power Delivery*, vol. 20, no. 2, p. 1080ff, April 2005.

[100] L. Baxter, *Capacitive Sensors, Design and Applications.* IEEE Press, 1997.

[101] W. Kliever, "Ice Indicator," US Patent 2 432 669, December 16, 1947.

[102] G. Codner, D. Pruzan, R. Rauckhorst, A. Reich, and D. Sweet, "Impedance Type Ice Detector," US Patent 5 955 887, 1999.

[103] R. Rauckhorst, "Ice Detector," US Patent 5 569 850, October 29, 1996.

[104] J. Geraldi, G. Hickman, A. Khatkhate, and D. Pruzan, "Apparatus for Measuring Ice Distribution Profiles," US Patent 5 398 547, March 21, 1995.

[105] J. Geraldi, G. Hickman, A. Khaktate, and D. Pruzan, "Measuring Ice Distribution Profiles on a Surface with Attached Capacitance Electrodes," US Patent 5 551 288, March 9, 1996.

[106] A. Troiano, E. Pasero, and L. Mesin, "An Innovative Water and Ice Detection System for Monitoring Road and Runway Surfaces," in *Proceedings of the 2010 Conference on Ph.D. Research in Microelectronics and Electronics (PRIME)*, July 2010, pp. 1–4.

[107] J. Weremczuk, "Dew/Frost Point Recognition With Impedance Matrix of Fingerprint Sensor," *IEEE Transactions on Instrumentation and Measurement*, vol. 57, no. 8, pp. 1791–1795, August 2009.

[108] K. Owusu, D. Kuhn, and E. Bibeau, "Capacitive Probe for Ice Detection and Accretion Rate Measurement: Proof of Concept," *Renewable Energy*, vol. 50, pp. 106–205, 2013.

[109] *Installation and operation manual of Instrumar IM101 v2.4., 2006.*

[110] J. Daniels, "Ice Detecting System," US Patent 4 775 118, October 4, 1988.

[111] R. Boström, R. Olingsberg, B. Nachebia, and D. Taits, "Device for Indicating Ice Formation," US Patent 6 456 200, April 29, 2002.

[112] J. Richard, "Ice Detection Apparatus," US Patent 3 276 254, October 4, 1966.

[113] F. Meyer, "Process and Measuring Probe for the Determination of Ice or Snow Formation," US Patent 4 755 062, July 5, 1988.

[114] R. Gaertner, "Detector for Measuring Icing Rates over a Plurality of Periods of Time," US Patent 3 571 709, March 23, 1971.

[115] I. Mackenzie, "Method and Apparatus for Measuring Ice Thickness on Substrates Using Backscattering of Gamma Rays," US Patent 5 821 862, October 13, 1998.

[116] R. Dehn and A. Macdonald, "Ice Detection System," US Patent 5 005 015, April 2, 1991.

[117] J. T. Abaunza, "Aircraft Icing Sensors," US Patent 5 772 153, July 30, 1998.

[118] H. Lee and B. Seegmiller, "Ice Detector and Deicing Fluid Effectiveness Monitoring System," US Patent 5 523 959, June 4, 1996.

[119] X. Huang, J. Li, W. Liu, J. Liu, and A. Song, "A New On-line Monitoring System of Transmission Line Icing and Snowing," in *Proceedings of IWAIS XIII, Andermatt, Switzerland*, 2009.

[120] D. Dondi, A. Bertacchini, D. Brunelli, L. Larcher, and L. Benini, "Modeling and Optimization of a Solar Energy Harvester System for Self-Powered Wireless Sensor Networks," *IEEE Transactions on Industrial Electronics*, vol. 55, no. 7, pp. 2759–2766, July 2008.

[121] J. Ramírez-Nino, M. Pacheco, J. Rodríguez, and V. M. Castano, "Design and Construction of a Pollution Monitor for Power Line Insulators," *Meas. Sci. Technol.*, vol. 7, pp. 876–881, June 1996.

[122] K. Sunderland and M. Conlon, "Estimating the Yield of Micro Wind Turbines in an Urban Environment: A Methodology," in *Universities Power Engineering Conference (UPEC), 2010 45th International*, 2010, pp. 1–6.

[123] D. Carli, D. Brunelli, D. Bertozzi, and L. Benini, "A High-Efficiency Wind-Flow Energy Harvester Using Micro Turbine," in *International Symposium on Power Electronics Electrical Drives Automation and Motion (SPEEDAM)*, 2010, pp. 778–783.

[124] X. Lu and S.-H. Yang, "Thermal Energy Harvesting for WSNs," in *Proceedings of the 2010 IEEE International Conference on Systems Man and Cybernetics (SMC)*, 2010, pp. 3045 – 3052.

[125] T. Becker, M. Kluge, J. Schalk, T. Otterpohl, and U. Hilleringmann, "Power Management for Thermal Energy Harvesting in Aircrafts," in *Proceedings of the 2008 IEEE Conference on Sensors*, 2008, pp. 681–684.

[126] C. Ugalde, J. Anzurez, and I. Lazaro, "Thermoelectric Coolers as Alternative Transducers for Solar Energy Harvesting," in *Proceedings of the 2010 IEEE Electronics, Robotics and Automotive Mechanics Conference (CERMA 2010)*, 2010, pp. 637–641.

[127] N. D. Sadanandan and A. H. Eltom, "Power Donut System Laboratory Test and Data Analysis," in *Souteastcon 90.* New Orleans, LA, USA: IEEE, April 1-4 1990, pp. 675–679.

[128] J. Engelhardt and S. Basu, "Design, Installation, and Field Experience with an Overhead Transmission Dynamic Line Rating System," in *Proceedings of the IEEE Transmission and Distribution Conference*, 1996, pp. 366–370.

[129] L. Du, C. Wang, X. Li, L. Yang, Y. Mi, and C. Sun, "A Novel Power Supply of Online Monitoring Systems for Power Transmission Lines," *IEEE Transactions on Industrial Electronics*, vol. 57, no. 8, pp. 2889–2985, August 2010.

[130] H. Zangl, T. Bretterklieber, and G. Brasseur, "A Feasibility Study on Autonomous Online Condition Monitoring of High-Voltage Overhead Power Lines," *IEEE Transactions on Instrumentation and Measurement*, vol. 58, no. 5, pp. 1789–1796, May 2009.

[131] B. George, H. Zangl, T. Bretterklieber, and G. Brasseur, "Seat Occupancy Detection System based on Capacitive Sensing," *IEEE Transactions on Instrumentation and Measurement*, vol. 58, no. 5, pp. 1487–1494, May 2009.

[132] D. Kuroiwa, "The Dielectric Property of Snow," *International Association of Scientific Hydrology*, pp. 52–63, 1954.

[133] W. Haynes, *CRC Handbook of Chemistry and Physics.* Taylor & Francis, 2011.

[134] *Telit Communications S.p.A., GM862 Modem QUAD GPS Data Sheet, 2009.*

[135] W. van Schalkwijk, *Advances in Lithium-Ion Batteries.* Kluwer Academic Publishers, 2002, ch. Charging, Monitoring and Control, pp. 459–481.

[136] J. A. Carcone, *Handbook of Batteries.* McGraw-Hill, 2002, ch. Portable Sealed Nickel-Cadmium Batteries, pp. 28.1–28.35.

[137] Arduino open-source electronics prototyping platform. http://www.arduino.cc, downloaded 4/9/2013.

[138] *IEEE Standard for Local and metropolitan area networks–Part 15.4: Low-Rate Wireless Personal Area Networks (LR-WPANs)*, IEEE Std., 2011.

[139] *Texas Instruments: CC1101 Low-Power Sub-1 GHz RF Transceiver, Data Sheet, 2011.*

[140] *Analog Devices: Programmable Controller for Capacitive Touch Sensors AD7143, Data Sheet, 2007.*

[141] *Analog Devices Inc., ADUM2251: Hot-Swappable Dual I2C® Isolators, 5 kV, Data Sheet, 2007.*

[142] *NXP Semiconductors, P82B96: Dual Bi-Directional Bus Buffer, Datasheet, 2004.*

[143] *Optek Technology, OPI155 High-Speed Optically Coupled Isolator, Datasheet, 2007.*

[144] A. Küchler, *Hochspannungstechnik.* Springer, 2009.

[145] H. Fischer, H. Hofmann, and J. Spindler, *Werkstoffe in der Elektrotechnik.* Hanser, 2007.

[146] *Dow Corning Sylgard® 170 Silicone Elastomer, Product Information.*

[147] G. Fercher, W. Smetana, and M. J. Vellekoop, "Contactless Conductivity Detection in LTCC Technology for Microfluidic Devices," in *31st International Spring Seminar on Electronics Technology, Budapest, 7-11 May 2008. ISSE '08.*, 2008, pp. 324–328.

[148] M. Weilguni, W. Smetana, G. Radosavlevic, J. N. A. Hofmann, and W. Goebl, "A ring-shaped LTCC/HTCC sensor for detection of finger forces in clarinet playing," in *Proceedings of the 2012 IEEE Sensors Conference*, 2012, pp. 1–4.

[149] *DuPont 951 Green Tape, Data Sheet.*

[150] LTCC@ÉTS, Folder. École de technologie supérieure, Montreal. http://www.ltcc.etsmtl.ca/documents/process.pdf, downloaded 8/7/2013.

[151] M. Gemeinert, "Über LTCC-Werkstoffe aus dem Stoffsystem CaO-La_2O_3-Al_2O_3-B_2O_3," Ph.D. dissertation, BAM, 2009.